DEPENDENCE OF RATES OF BREAKAGE ON FINES CONTENT IN WET BALL MILL GRINDING

by

Anirban Bhattacharyya

A thesis submitted to the faculty of
The University of Utah
in partial fulfillment of the requirements for the degree of

Master of Science

Department of Metallurgical Engineering

The University of Utah

December 2014

The University of Utah Graduate School

STATEMENT OF THESIS APPROVAL

The thesis of **Anirban Bhattacharyya**

has been approved by the following supervisory committee members:

Raj K. Rajamani	, Chair	**22nd August, 2014** Date Approved
Manoranjan Misra	, Member	**22nd August, 2014** Date Approved
Swomitra Mohanty	, Member	**22nd August, 2014** Date Approved

and by **Manoranjan Misra** , Chair of

the Department of **Metallurgical Engineering**

and by David B. Kieda, Dean of The Graduate School.

ABSTRACT

The following research fundamentally deals with the cause and implications of nonlinearities in breakage rates of materials in wet grinding systems. The innate dependence of such nonlinearities on fines content and the milling environment during wet grinding operations is also tested and observed. Preferential breakage of coarser size fractions as compared to the finer size fractions in a particle population were observed and discussed. The classification action of the pulp was deemed to be the probable cause for such a peculiarity. Ores with varying degrees of hardness and brittleness were used for wet grinding experiments, primarily to test the variations in specific breakage rates as a function of varying hardness. For this research, limestone, quartzite, and gold ore were used. The degree of hardness is of the order of: limestone, quartzite, gold ore. Selection and breakage function parameters were determined in the course of this research. Functional forms of these expressions were used to compare experimentally derived parameter estimates. Force-fitting of parameters was not done in order to examine the realtime behavior of particle populations in wet grinding systems. Breakage functions were established as being invariant with respect to such operating variables like ball load, mill speed, particle load, and particle size distribution of the mill. It was also determined that specific selection functions were inherently dependent on the particle size distribution in wet grinding systems. Also, they were consistent with inputs of specific energy, according to grind time. Nonlinearity trends were observed for 1^{st} order

specific selection functions which illustrated variations in breakage rates with incremental inputs of grind time and specific energy. A mean particle size called the fulcrum was noted below which the nonlinearities in the breakage trends were observed. This magnitude of the fulcrum value varied with percent solids and slurry filling, indicating that breakage rates were being influenced by the milling environment as a whole. Primarily, there was always an increase in the breakage rates of coarser fractions with an increase in the amount of fines in the particle population. Consequently, the breakage rates of the finer size fractions were observed to decrease with an increase in grind time. Similar trends were noticed for 2^{nd} order specific selection functions, where incremental inputs of specific energy were provided to observe realtime trends in the nonlinearity of breakage rates closely. Although the breakage rates for coarser size fractions increase with an increase in the amount of fines, the nature of nonlinearities varied with extended grind times. 1^{st} order and 2^{nd} order energy-specific breakage rates were observed to notice the variation in trends with extended grind times. Implications of such nonlinearities in specific breakage rates of various materials were tested on predictive simulation techniques, using the normalized linear population balance model and compared with an incremental methodology of specific energy input.

“BELIEVE YOU CAN AND YOU‘RE HALFWAY THERE”

- *Theodore Roosevelt*

I dedicate this thesis to my family. A special feeling of gratitude towards my beloved parents, **Kalyan Kumar Bhattacharyya** and **Gargi Bhattacharyya,** who have always encouraged me to stay motivated. My brother **Dhiman** and my girlfriend **Aayushi** have been very special and have always stood there beside me.

TABLE OF CONTENTS

ACKNOWLEDGEMENTS

I would sincerely like to express my heartfelt gratitude to Prof. Raj K. Rajamani for providing me with such a wonderful opportunity to work on this project. His guidance, persistence, and words of encouragement have been a constant source of inspiration for me, throughout my thesis research. I have always tried to imbibe maximum knowledge on this subject through his course lectures and the scientific research discussions.

I would also like to express my sincerest thanks and gratitude to members of my supervisory committee, Prof. Manoranjan Misra and Prof. Swomitra Mohanty, for their valuable inputs and suggestions and for their precious time reviewing my thesis.

Special thanks to Patricia (visiting researcher from Brazil), with whom I have had several scientific discussions. Her expertise and guidance on grinding is greatly acknowledged. I cherish the time spent with her here at the University of Utah.

Also, I would like to thank Solomon Tucker for the valuable discussions I had with him during the course of my thesis project.

Thanks are extended to Newmont Corporation for providing financial support to carry out parts of this study.

I would like to thank the entire faculty, staff, and my colleagues and friends in the Department of Metallurgical Engineering at the University of Utah for helping me in some way or other during my thesis research.

Last but not the least, I would like to express my love and appreciation towards my parents, brother, my girlfriend, and all those who had indubitable faith in my abilities, and for the endless support I received from them throughout my research work.

CHAPTER 1

INTRODUCTION

Comminution has predominantly been the fundamental step in the process of extraction of valuable minerals and metals from corresponding ore bodies. Grinding processes and operations, in particular, have always been at the forefront of comminution-related works. Grinding operations are of immense and specific importance to mineral processing and cement industries, which, in turn, are directly responsible for boosting or causing a slump in the U.S. economy. Whilst considering a global scenario for mineral and cement industries, grinding operations play an even more imperative role as the major expenses incurred are due to consumption of huge quantities of energy during the aforementioned processes. This, in turn, affects the net annual turnover generated from such industries. Industrial grinding operations in the United States consume more than 1% of net U.S. steel production annually as grinding media. These operations also consume more than 1.5% of the net energy production in the United States.

The end product is directly affected as a result of the grinding process. The primary objective of any mineral processing plant is to liberate and extract valuable minerals and metals from ore bodies. The degree of liberation of valuable minerals from

ore bodies is directly dependent on the degree of size reduction, which in turn, will dictate the process parameters for subsequent mineral processing and extraction operations. The primary concerns with such grinding circuits are those that involve colossal capital investments and even higher operating costs. In addition to such discrepancies, grinding circuits are infamous for their low efficiency. This is the singular reason why advancements are being made to improve milling efficiency, thereby reducing operating costs and increasing net annual turnover. In the past several decades, automation has replaced manual labor extensively. Owing to this, the increase in generated revenue has been significant. In order to improve milling efficiency, mill scale-up design is the area of research with maximum potential.

For a good part of the twentieth century, most mill scale-up designs were dictated by Bond's empirical model that related expended energy to size reduction of particles [1]. This empirical approach, though not without its fair share of mill design errors, has been used extensively in the mineral processing industry. Industrial surveys that evaluate risks pertaining to traditional design scale-up methods have assessed errors up to ± 20 percent [2, 3]. Design limitations and shortcomings in Bond's empirical model are primarily due to nonconsideration of imperative secondary processes in the grinding circuit, i.e., particle breakage kinetics, transport of particles through the mill, and explicit classification of particle size. All of the aforementioned factors contribute vehemently to the reason why nonlinearity inherently exists for wet grinding systems. Bond's model does not fully assert the significance and influence of these secondary processes on the grinding efficiency; instead, correlates each of them into an empirical equation [1]. Bond's model and other models have always explicitly accounted available grinding data

in terms of intrinsic energy-size reduction relationships [4, 5, 6], better known as laws of comminution [7, 8, 9]. These simplified grinding process models do not provide enough justice to the complicated breakage or fracture process of particles. Although these models provide a rudimentary basis for correlation of operating variables in the grinding process, they do not provide for descriptive process simulation.

Optimum process design and control of process parameters in comminution circuits require a comprehensive mathematical model proficient at predicting size-reduction dynamics of particles for every size fraction during the grinding process. Two discrete perspectives toward pragmatic simulation of the grinding process have been adopted widely. The first viewpoint concentrates primarily on discretized or singular events, i.e., involving breakage and fracture of single or unit mineral particle specimens. The essential goal of this operation is to represent the entire grinding process in terms of the fracture and breakage dynamics of individual specimens, and thereafter delineate their stress field characteristics. Information derived from single-particle fracture events cannot account explicitly for multiparticle breakage systems, since secondary grinding processes are not taken into consideration [10, 11]. For single-passage grinding systems, the Schonert model only analyzes the distribution of effectual loads acting on a particle, along with effective distribution of particle breakage energy, and dissemination of product particle size [10]. For the very same reason, the Schonert model is incompetent in depicting multiparticle environments in tumbling mills where the particle residence time distinctly varies from the time required to apply adequate stress on a single particle.

Multipassage systems and systems involving multiparticle environments are best depicted by a second perspective featuring mathematical modeling. The past two decades

have seen gradual, yet significant progress in the research and development of detailed grinding circuit and process models that fully assert the influence of secondary grinding processes. These phenomenological models have been derived from population balance modeling of particle populations and their behavior in mills [1, 12, 13, 14]. These models present a detailed relationship amongst various grinding subprocesses like particle breakage kinetics and size reduction, classification of product particle size, and transport of material or particle transport through the mill. Such a detailed relationship between interdependent grinding subprocesses provides considerable advantage over grassroot correlations like reduction in particle size and expended energy. This information, in turn, can be used to proactively simulate grinding data for mill scale-up design purposes. The phenomenon of particle breakage from parent particle to progeny particles or daughter fragments is characterized by two physically decipherable and intelligible quantities. Firstly, there is a selection function, which provides with the fractional rate of breakage of particles in their respective size intervals. Secondly, there is a breakage function, which explicitly accounts for the average particle size distribution of progeny fragments or daughter particles formed as a simultaneous consequence of primary breakage occurrences. The aforementioned physical quantities account for mathematical representation of individual size fractions in the mill. This, in turn, helps in determining optimum conditions for industrial grinding purposes from a mathematical perspective [1]. These are the most imperative reasons for choosing phenomenological models over other simpler models. As a result of this, these phenomenological models are more accurate at predicting mill scale-up designs with closer tolerances and reduced design risks than would have been possible with traditional scale-up methods.

Until very recently, population balance models were primarily used for the prediction of performance and analysis of laboratory-scale grinding mills, primarily batch grinding mills. Several attempts at predicting and determining the accuracy of population balance modeling for industrial mill scale-up designs for dry ball mill grinding systems have been made in the recent past [1, 14, 15]. Correlation of derived selection and breakage functions with mill diameter is the most fundamental step [14, 15]. The following step involves correlating and linking of derived model parameters to the specific power draft of the mill [1, 14, 15].

Population balance modeling for scale-up of ball mills for wet grinding purposes is a relatively new and novel approach. From an industrial perspective, wet grinding is more significant and important than dry grinding. Wet grinding processes encumber the treatment and analysis of inherent and innate nonlinearities that result directly due to the breakage process of particle populations in ball mills [12, 16]. A linearized population balance model adept for wet grinding purposes can have its parameters correlated with specific mill operating variables in a metaphoric fashion, quite akin to its correlation with the specific power draft used in dry grinding processes [16]. This, in turn, can help explain the exact consequence of mill design variables on the grinding process and on scale-up [16].

1.1 Research Objectives

The primary objective of this thesis research is to investigate reasons and causative factors contributing to nonlinearities in breakage rates for wet grinding systems. An energy-discretized approach will help understand the relationship between particle

breakage rates and specific energy input, which, in turn, may prove useful for improving mill efficiency for wet grinding processes. Three different ore bodies have been used to illustrate the variation in breakage rate behavior. Narrow inputs of specific energy in an incremental manner will be used to illustrate the ability of the population balance model to predictively simulate product particle size distributions. 1st order incremental inputs of specific energy will fully illustrate the increase in breakage rates for coarser size fractions of the particle population, with a subsequent decrease in the breakage rates for finer size fractions, as a function of fulcrum position. Detailed description of parameter estimation for predictive simulation and scale-up procedures has also been discussed. Effect of variation in percent solids and slurry filling have also been discussed, with close focus on specific energy input and described by fulcrum positions. Comparison of breakage rates during grinding of mono-size material and natural size material has also been discussed. The ores used in this study are limestone ore (softest), quartzite ore (extremely hard and brittle), and gold ore (extremely hard due to presence of granitic and gneissic rock). Particulate environment present in the mill during wet grinding processes has been effectively used to study and describe the nonlinearities in breakage rates. 1st order and 2nd order breakage kinetics have been considered in this research work to provide detailed insight into the mechanism of milling during wet grinding operations. Two methods have been used for breakage rate parameter estimation. Method I has a cumulative input procedure whilst Method II has an incremental input procedure for parameter estimation. These methods are compared against each other to get a better understanding of how breakage rates work. Results derived from both methods have been lucidly explained with respect to the research work performed here.

1.2 Thesis Organization

Chapter 1 gives a detailed overview on the importance of comminution in the field of mineral processing, pertaining to the mining and metallurgical industries. It also gives a conclusive relationship between size reduction and liberation of minerals from ore bodies. Bond's model provides an empirical approach to mill scale-up, and as such, shortcomings in the model have also been discussed. Primary focus of this research is on deducing a comprehensive and veritable relationship between nonlinearities in breakage kinetics and the fines content and milling environment for wet grinding systems.

Chapter 2 provides a detailed overview of information assimilation for this research work. It emphasizes on the phenomenon of wet grinding, the various forces acting on particles in the milling environment, and the mechanism via which grinding of particles actually takes place. Preferential breakage of particles has also been discussed, along with probable reasons for nonlinearities in wet grinding, linking the particle breakage kinetics to percent solids and interstitial void filling. The population balance model has been explained in detail, depicting fundamental relationships for material mass balance in wet grinding systems with respect to fractional rate of breakage out of various size intervals and also the fraction of product material received as a consequence of breakage events in the immediately preceding size interval. Descriptions have also been provided regarding energy normalized expressions derived from the original population balance model. An overview on causes and implications of nonlinearities in breakage rates for wet grinding has also been presented, with emphasis on 1^{st} order and 2^{nd} order breakage rates, along with implications of such nonlinearities on various methods of product size distribution simulations.

Chapter 3 gives an overview of the methods and materials that were utilized during experimental work. It also includes a detailed description of the test conditions and ore characteristics, along with a skeletal framework for all experiments done. A standard procedure for all wet grinding experiments performed has also been discussed, along with pictorial illustrations of various components of the grinding equipment used at different stages of the experimental process

Chapter 4 provides a logical analysis of all experimentally derived data. A detailed analysis of breakage kinetics has been done and initial estimates for selection functions and breakage functions for various ores have been derived. Graphical illustrations depicting various imperative relations in the wet grinding process have also been portrayed. Effect of nonlinearities on incremental 1^{st} order breakage kinetics have also been described, with the added mention of mean particle size below which nonlinearity is pronounced under varying test conditions. Incremental 2^{nd} order breakage kinetics have also been described with graphical depiction to provide information on the degree of nonlinearity with extended grinding times, linking ore characteristics and milling environment scenarios to explain such phenomena. Use of the function fitting software code called ESTIMILL has also been enunciated, along with applied logic with which predictive simulations are derived from experimental product size distributions.

Chapter 5 provides a compact framework, describing various kinds of inference drawn from the analysis of experimental data, along with stated conclusions, to help understand the mechanism and characteristics of wet grinding in a lucid manner.

CHAPTER 2

LITERATURE REVIEW

This chapter broadly encompasses all aspects of ball-milling, along with detailed investigation and review of population balance modeling, delving deep into its relevance in depicting multiparticle breakage environments, along with inspection of its legitimacy and corroboration with respect to existing and present experimental knowhow.

2.1 Postulates of Ball Milling

The process of milling or the milling phenomenon in tumbling ball mills is exemplified through dry and wet milling or grinding operations. Such operations utilize repetitive colliding of milling and grinding media like steel balls to achieve size reduction of particle populations as a consequence of expended energy. Particles ranging from one to several thousand in number may be present in between two colliding balls during a single time-discretized breakage event. Limiting factors for the number of particles present between two colliding balls or ball and mill shell include the density of balls, pertinent particle size, effective ball diameter relative to the diameter of the particle, and the amount of fine particles present [17]. In wet grinding operations, finer particles are suspended in slurry. This acts as a viable cushion during collision of balls, thereby dampening the full effect of the collision phenomenon. Consequently, the dampening

effect is missing if slurry viscosity is not high, thereby causing the finer fractions in the particle population to transmit energy to the coarser size fractions, and leading to an increase in their breakage rates. Figure 2.1 enunciates the phenomenon of collision of two grinding balls with entrapped particles in between. From a three-dimensional perspective, the trapped volume comprises all particles present within **BB'-BB'**. Therefore, this region is tightly packed and compacted with particles. This creates a region of comparatively higher density within the entrapped volume. The particles present outside this region have relatively lower density, quite akin to that of loose fine powder. Figure 2.2 portrays the entrapment of particles between colliding grinding balls. If the force due to collision is adequate, the entrapped particles are compressed (due to the constant compressive regime of the grinding media), causing impact breakage and interparticle breakage, as illustrated in Figure 2.2d. Adequate collision force ensures a strong probability that the concerned particles will disintegrate fully and form multiple progeny particles in the zone with diameter $\mathbf{X_c}$ associated thickness t in the region **BB'-BB'**, depicted in Figure 2.1. Inadequate impact force provides an impending possibility of the particles experiencing microforging and cracking at areas of maximum stress concentrations. Fundamentally, the zone of compaction is present within the region **AA'-AA'**. The entrapped volume in the zone of compaction comprises whole parent particles, along with progeny particles derived as fragments after fracture from other particles during previous breakage events. Maximum density is observed at that specific point where the balls collided and had initial contact. That region is given by **CC'**. The density decreases from the region **CC'** and goes down to a minimum value outside the **AA'-AA'** region where the density is all of loose fine particles, as portrayed in Figure 2.1 [18].

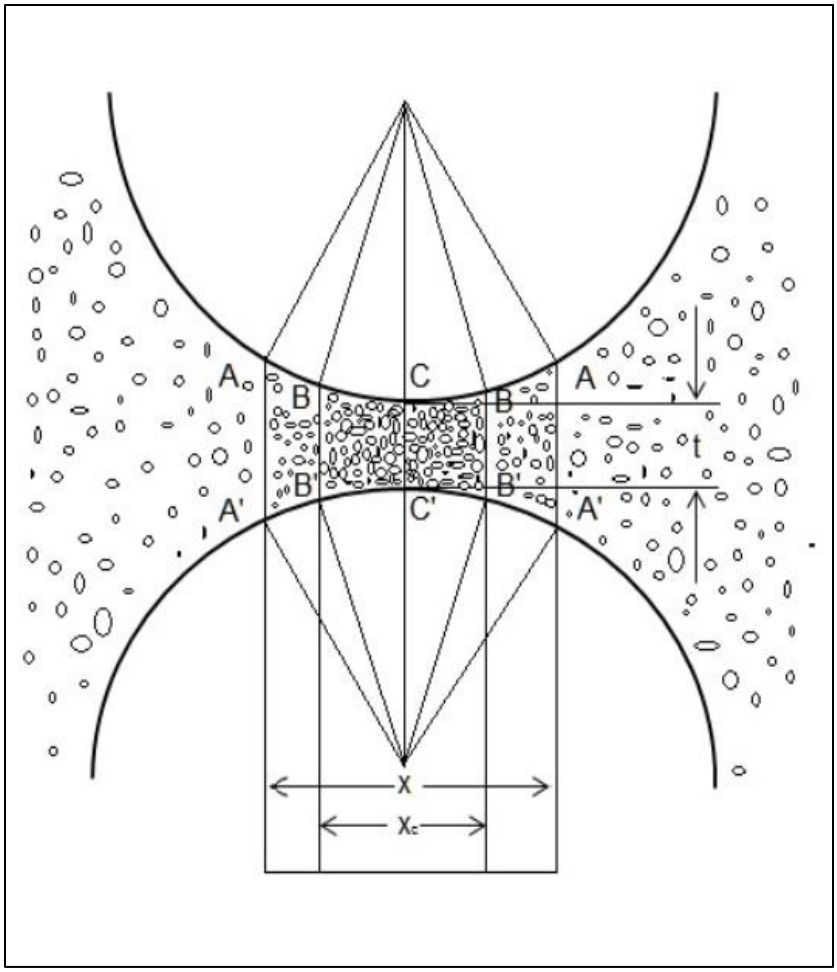

Figure 2.1.Model of collision/impact occurrence between two balls at a time of maximum impacting force.

Interparticle breakage is relatively higher in an area with maximum particle density (**CC'**). During the collision phenomenon, the impacting balls are decelerated due to energy being elastically expended. Fine particles incur radial displacement in the direction of minimal resistance to the flow of particles, as depicted in Figure 2.1. The interparticle spacing is relatively larger as compared to the particle size. Throughout the process of compaction, the interparticle spacing is reduced to an extent where it becomes nonexistent or negligibly minute as compared to particle size.

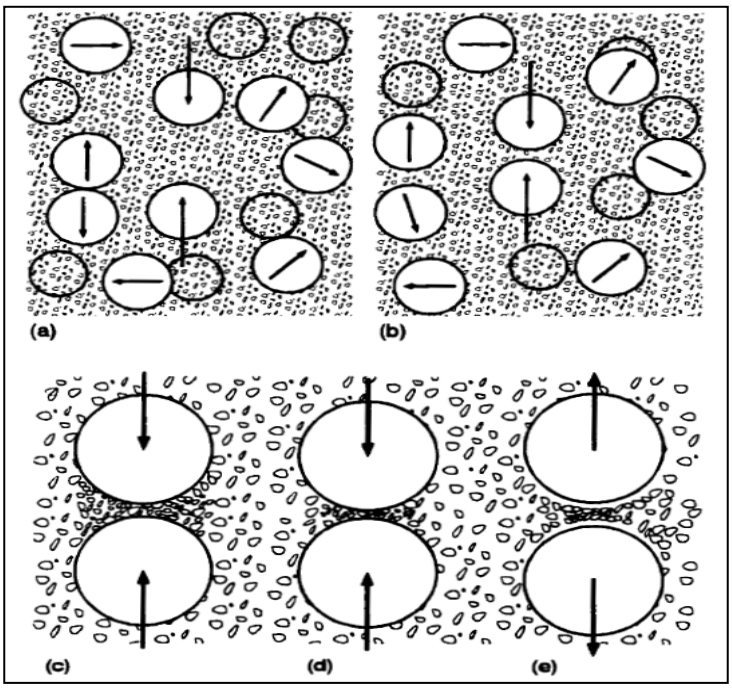

Figure 2.2. Procedure for entrapment of an incremental volume of ore material between two grinding balls. (a,b) Movement of grinding balls in the mill. (c) Entrapment and compressive action on particles. (d) Process of microforging, impact fracture, and interparticle breakage observed. (e) Particles released through elastic energy.

It is at this point that the particle density within the entrapped volume is maximum in a time-discretized framework, causing the finer particles to transmit the impact energy to the comparatively coarser particles in the entrapped volume. Compaction at the initial stage involves disarticulation and rearrangement of particles. Particle fracture and breakage comprise the final stage of an independent breakage event. Another imperative factor that determines the degree of fracture during a breakage event between particles is the type of material being worked upon in the milling environment, that is, particle characteristics like hardness and brittleness [19, 20, 21]. The end product

is a particle size distribution doing justice to the net specific energy absorbed during the entire grinding process.

2.2. The Phenomenon of Milling

Milling of material particles provides for in-situ changes in the particle morphology. Changes that occur are due to processes like microforging and impact fracturing. Initially, material particles that are ductile in nature are compressed by repetitive collision forces derived from colliding grinding balls. Brittle particles experience instantaneous breakage on impact due to their brittle nature. For harder materials, impact collisions may either cause instantaneous breakage or increase stress-concentrations in particles, which will subsequently cause fracture after repetitive impacts. Repeated impacting action by colliding grinding balls as well as interparticular encounters cause crack propagation that ultimately leads to failing and fracture, thereby leading to size reduction. After a stipulated duration of milling, individual and groups of particles deform and are stressed to such an extent that crack initiation takes place. Particle defects, irregularities, and inherent crack and inclusions help in buildup of inconsistent stress fields that ultimately lead to particle fracture.

The mechanism of milling is propagated by an initial stage of microforging. This stage comprises deformation of particles, primarily through fracture occurrences. Repetitive collisions cause the deformed particles or clusters of particles to be subjected to various stress-related forces like shearing, thereby causing fragmentation and failure. Progeny particles formed from the fragmentation and failure processes are subject to a

chain reaction wherein repetitive impact by grinding balls causes size reduction and fracture alternatingly.

2.3. Objectives of Milling

The process of milling has many prerogatives and objectives, but augmented and escalated interests vested in deriving particle sizes lower than that obtained through the process of atomization have given it a fresh start. Ball milling research, from a current and unbiased perspective, is fundamentally empirical, theoretical, and aimed at developing viable models for better and more energy-efficient milling processes. The primary prerogative of the milling process is reduction in particle size. The physical and mechanical properties of the material determine the definitive effect of the milling process on such materials. Secondly, the milling environment wherein the particle population will be subjected to the milling process also plays a specific role in shaping the properties of the material particles. The outcome and the result obtained from the milling process directly govern the kind of milling process required. Additionally, the behavior of particles when exposed to such milling conditions, along with their physical and mechanical properties, governs the choice of milling process to be used. The process of milling involves various forces acting on the particle population present within the milling environment. From the perspective of ball milling, instantaneous ball-particle collisions are defined by impact or collision forces. In such a situation, both objects may either be in relative motion or alternatingly stationary. Ball-particle and particle-particle collisions lead to size reduction and subsequent generation of finer particles. The underlying force determining such vehement deformation in particles is better known as

shear force. The first stage of milling involves crushing, truncation, and squashing of parent particles, thereby causing initial shape change and weakening. The underlying force prevalent during this stage of operation is better known as compressive force. Energy expended during the milling process provides impetus for these forces to act within the milling environment. Design and development of energy-efficient milling models is another imperative objective of the milling process. As a whole, it is the constant compressive force regime which causes size reduction and particle breakage in wet grinding systems.

2.4. Modus Operandi of a Tumbling Mill

Tumbling mills have steel balls as grinding media. The milling environment within a tumbling mill in operation observes augmented particle size reduction due to attrition action, rather than cataracting action of the grinding media. Therefore, it can be safely assumed that abrasion is the dominant force for particle size reduction in a tumbling mill. Ball mills are mostly employed to derive fine particulate product material as a result of the grinding process. Tumbling mills generate more fine particles during dry grinding, as compared to wet grinding. This can be attributed to the augmented settling speeds of solid particles held in suspension within the milling environment. More recently, there have been technological developments leading to increased production of fine particles through wet grinding processes. Mill rotation forces and provides impetus to grinding media and the loaded particle population into tumbling motion within the mill. The tumbling and cataracting motion of the grinding balls within the mill initiates the grinding process. They collide with other grinding balls and material particles

entrapped between them, in addition to impacting already partially cleaved parent particles and newly formed progeny particles. Another adjunct and supplementary process to the fundamental grinding process is the shearing of particles in the particle bed present within the tumbling mill. Shearing of particles occurs in the particle bed entrapped between two colliding grinding balls. Cleaving and rubbing between two particles promote superficial crack initiation, which propagates under the influence of existing forces within the milling environment. This subsequently results in fracture and fatigue failure of the particles. The phenomenon of particle fracture can be categorized into various types. Complete and utter fragmentation and disintegration of particles may occur due to colossal impacts exerted by the grinding balls on the particles. An impact of such magnitude causes instantaneous cleaving and fracture of parent particles, thereby forming progeny particles. Chipping is another mode of fracture which occurs due to glancing, grazing, and slanted collisions of grinding balls with particles. Angular and sideways impact of grinding balls on particles cause chipping and chiseling. Irregularly shaped particles having protruded edges and other relevant sharp features are smoothened by the chipping process. A third process causes gradual but progressive wear of particles surfaces. Rubbing and mowing of rough spherical particle surfaces previously obtained from the chipping process causes profound smoothening. At lower rotational speeds of the mill, the particle bed along with the ball charge is in a cascading state of motion. As the rotational speed of the mill is increased, grinding balls are released from a higher position within the mill shell, thereby causing comparatively more cataracting action than cascading action [22, 23]. Notably, there are three distinct modes and approaches of grinding media and particle bed movement. Movement utilizing the cascading

phenomenon causes grinding media to move in a counter direction or angularly opposite to drum rotation. Feed velocity gradient as well as velocity gradients between the feed and mill shell generate absolutely optimum conditions for profound and effectual attrition of particles. Another mode of operation is cataracting of grinding media. In this mode of operation, a narrow zone within the milling environment accounts for all the mill feed, that is, the entire feed material is concentrated within that particular volume, as it tumbles and traverses along a skewed or arced trajectory. A third mode of operation is known as the hurricane mode of operation, wherein a relatively similar curved trajectory distributes and disseminates the feed material over the absolute volume of the mill. A veritable synthesis of shear stresses, impact and collision forces, and compressive action generate the hurricane mode of operation [20, 22].

2.5. Transfer of Energy during the Milling Process

In all kinds of mills, kinetic energy is transmitted from the drive shaft to the mill shell and subsequently, the energy is transferred and imparted to the grinding media and the feed material present within the mill. Compression, friction, attrition, and other forces exert the energy expended from grinding balls onto feed particles, thereby causing size reduction in particles. Wet grinding systems have acceptable efficiency when it comes to transmission of energy for particle size reduction purposes. Slurry generation in wet grinding systems provide for the formation a suspension of fine particles. This partly dampens and absorbs the energy expended by colliding grinding balls. Therefore, only a considerable fraction of energy expended by colliding grinding media is utilized for particle size reduction in wet grinding systems. As mentioned earlier, various modes of

operation of material movement provide for expended energy to be utilized through application of a medley of forces like fracture, chipping, compression, and attrition. Transmission, transfer, and conversion of energy during the milling process is carried out in three major steps. Firstly, there is a net conversion or alteration of the kinetic energy expended by the drive shaft into mechanical movement that rotates the mill. The energy derived from the mechanical movement of the mill is transmitted to the grinding media present within the mill, which, in turn, is transferred to the feed material present. The third stage comprises comparison and equitability of stresses produced due to the movement of material inside the mill, and equating that with the stress required to produce fatigue failure and subsequent fracture in particles. Colliding grinding balls produce compressive and shear stresses, along with crushing and attrition forces. Therefore, particles or clusters of particles entrapped within the volume present in between two colliding balls are subjected to such forces. This causes the entrapped particles to be stressed. Repetitive impacts cause anelastic and elastic deformation in particles, along with simultaneous and instantaneous generation of a stress field caused by ball-particle contact. Energy waves traverse from primary sites of stress energy concentration and into the milling environment. These primary sites of stress energy are found in particles within the mill as well as the rotating mill and other tools. Repeated and persistent collisions cause stress buildup in particles to such a degree that the magnitude is in the proximity of stress that may result in fatigue failure of particles. Along with transmission of energy as energy waves from concentrated stress energy sites, a second phenomenon of energy dissipation occurs in the form of heat loss. This is due to the fact that friction and attrition forces due to ball-particle interaction, particle-particle

interaction, ball-ball interaction, and interaction of balls and particles with the mill shell, as well as friction due to the rotating mill, and other associated moving parts cause a considerable fraction of the expended energy to be lost due to heat generation [18, 22]. Usually, the collision interactions between balls and particles cause irreversible stressing of entrapped particles, thereby causing localized stress buildups. Elastic stresses caused by initial impacts can be reversed completely, but only under certain situations. Firstly, if the stressing rate caused by repeated impacts of grinding balls against particles can be lowered, the elastic stress can possibly be reversed. Secondly, if the distribution and spread of magnetic moments is not varied due to forces acting during the milling process, the stresses can be reversed. Also, if the distribution and variation of lattice defects in particles is low or negligible, the elastic stresses generated during the milling process can be relieved. Variations in mechanical stress result after a certain period of operation of the mill. After a stipulated number of cycles or runs in plastic or anelastic deformation, stresses are consistently produced. The magnitude of such stresses in the milling environment determine whether the stresses induced remain elastic in nature, or whether they lead to fracture by fatigue failure of particles [24, 25]. Cyclic loading and repetitive stress-imparting collisions cause fatigue failure below the yield strength of the material, caused by irreversible stress concentration buildup.

2.6. Postulates and Overview of Population Balance Modeling

Preliminary investigations done by Bond did not take into account the effects of secondary grinding processes or subprocesses on the entire grinding model. Particle breakage kinetics, explicit classification of particle size, and transport of particles through

the mill are just a few of a plethora of grinding subprocesses not taken into consideration by Bond's model. Lack of a comprehensive model describing all the parameters and subprocesses negated in Bond's model brought in an urgent need for the development of a descriptive and detailed model that would have accounted for everything. Exhaustive research and development brought in a new era of mathematical modeling and simulation of grinding processes. The most comprehensive and least erroneous of all was the population balance model, aimed at precise modeling and simulation of the grinding process. The efficiency and efficacy of a phenomenological mathematical model is determined by its complexity and details of its computational ability, along with the accuracy with which it can explicitly describe the intricacies and physical details, along with various intended applications. Simple models like Bond's model do not take secondary processes into consideration, whilst precisely predictive models will always decipher a simple yet analytical solution that invariably include all subprocesses. Primary features of Bond's equation include a feed size variable, a product size variable, and a work index. Bond's empirical equation gives a generalized idea of specific energy correlation with the work index and other associated variables [26, 27, 28]. Earlier, specific energy needs of industrial grinding processes were fulfilled by Bond's empirical model. Various subprocesses like transport of material through the mill, breakage kinetics, and size classification were accounted for by Bond's work index. The primary underlying assumption taken into consideration in Bond's empirical equation is coherence and similarity in breakage kinetics of all materials, as compared to 'Ideal Bond Material' [1]. The primary flaw in such an assumption is the fact that the work index is varied with variation in product size [27].

Bond's work index is determined through impeccable and precise classification in a standard grinding mill using locked cycle grinding tests. Scale-up is a herculean task in such situations because flawless classification is impossible in industrial-scale grinding mills, as compared to their laboratory counterparts. Another major assumption in Bond's solution to the grinding model problem is consideration of plug flow behavior for industrial-scale mills. Additionally, equilibrium is assumed to be achieved at steady state flow in closed circuit, in a continuous plug flow mill.

Contrary to Bond's empirical model, population balance models explicitly define grinding subprocesses in a physically legible and comprehensible manner [1, 12, 13, 16, 29]. Precise predictions of product size distribution in batch milling, locked cycle tests, and industrial-scale milling is provided by population balance modeling [1]. Time and again, it has been unequivocally proven that population balance modeling provides a comparatively more comprehensive alternative to Bond's empirical model [1, 12, 30, 31].

Various authors have pursued and presented several characteristics and processes of formulation of population balance models in their discussions [1, 12, 14, 16, 29, 31]. The most comprehensive of these models is the one that pertains to modeling and simulation of a size-discretized grinding process, in an incessant, uninterrupted, and continuous time frame. This size-discretized grinding process is wholly accounted for by two physically explicable and intelligible quantities. These are the size-discretized selection function and the size-discretized breakage function. The basic skeletal and fundamental framework of the model is lucidly described in the following pages.

Consider a batch mill with holdup mass H, which comprises particles with a size distribution range, intelligibly segregated into n intervals with maximum particle size

given as x_1 and the minimum particle size given as x_{n+1}. x_i as the limiting top size and x_{i+1} as the limiting bottom size define the particle size range given by the ith interval, and thus contain material mass fraction $m_i(t)$ at a given time t. Most instances witness an unequivocal relationship between x_i and x_{i+1}, given by $x_i = r.x_{i+1}$ (i=1, 2,……., n-1), where r is the geometrically determined sieve ratio. The kinetic model derived from the material mass balance for the ith size interval is illustrated as:

$$\frac{d[H\, m_i\,(t)]}{dt} = -S_i(t) H\, m_i\,(t) + \sum_{j=1}^{i-1} b_{ij}\, S_j(t) H\, m_j\,(t) \qquad \ldots 2.1$$

In the equation illustrated above, $m_i(t)$ defines the material mass fraction present in the ith interval at any given time t. $S_i(t)$ characterizes the size-discretized selection function for the size interval i, thereby accounting for the fractional rate of breakage of material from the ith size interval and into the following lower and finer sieve size intervals. b_{ij} defines the size-discretized breakage function that clearly elucidates the fraction of product material derived from primary breakage in the jth interval and subsequently found in size interval i [1,12]. Size-discretized selection functions are usually dependent upon the holdup particle size distribution in the mill at any arbitrary time t, given as;

$$S_i\,(t) = S_i\left(H, m_k\,(t)\right), \qquad for\ k = 1,2,\ldots\ldots,n \qquad \ldots 2.2$$

Although these size-discretized selection functions are dependent on holdup particle size distribution, these are not categorically and unequivocally dependent on time [1, 12, 16]. A case of linearity of such a kinetic model with constant coefficients is considered valid when the size-discretized selection and breakage functions are individually independent of the holdup particle size distribution in the mill.

A plethora of assumptions have been considered during formulation of the population balance Equation 2.1 [12, 16]. These are:

1. The ith size interval should be constricted and narrow enough to allow for coherent and pertinent description of particle behavior within that interval by interval parameters like $S_i(t)$ and b_{ij}.
2. The holdup particle size distribution does not dictate variations in size-discretized breakage functions, i.e., the size-discretized breakage functions are independent of the holdup particle size distribution within the mill. This is given by:

$$b_{ij} \neq b_{ij}\left(H, m_i(t)\right) \qquad for\ i = 1,2,\ldots\ldots\ldots,n \qquad \ldots 2.3$$

3. Particle agglomeration and clustering is unsubstantial and nonexistent, whereas attrition forces are meager and negligible.

The relationship illustrated in Equation 2.1 clearly enunciates the advantage that $S_i(t)$ and b_{ij} can be determined directly from milling experiments [17, 32, 33]. Size-discretized selection and breakage functions are independent of the holdup particle size distribution during dry ball-milling processes. The mass holdup H does not dictate variations in size-discretized breakage functions. Therefore, size-discretized breakage functions are independent of mass holdup in the mill. On the contrary, size-discretized selection functions are innately dependent on mass holdup within the mill [16]. This is given as:

$$S_i(t) = S_i\left(H, m_k(t)\right) = S_i(H) \qquad for\ k = 1,2,\ldots\ldots\ldots,n \qquad \ldots 2.4$$

Since the holdup particle size distribution does not vary the size-discretized selection functions, i.e., the selection functions are invariant to effects of holdup particle size distribution, and are therefore represented by an array of n differential equations

portrayed in Equation 2.1. A singular matrix equation with constant and uniform coefficients can express Equation 2.1 [1, 12, 16]. This is given as:

$$\frac{d\,\underline{m}\,(t)}{dt} = -[\ \boldsymbol{I}\ -\ \boldsymbol{B}\ ]\boldsymbol{S}\,(H)\,\underline{m}\,(t) \qquad \ldots 2.5$$

In the equation above, $\underline{m}(t)$ depicts a nx1 vector which illustrates mass fractions in n particle size intervals at any given time t, better denoted as $m_i(t)$ (for i=1, 2,……., n). The breakage functions are given by an n x n triangular matrix denoted by **B**. Selection functions are the diagonal matrix given by **S**(H), whereas the identity matrix is denoted by **I**. The analytical and logically derived solution for Equation 2.5 for a batch grinding process with arbitrary or random initial feed H $\underline{m}(0)$ is given as:

$$\underline{m}(t) = \exp[-(\ \boldsymbol{I} - \ \boldsymbol{B}\ )\boldsymbol{S}\,(H)\ t]\ \underline{m}(0) \qquad \ldots 2.6$$

The exponential present in the above expression can be explicitly simplified and explained by similarity transformation, when two selection functions are unequal [1, 12, 16, 30, 34], and this is given as:

$$\underline{m}\,(t) = \ \boldsymbol{T}\,\boldsymbol{J}\,(t)\,\boldsymbol{T}^{-1}\,\underline{m}\,(0) \qquad \ldots 2.7$$

Matrices **T** and **J** in Equation 2.7 have elements illustrated as:

$$T_{ij} = \begin{cases} 0 & i < j \\ 1 & i = j \\ \sum_{k=1}^{i-1} \dfrac{b_{ik}\ S_K\ (H)}{S_i\ (H) - \ S_j\ (H)}\ T_{kj} & i > j \end{cases} \qquad \ldots\ 2.8$$

$$J_{ij} = \begin{cases} \exp[-S_i\ (H)t & i = j \\ 0 & i \neq j \end{cases} \qquad \ldots 2.9$$

As the population balance models are phenomenological in essence, there is no deductive or postulated method to determine the dependence or effect of grinding model parameters on process variables and grinding mill design [12,16]. A grassroot and basic

analysis of particle breakage kinetics and associated correlations are fully functional and responsible for the formulation of a medley of parameter relationships within the model. There have been several instances where breakage kinetic parameters have been explicitly correlated with grinding media shape and structure, ball mill speed, mill dimensions, grinding ball size distribution, ball charge loading percentage by weight, ball density, and the mass of material holdup in the mill [1, 14, 15, 37]. A lot of experiments have been carried out to validate these correlations and have hence been precisely concretized. A relatively different approach at defining and determining such a correlation has been used for the case of dry ball-milling process [12, 13, 14]. The dry ball-milling process involves determination of proportionality of size-discretized selection functions when correlated to the specific power input of the mill, given by (P/H), i.e.,

$$S_i = S_i^E\ (P/H) \qquad \ldots 2.10$$

In the Equation 2.10, S_i^E is defined as the specific selection function, which is fundamentally and inherently independent of operating conditions in the mill. This can be directly applied to wet grinding with the assumption that the linear normalized model, over narrow ranges of specific energy input, provides breakage kinetics that are "nearly linear" in the "near neighborhood" of experimental data. Similarly, it was determined that the breakage function b_{ij}, is approximately homogeneous, invariable, and undeviating with respect to mill operating conditions. For maximum particle size, the ith interval will have i=1, and the Equation 2.10 can be substituted in Equation 2.1 to give a solution:

$$m_1(t) = m_1(0)\exp\ [-S_1^E\ (P/H)\ t] \qquad \ldots 2.11$$

The specific energy input of the mill ($\overline{E}$) is given by the product of material grinding time in the mill and the specific power derived for the milling operation. Equation 2.11 can therefore be described as:

$$m_1\,(\overline{E}) = m_1(0)\exp\left[-S_i^E\,\overline{E}\right] \qquad \ldots 2.12$$

Equation 2.1 can therefore be expressed in the normalized framework as:

$$\frac{dm_i(\overline{E})}{d\overline{E}} = -S_i^E\,m_i\,(\overline{E}) + \sum_{j=1}^{i-1} b_{ij}\,S_j^E\,m_j\,(\overline{E}) \qquad \ldots 2.13$$

Normalized forms of Equation 2.5 and Equation 2.6 can be written in a similar manner by substituting t with $\overline{E}$ and S_i with S_i^E. Predictive simulation of dry grinding performance and behavior has been accurately deduced by the implementation of such normalized equations, and these have been successfully enforced for performance prediction in batch mills of different sizes [14, 15]. The procedure involving scale-up predictions for industrial-scale mills comprise obtaining product particle size distribution data and other batch grinding information along with data on net power consumed in a laboratory-scale batch mill. It also involves estimation of selection and breakage functions from batch grinding data. These selection and breakage functions are then used in correspondence with specific power draft data to predict particle size distribution for mills with larger diameters. For our research, we will primarily be concerned with predictive simulations of experimentally derived wet grinding batch data.

Although no concrete information has been obtained to be directly implemented into scale-up population balance modeling for wet grinding models, data obtained from wet grinding operations by Kim [16] suggest that such data has impending and imperative implications on wet grinding model scale-ups. A volley of batch mill

experiments performed in a 10-inch diameter mill with a variety of different ball loads, percent solids in pulp, percent slurry filling, and mill speeds proved apt approximation of selection functions, which are nearly directly proportional to the specific power draft (P/H). Also, these selection functions are inversely proportional in nature to the percent solids in pulp. Mill speed, to a good extent, does not affect or vary deduced breakage functions for a definitive or given percent solids of material by weight. In close coherence, grinding media or ball load, along with material particle load, do not affect variations in breakage functions. Such results can be accurately extended to wet grinding processes in mills of varying diameters in a manner similar to that applied by earlier researchers to scale-up procedures for dry grinding processes in differently sized mills. Based on the inferences derived from scale-up population balance modeling of dry grinding processes in mills of different diameters, the idea can be extended to formulation of a concrete and accurate population balance model for wet grinding process in mills of different sizes. Incorporating the effects of inherent nonlinear breakage mechanisms and characteristics into the population balance modeling of wet grinding processes is most viable to accurate modeling and simulation, along with inculcating a competitive scale-up procedure.

2.7. Overview of the Nonlinearities in Breakage Rates in Wet Grinding Systems

The normalized linear mathematical population balance model depends on the specific rate of breakage of materials in wet grinding systems to accurately and intelligibly describe specific milling conditions. As it is known, both are strong functions

of the milling environment. There are various factors which affect the rate of breakage in wet grinding systems, and the most imperative are particle hold-up, percent solids, slurry filling, and media ball size. The most prominent functional dependence is that of the specific rate of breakage on the particle size distribution in the mill. A prominent observation is that the specific rate of breakage is augmented steadily with a decrease in average particle size. This observation is consistent with the fact that the strength of a particle decreases with an increase in size, and subsequently, the reverse seems to be true in a way that finer size fractions in a wet grinding system transmit most of the impact energy to the coarser size fractions, thereby resisting becoming even finer. The notion that the specific rate of breakage for finer size fractions decreases with an increase in grind times is true due to the increasing amount of fines being generated with extended grind times [38]. This, in turn, can be attributed to the comparatively greater density of stress-concentration and microflaws in coarser size fractions, thereby supporting the notion that such coarse particles will innately have a high probability of containing microfissures and flaws that would ultimately lead to fracture under persistent stress conditions governing the milling environment [39]. Consequently, it would be inadequate to state that this is an infinite process as the decrease in particle strength for the coarser particles does not lead to an indeterminate and unrestricted increase in the specific rate of breakage. The limiting factor in this case is the size of the smallest balls in the grinding media, such that the specific breakage goes through a maximum and starts decreasing for extended grind times. If the particle size distribution in the ball mill has top size particles comparable with ball charge top size and significant in comparison to the smallest ball size, this would directly affect the specific rate of breakage, as these particles would

themselves act as part of the grinding media, and not be appropriately fractured under prevailing stress conditions in the mill. Extended grind times would increase slurry viscosity and have a somewhat "cushioning effect", inhibiting further breakage of the coarser size fractions by partially absorbing the impact energy. As such, energy-specific breakage rates would start decreasing, even for the coarser size fractions in the particle population.

It is known that breakage rates are calculated from grassroot breakage characteristics of the particles. As is known, the selection function is an effective measure of the probability that a particle will be fractured during a time-discretized specific breakage event. In order for the particle to be fractured, it must be involved in the impact or compression zone between two media particles, such that it receives a considerable fraction of the event impact energy, thereby causing its fracture energy to exceed, ultimately leading to fragmentation due to failure. Wet grinding is inherently nonlinear due to the classification action of the pulp under prevailing milling conditions, which causes "preferential breakage" of coarser size fractions in comparison to the finer size fractions. Also, multiparticle interactions during wet grinding change in a spatiotemporal manner, rendering 1st order breakage kinetics not fully equipped to describe the classification action in wet grinding. Interparticle stress concentrations for the average particle population tend to reduce with an increase in the amount of fines for extended grind times, primarily due to presence of an augmented number of contact points which cause partial dispersion of impact energy and not complete transmission. Consequently, the energy-specific breakage rates decrease with an increase in the amount of fines and this can prominently be witnessed for harder and more brittle materials. Incremental

inputs of specific energy and grind times should be implemented to notice the gradual change in 1^{st} order and 2^{nd} order breakage kinetics, thereby enabling realtime observation of nonlinear breakage kinetics and its dependence on the fines content and milling environment during wet grinding. Incremental 2^{nd} order energy-specific breakage rates provide an insight into realtime interactions between various size fractions of the particle population during wet grinding, and as such, definitive information can be obtained by varying test conditions like percent solids and interstitial/void filling (percent slurry filling) to observe consequential results. These, in turn, would help provide a veritable framework for predictive simulation and mill scale-up and design, as required.

CHAPTER 3

EQUIPMENT AND EXPERIMENTAL PROCEDURES

This chapter illustrates the materials, equipment, experimental procedures and various other methods that have been used for this particular research work. The experiments have been carefully outlined and carried out to determine a quantitative and qualitative relationship between the breakage rate dependence and the quantity of fines generated during the milling process, correlating it with the particle size distribution within the milling environment. All the experiments have been carried out in a 10-inch diameter mill and a veritable correlation has been established between the size distribution of finer particles and the specific rate of breakage into successive sieve sizes.

Experiments were performed on three different types of ore bodies, as a basis to compare specific rates of breakage for each mineral as a function of fines generated. Natural (-10 mesh) size distribution and mono-size (10 x 14 mesh) distribution of each ore body were used for wet grinding experiments. Limestone was sourced from operations at Graymont Delta, Utah. Specific gravity of limestone, as measured by a picnometer, was deduced to be 2.65. Limestone was primarily comprised of opaque limestone crystals with a few instances of translucent calcite crystals, which did not hinder homogeneous and uniform breakage characteristics, owing to the fact that both

minerals had similar and closely correlated breakage kinetics. Quartzite was sourced from Staker-Parson Ltd. Homogeneity of breakage kinetics was ensured as the derived mineral was highly pure in content. Density of quartzite, as deduced by the picnometer, was found out to be 2.74. In the case of quartzite, natural size distribution (-10 mesh) was derived by passing rocks (3 x 4 mesh) through a roll crusher with a roll gap of 2 mm. The resultant product obtained was then screened using a 10 mesh screen on a Sweco machine. The oversize was discarded and the undersize was used as natural size (-10 mesh) distribution for wet grinding experiments. This ensured uniformity of feed size distribution for natural size experiments. The third material used was gold ore derived from Newmont Gold operations, sourced from the Boddington mines in Australia. The specific gravity of the ore was determined with the help of a picnometer and it was observed to be around 2.86. A procedure similar to that used for quartzite was used to derive natural size and mono-size material for wet grinding experiments.

3.1. Grinding Equipment

Primary equipment comprises a laboratory batch mill, with its dimensions being 10 inches in diameter and 11.5 inches in length. The batch mill is constructed out of stainless steel and is fitted with eight square lifter bars, as shown in Figure 3.1 and Figure 3.2. The mill shell, as shown in Figure 3.3, illustrates a replaceable end plate with two stainless steel handles to aid in lifting the plate after completion of each experiment. The end plate is affixed firmly to the mill shell with the help of sixteen mild steel bolts, put rigidly in place with the help of a torque gun. The torque gun also aids in providing uniform torque to each of the bolts, enabling the opening plate to rest uniformly and

Figure 3.1.Partially loaded 10-inch batch grinding mill depicting square lifters configuration.

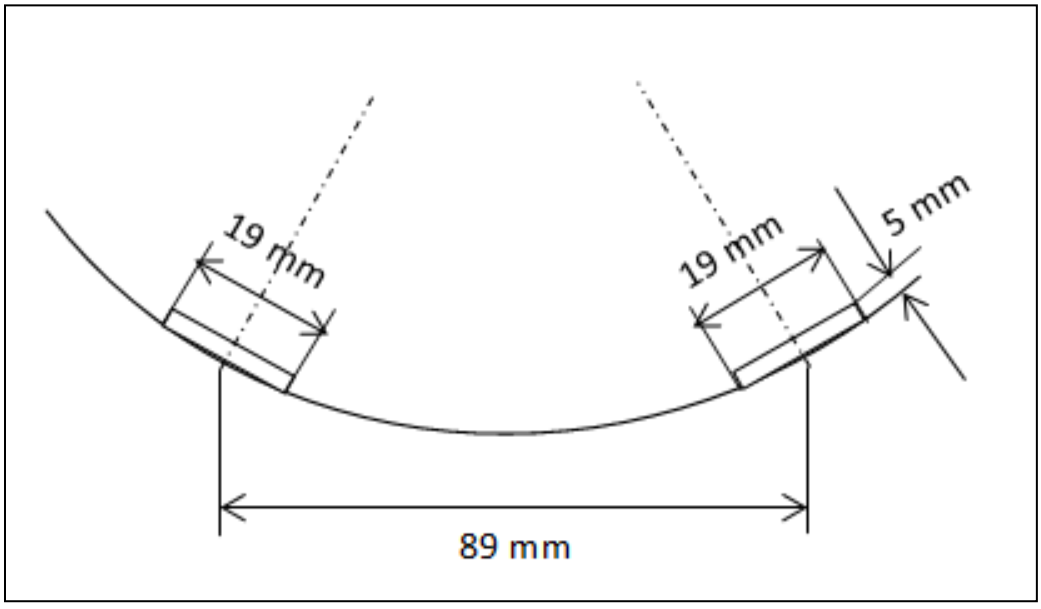

Figure 3.2.Configuration of 8 rows of square lifters present in the 10-inch mill.

firmly on the mill shell. A counterweight illustrated in Figure 3.4, in the form of a stainless steel bar, is present to neutralize the combined weight of the additional handles and bolts on the opposite side, thereby maintaining the centre of gravity precisely, such that the results can be used for scale-up and simulation for mills of larger diameters without these contraptions. This also provides scope for the transmission system to deliver power to the mill shaft in a uniform and steady manner. Wet grinding tests performed before and after mill modifications, but under similar test conditions, yielded exact results. A Graham variable speed transmission mechanism is used to transmit power to the mill shaft. The mill shaft is conveniently coupled with a torque sensor to measure power draft or torque, as is shown in Figure 3.5. This allows for direct and realtime measurement of power draft from the drive shaft connecting the ball mill to the transmission system. The maximum capacity of the torque sensor is 100Nm and the model is a Futek Sensor. Figure 3.6 illustrates a fully loaded mill before operation. Stainless steel balls were used for all wet grinding experiments. Ball sizes used in the batch mill for wet grinding experiments ranged from 1/2 inch to 1 1/2 inch. The batch ball mill was loaded with an equilibrium ball charge distribution. An equilibrium ball charge distribution is defined by balls of various sizes present in a commercial mill during operation, such that the wear rate of steel balls comprising the top size is accounted for. The ball load was perfectly consistent with a ball filling of 30% (M_B = 0.3) of the struck volume, which amounted to 20.7 kg. The precise and absolute distribution of ball charge used for wet grinding experiments is given in Table 3.1. The following figures, as mentioned above, provide information regarding batch mill equipment, followed by tables with information regarding experimental conditions.

Figure 3.3.Mill shell replaceable cover plate with stainless steel handles.

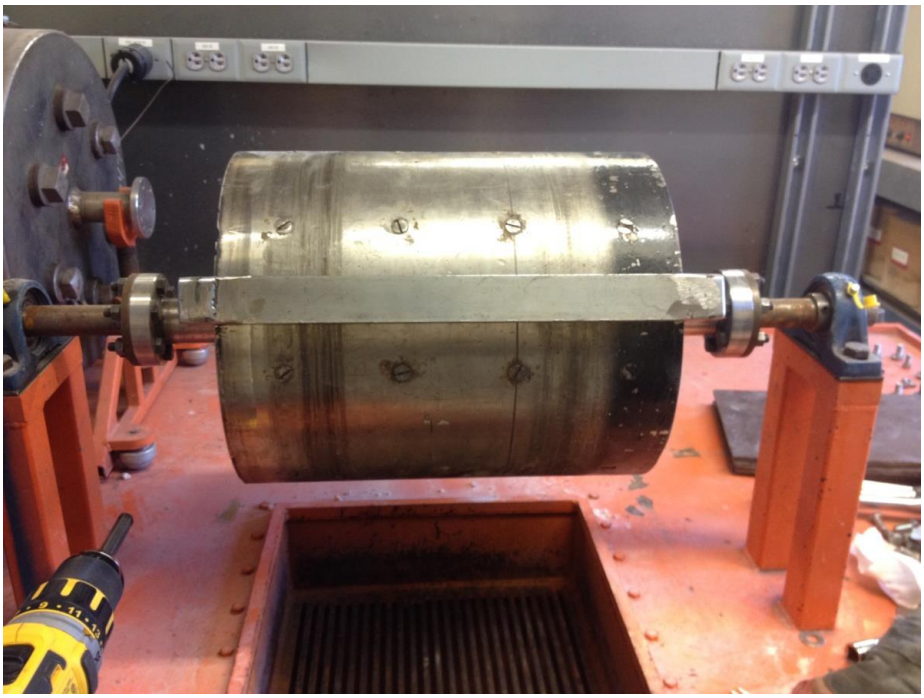

Figure 3.4.Counterweight to neutralize variation in center of gravity due to presence of steel handles.

Figure 3.5.Illustration of torque meter coupled to the mill shaft.

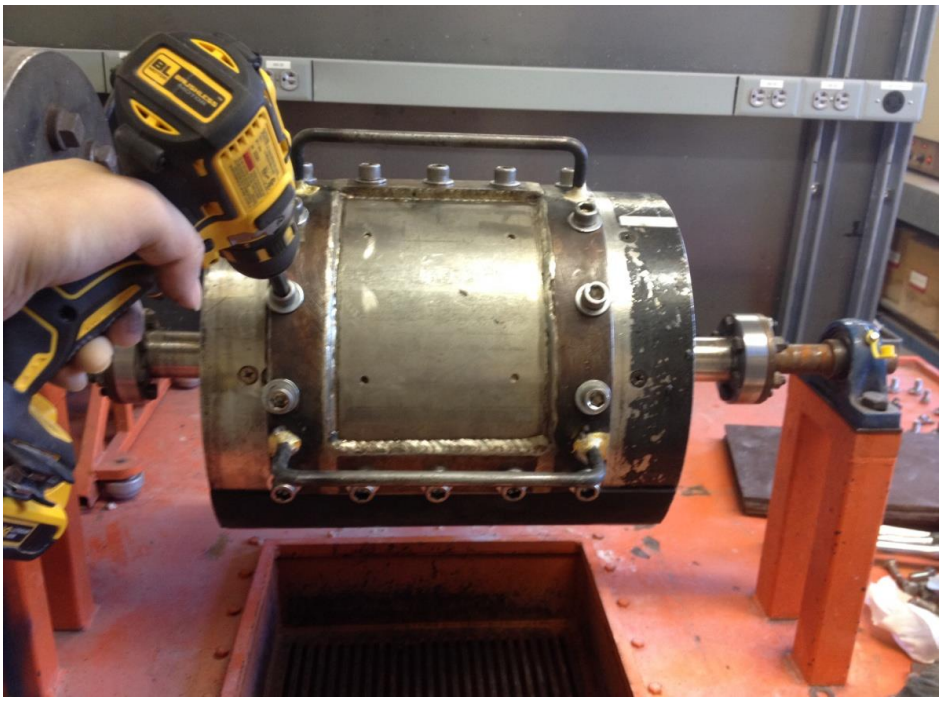

Figure 3.6.Fully loaded mill depicting uniform torque being applied to the bolts before operation.

Table 3.1.The Equilibrium Ball Charge Distribution Used in the 10-Inch Mill.

Ball Diameter (inches)	Total No. of Balls	Percent (by wt)	10-inch mill (30% filling) (kg)
1.50	28	30.94	6.41
1.25	62	39.06	8.09
1.00	69	22.27	4.61
0.67	70	6.73	1.39
0.50	25	0.99	0.21
Total	254	100.00	20.70

3.2. Experimental Procedure

For each of the three ores used for wet grinding experiments, the "as received" material was first prepared according to requirements. Limestone ore received was first screened through a 10 mesh Sweco screen to derive -10 mesh "natural size" distribution. Enough ore was screened to get an adequate amount of "natural size" material for wet grinding purposes. The remaining ore was then screened through a set of two Sweco screens, subsequently retaining all material in the 10x14 size interval, whilst discarding all material that were either +10 mesh or -14 mesh. This provided for enough mono-size (10x14 mesh) to be used for wet grinding purposes. The procedure used for deriving material for wet grinding of quartzite ore was quite different than that followed for limestone. Rocks (3x4 mesh) were passed through a roll crusher with a roll gap of 2 mm. The material thus obtained was screened through a 10 mesh Sweco screen to derive -10 mesh "natural size" distribution. The remaining roll crusher product was then passed through a set of two Sweco screens, thereby deriving mono-size material in 10x14 size interval. For gold ore, the process used to obtain "natural size" and mono-size material is the same as that implemented for quartzite ore.

3.2.1. Wet Grinding Experimental Conditions

The purpose of this research work was to determine the dependence of the specific rate of breakage on the fines content and the material environment in a ball mill for wet grinding systems, and subsequent scope for scale-up procedures. This involved deducing impending reasons and causes for the nonlinearity observed in wet grinding systems. Particle behavior and size distribution inside the mill during wet grinding operations have pronounced effect on the rate of breakage of particles during the grinding process. A feasible experimental structure was devised to enable and observe the effect and behavior of varying percent solids and percent slurry filling of interstitial or void volume on the material environment and the size consist on the mill, thereby directly affecting the specific rate of breakage. Table 3.2 gives the skeletal framework for the wet grinding experiments performed. Table 3.3 through Table 3.5 gives an overview about actual test conditions applied for wet grinding, along with the various masses of material and water, in accordance with percent solids and slurry filling considerations.

Table 3.2.Experimental Structure for Wet Grinding Experiments

Wet Grinding Experimental Conditions for Limestone, Quartzite, and Gold Ore				
Natural Size Distribution				
Percent Ball Load (%)	Percent Slurry Filling (%)	Percent Solids (%)	Grind Time (min)	Percent of Critical Speed (N*)
30	100	65	1,2,4,5,6,8	68.3
30	100	72	1,2,4,5,6,8	68.3
30	260	65	1,2,4,5,6,8	68.3
30	260	72	1,2,4,5,6,8	68.3
Mono-size Distribution				
30	100	72	1,2,4,6	68.3

Table 3.3.Wet Grinding Test Conditions for Limestone

Test Conditions for Limestone							
Natural Size Distribution							
Percent Ball Load (%)	Percent Solids (%)	Weight of Material (gms)	Percent Slurry Filling (%)	Weight of Water (gms)	Grind Time (min)	Percent of Critical Speed (N*)	Mill speed (rpm)
30	65	1925.7	100	1036.89	1,2,4,5,6,8	68.3	62.2
30	72	2250.7	100	875.27	1,2,4,5,6,8	68.3	62.2
30	65	5006.7	260	2695.92	1,2,4,5,6,8	68.3	62.2
30	72	5851.8	260	2275.70	1,2,4,5,6,8	68.3	62.2
Mono-size Distribution							
30	72	2250.7	100	875.27	1,2,4,6	68.3	62.2

Table 3.4.Wet Grinding Test Conditions for Quartzite

Test Conditions for Quartzite							
Natural Size Distribution							
Percent Ball Load (%)	Percent Solids (%)	Weight of Material (gms)	Percent Slurry Filling (%)	Weight of Water (gms)	Grind Time (min)	Percent of Critical Speed (N*)	Mill speed (rpm)
30	65	1954.5	100	1052.43	1,2,4,5,6,8	68.3	62.2
30	72	2338.9	100	909.58	1,2,4,5,6,8	68.3	62.2
30	65	5081.8	260	2736.33	1,2,4,5,6,8	68.3	62.2
30	72	6081.2	260	2364.91	1,2,4,5,6,8	68.3	62.2
Mono-size Distribution							
30	72	2338.9	100	909.58	1,2,4,6	68.3	62.2

Table 3.5.Wet Grinding Test Conditions for Gold Ore

Test Conditions for Gold Ore							
Natural Size Distribution							
Percent Ball Load (%)	Percent Solids (%)	Weight of Material (gms)	Percent Slurry Filling (%)	Weight of Water (gms)	Grind Time (min)	Percent of Critical Speed (N*)	Mill speed (rpm)
30	65	2203.4	100	928.98	1,2,4,5,6,8	68.3	62.2
30	72	2388.8	100	856.87	1,2,4,5,6,8	68.3	62.2
30	65	5728.8	260	2415.34	1,2,4,5,6,8	68.3	62.2
30	72	6210.9	260	2227.85	1,2,4,5,6,8	68.3	62.2
Mono-size Distribution							
30	72	2388.8	100	856.87	1,2,4,6	68.3	62.2

A detailed and elaborate description of the experimental procedure used during wet grinding operations in the 10-inch batch mill is as follows:

- A layer loading manner was used to charge or load the mill with balls and feed material, that is, feed material and balls were put alternatingly atop each other in a layered manner to ensure thorough and uniform mixing at the beginning of each wet grinding experiment. This operation was subsequently followed by addition of water according to predetermined percent slurry filling values.
- Thereafter, the mill speed was adjusted using the variable speed controller and was set to 68.3% of critical speed, which corresponded to 62.2 rpm. The mill was then put in operation for a predetermined span of time. Mill revolutions were recorded periodically and the torque was measured by the torque sensor, which was connected to the computer and hence gave a realtime plot of the variation in torque.

- The mill was unloaded after completion of a particular grind or experiment. The replaceable end plate was removed and the contents of the mill were discharged over a grizzley. It was simultaneously washed with water and collected in buckets placed underneath.
- The slurry thus collected in buckets was filtered using a pressure filter. The cakes of material obtained thereafter were put to dry in an oven set at a temperature of 110^{o} C.
- The dry cake obtained was weighed and pulverized by hand to get enough consistency for sampling. Thereafter, a rotating sampler splitter was used to derive a representative sample for a particular experiment. Depending on the test conditions for each wet grinding experiment performed, the weight of the representative sample differed accordingly.
- The representative sample thus obtained was dry screened up to 100 mesh (150 microns), and all the material below it was wet screened through sieves 140 mesh (106 microns), 200 mesh (75 microns), 270 mesh (53 microns), and 400 mesh (38 microns). The material retained on each screen was collected and dewatered using a pressure filter. This was followed by drying the cakes that followed, in an oven.
- A two place Mettler balance was used to measure the weight of each size fraction. This was subsequently followed by proper cleaning of each screen to ensure maximum recovery of the material retained at each size fraction.
- The mill torque for each wet grinding experiment was noted.

Actual wet grinding experiments were subjected to a number of precautionary and corrective checks to ensure optimum efficiency of the entire process, from grinding of

material in the ball mill to measurement of the weight of the representative material after completion of each experiment. These are as follows:

- Preliminary inspection was carried out to ensure that all grinding equipment are in optimum condition and do not have any loose parts that might be a concern for failure.
- The mill speed controller was set to the required mill speed and the subsequently, the mill speed was measured with the help of a tachometer.
- Empty mill torque was measured to prevent incorrect inputs during determination of net power draft and specific energy for each wet grinding experiment.
- Grinding media in the form of an equilibrium ball charge distribution was hence prepared, and loaded into the batch ball mill.
- Calculations were done to determine the weight of solids and water for each wet grinding experiment, according to predetermined test conditions. This was done to ensure desired percent solids and percent slurry filling, along with desired percent void filling or interstitial void filling.
- Percent ball load present in the mill was rechecked.
- A layer loading mechanism was applied for filling up the mill with solids, water, and grinding media.
- The torque sensor present on the mill shaft was connected to the computer.
- According to predetermined test conditions, the mill was run for a stipulated duration of time. Realtime torque data were recorded during this time.

- After completion of each grinding experiment, the contents of the mill were emptied into a grizzley. Water was used to wash the mill and recover any leftover material. Thereafter, the slurry was collected in buckets underneath.
- Care was taken not to apply excessive pressure during pressure filtration, in order to prevent tearing of the filter paper.
- Cakes were prepared during the filtration process and all the cakes were dried in an oven.
- The entire product was weighed and a representative sample was derived using a rotary sampler splitter.
- This representative sample was used for size analysis. Size analysis was done using Retsch AS200 wet and dry sieve shakers shown in Figure 3.7.
- After completion of product size, the sample was uniformly mixed with the remaining product and re-used for further grinding experiments. Any loss in mass during the entire procedure was compensated using material below 400 mesh (-38 microns).

The following Figure 3.7 gives a detailed illustration of the dry sieving and wet sieving process. Dry sieving is done in order to separate the coarser size fractions in the product particle size distribution, whereas wet screening is done to segregate the finer size fractions. Sieving helps in getting representative information regarding the product particle size distribution for the entire population of particles used for a particular experimental run. For wet grinding of mono-size material, it helps deduce the variation in selection functions for various ore bodies, which, in turn, help us get information regarding the breakage characteristics for the same.

Figure 3.7.Illustration of Retsch AS200 wet and dry sieve shakers in operation.

CHAPTER 4

RESULTS AND DISCUSSION

4.1. Analysis of Breakage Kinetics

This chapter provides a detailed overview of the analysis performed on the data derived from all wet grinding experiments performed. Breakage kinetics for limestone, quartzite, and gold ores has been enunciated in this chapter. The relationship and dependence of selection and breakage functions on mill operating variables, fines content in the mill during operation, and particulate environment in the mill have been described broadly. Variation in ore characteristics contributed directly to an understanding of these parameters, thereby providing a relationship between ore characteristics and parameter dependence. Limestone is generally a medium hard ore, more toward the soft side. The Mohs hardness scale tips the hardness of limestone as approximately 3. Quartzite is a comparatively harder material with a hardness value of 6.5 - 7 on the Mohs scale. Along with this high hardness value, quartzite is an extremely brittle material, providing for an interesting comparison with properties of other ores used. Gold ore derived from Boddington mines in Australia is even harder in nature, due to it being comprised of extremely hard granitic and gneissic rock. Hardness values are comparable with that of quartzite, with this being slightly higher, but a lot less brittle in nature. The preliminary step in determining selection and breakage function parameters is performing wet

grinding experiments on mono-size material, usually the top size that would be present for natural size wet grinding experiments. Figure 4.1, Figure 4.2, and Figure 4.3 provide an insight into the product particle size distributions for limestone, quartzite, and gold, respectively, derived after wet grinding of mono-size material of each ore for various grind times. Four grind times for each ore have been used. This has been done in order to witness the trends in product particle size distribution with extended grind times.

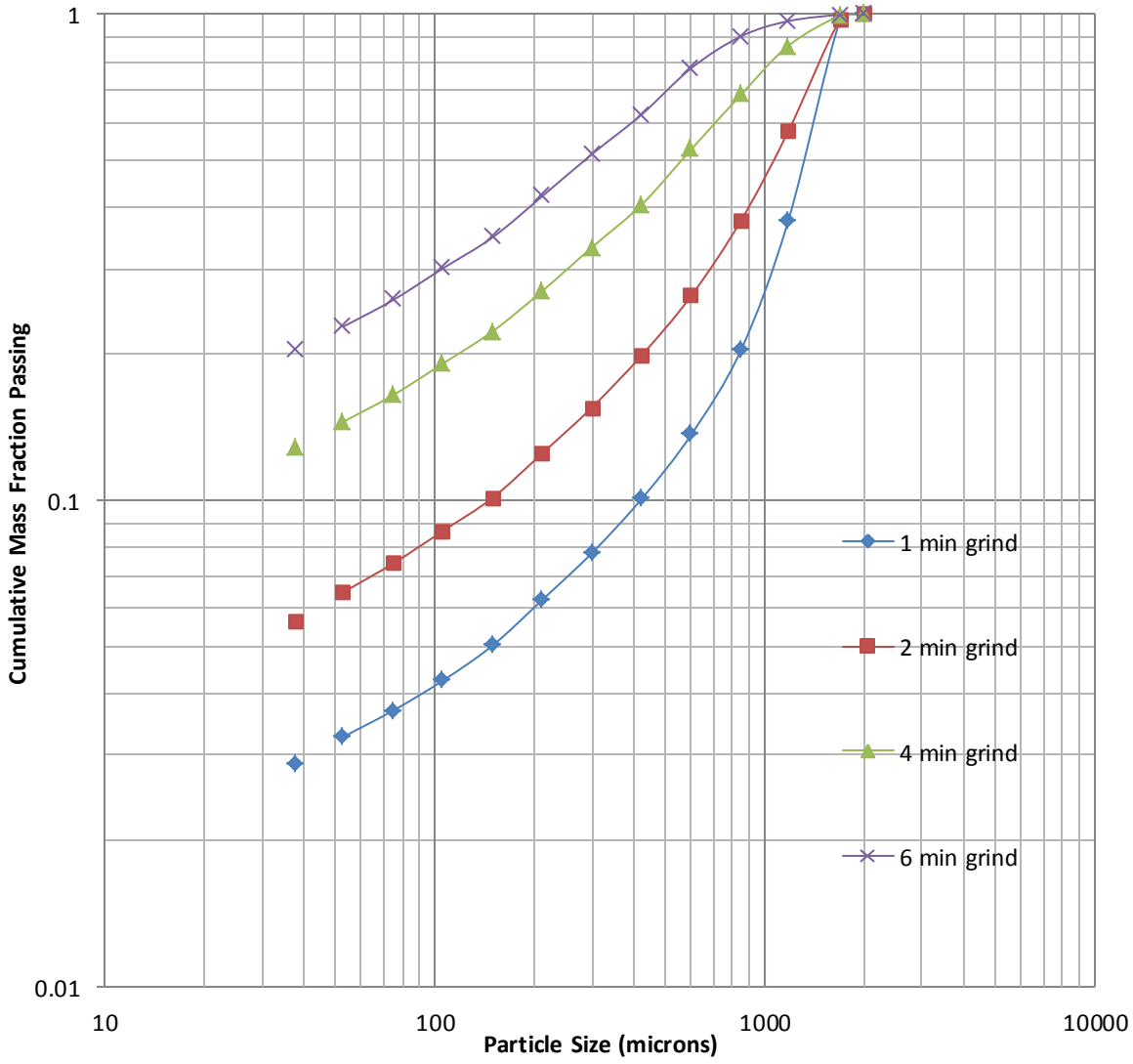

Figure 4.1.Cumulative Mass Fraction Passing versus Stated Size in batch grinding of mono-size limestone Ore.

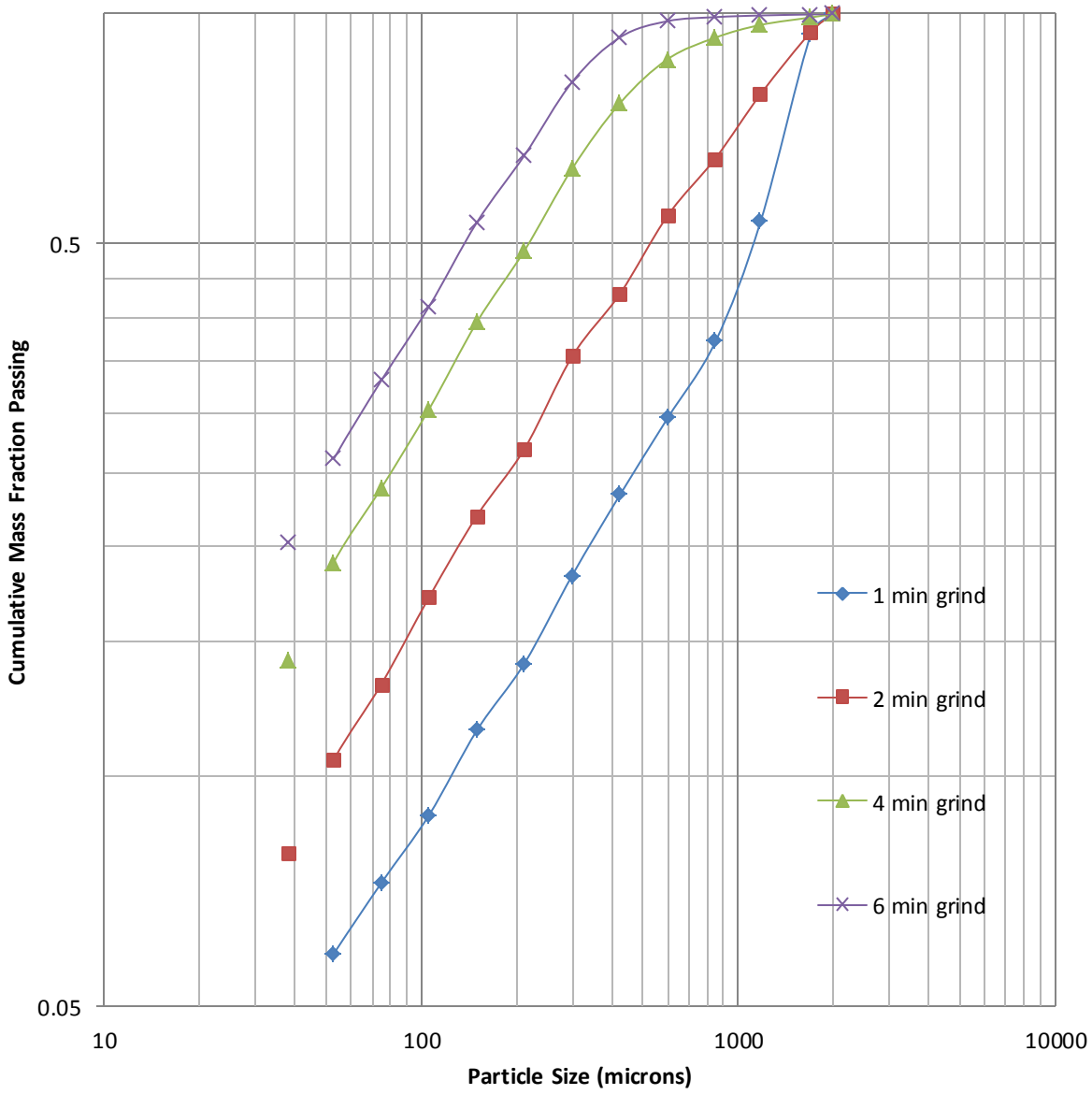

Figure 4.2.Cumulative Mass Fraction Passing versus Stated Size in batch grinding of mono-size quartzite Ore.

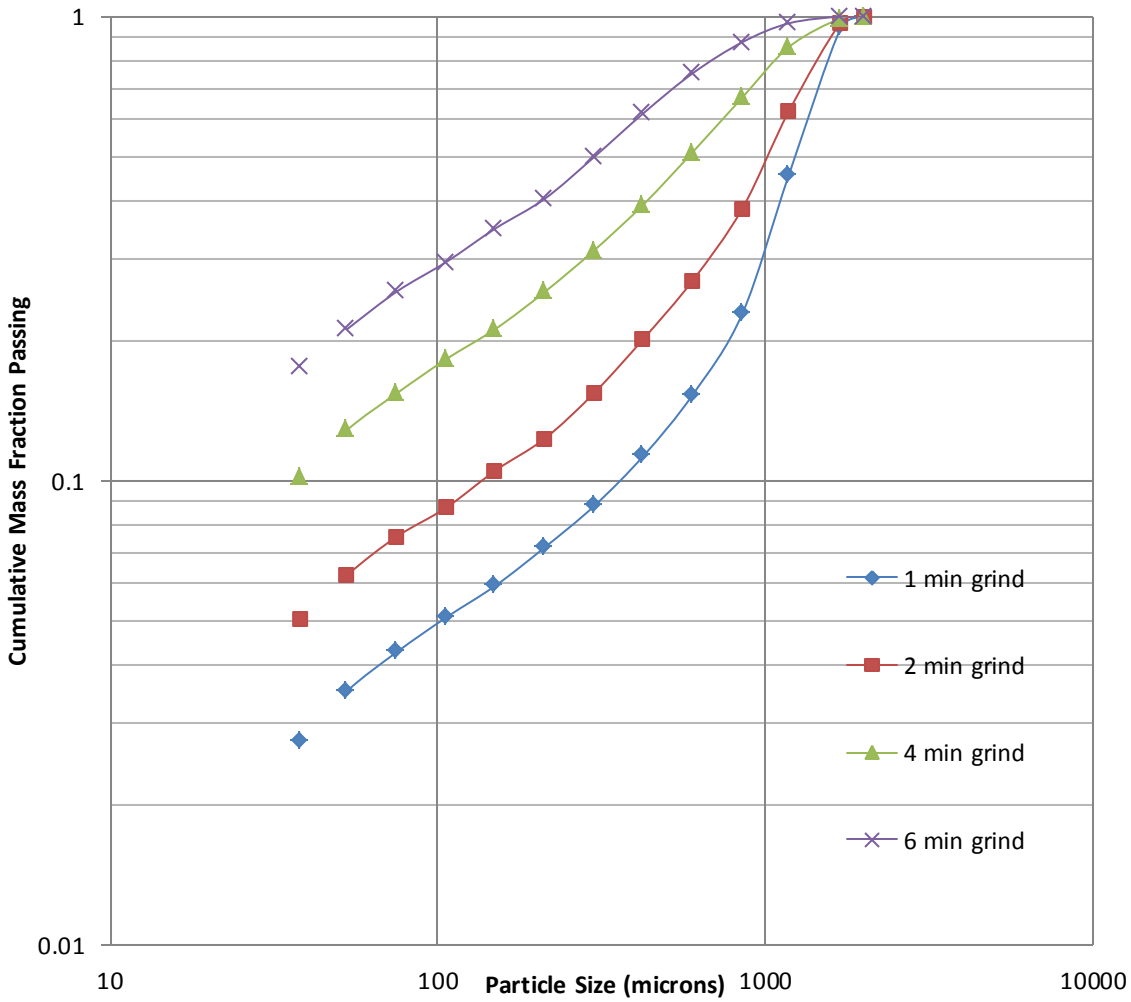

Figure 4.3.Cumulative Mass Fraction Passing versus Stated Size in batch grinding of mono-size gold ore.

As is known, dry grinding is inherently linear whereas wet grinding is inherently nonlinear in nature, that is, they exhibit a profound deviation from linearity during the milling process. Explicit classification of particles during wet grinding causes this phenomenon. Feed size selection functions can be directly deduced from the slope of feed disappearance plots ($\ln(m_i\ (t)/m_i\ (0))$ vs t) derived directly from the equation:

$$S_1(t) = -\frac{d}{dt}\left[\ln(m_i\ (t)/m_i\ (0))\right] \qquad \ldots 4.1$$

Figure 4.4, Figure 4.5, and Figure 4.6 illustrate plots for the fraction of feed size remaining after each wet grinding experiment $m_i(t)/m_i(0)$) versus time (t) for limestone, quartzite, and gold ore, respectively. They also illustrate normalized feed size selection functions with respect to grind times. Dry grinding systems have breakage kinetics absolutely linear in nature, thereby indicating that the feed size selection function (S_1) is independent of time. For wet grinding, a certain deviation from linearity is profoundly prominent once the fraction of feed size remaining in the top size interval falls below 0.1. It is evidently independent of ore characteristics like hardness and brittle nature, and is directly dependent on the particulate environment in the mill. The first order feed size disappearance equation for the normalized model as illustrated in Equation 4.2 provides the following expression:

$$m_1(\bar{E}) = m_1(0)\exp[-s_1^E\ \bar{E}] \qquad \ldots 4.2$$

The purpose of this expression is to predict the capacity for normalizability of the kinetics of breakage for the top size interval. Replacing $\bar{E}$ with t would give a normalized feed disappearance plot versus grind time, more like a least squares fit for the data obtained. For wet grinding, Kim [16] has provided detailed description of the normalizability phenomena with various operating variables like mill speed, grinding media load, particle load, percent solids, and slurry filling for a 10-inch mill. Feed size selection function S_1 values are 0.465, 0.877, and 0.538 minute $^{-1}$ for limestone, quartzite, and gold ore, respectively. As is known, preferential breakage is an inherent characteristic for wet grinding systems.

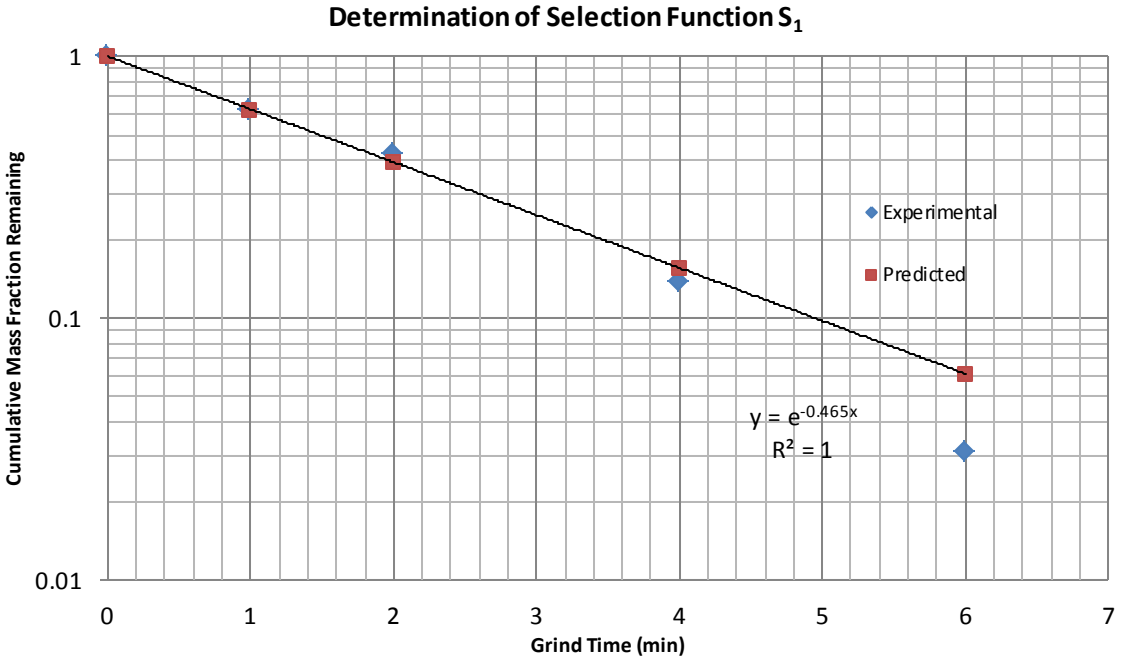

Figure 4.4.Feed Size disappearance plot for Limestone Ore depicting experimental and normalized predictions, showing wet grinding nonlinearity.

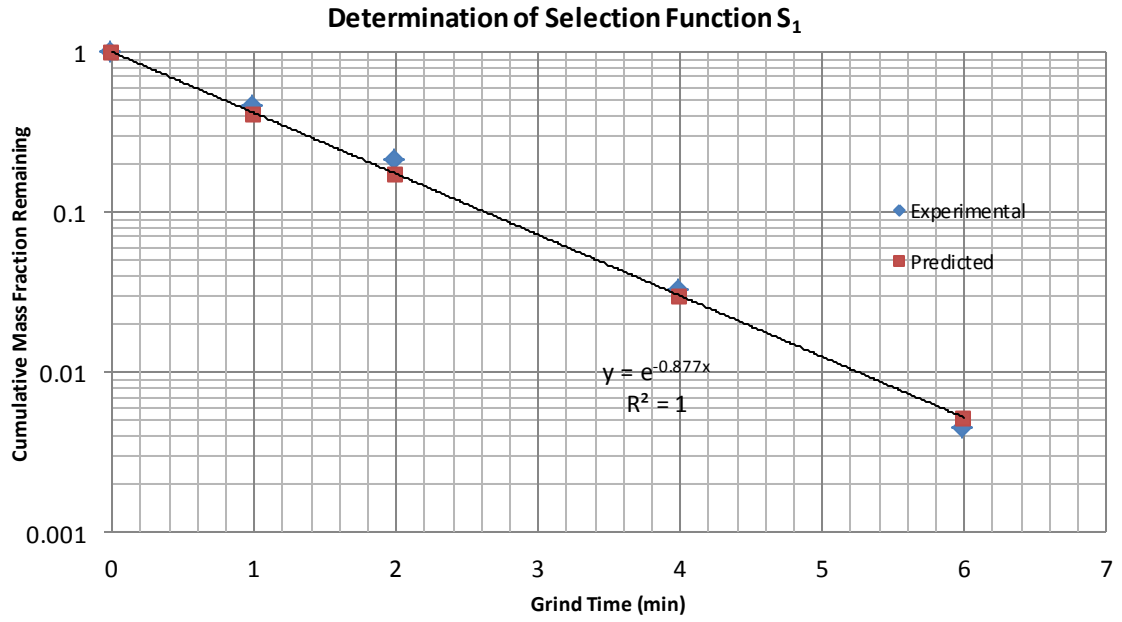

Figure 4.5.Feed Size disappearance plot for Quartzite Ore depicting experimental and normalized predictions, showing wet grinding nonlinearity.

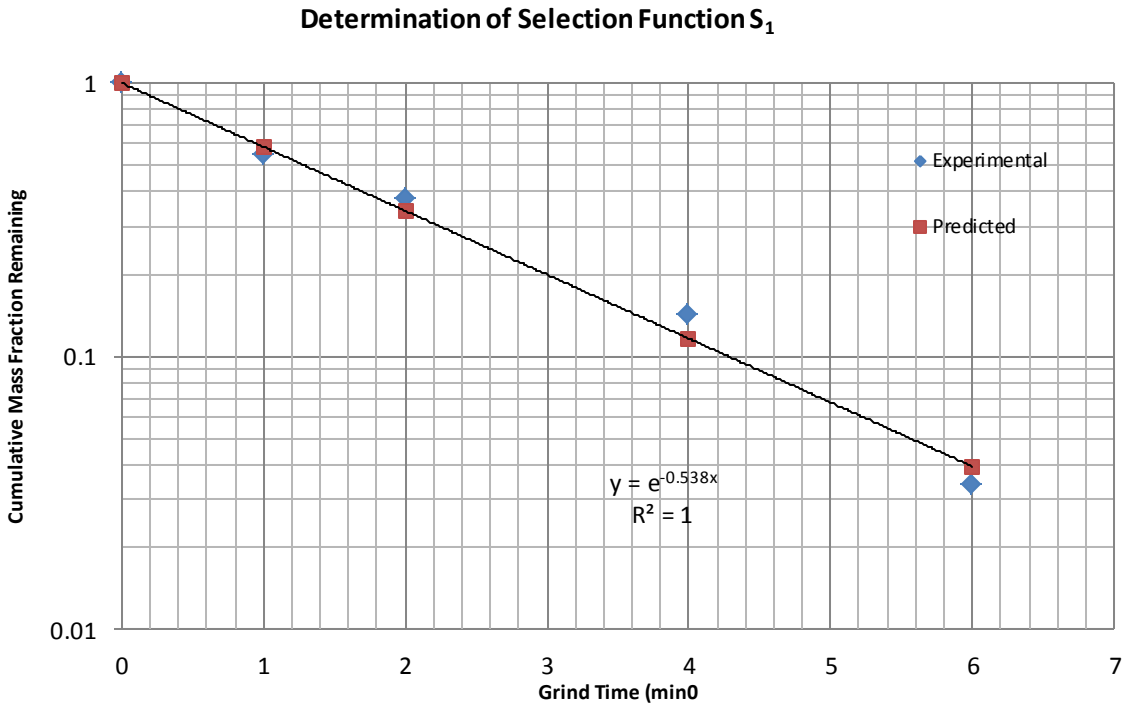

Figure 4.6.Feed Size disappearance plot for Gold Ore depicting experimental and normalized predictions, showing wet grinding nonlinearity.

Preferential breakage defines the probability of coarser particles in a particle population being subjected to breakage much more readily than the finer particles. This results in higher rates of breakage for coarser particles in the population present in the upper size intervals, as compared to the finer particles in the lower intervals. s_1^E values for wet grinding of limestone, quartzite, and gold ore are 0.975 $(kWh/ton)^{-1}$, 1.943 $(kWh/ton)^{-1}$, and 1.263 $(kWh/ton)^{-1}$, respectively. It is interesting to note that a brittle material like quartzite has the highest s_1^E of all the three ores.

Feed size cumulative breakage functions B_{i1} are computed from the relationship as mentioned [11] :

$$B_{i1} = \frac{F_i}{S_1} \qquad \ldots 4.3$$

S_1 is the feed size selection function determined directly from a feed disappearance plot versus time, whereas F_i is the initial slope of the cumulative fines production plot for material finer than stated size X_i. It is also known as the Zero Order Rate Production Constant. Figures 4.7, 4.8, and 4.9 provide plots for the same for limestone, quartzite, and gold ore, respectively.

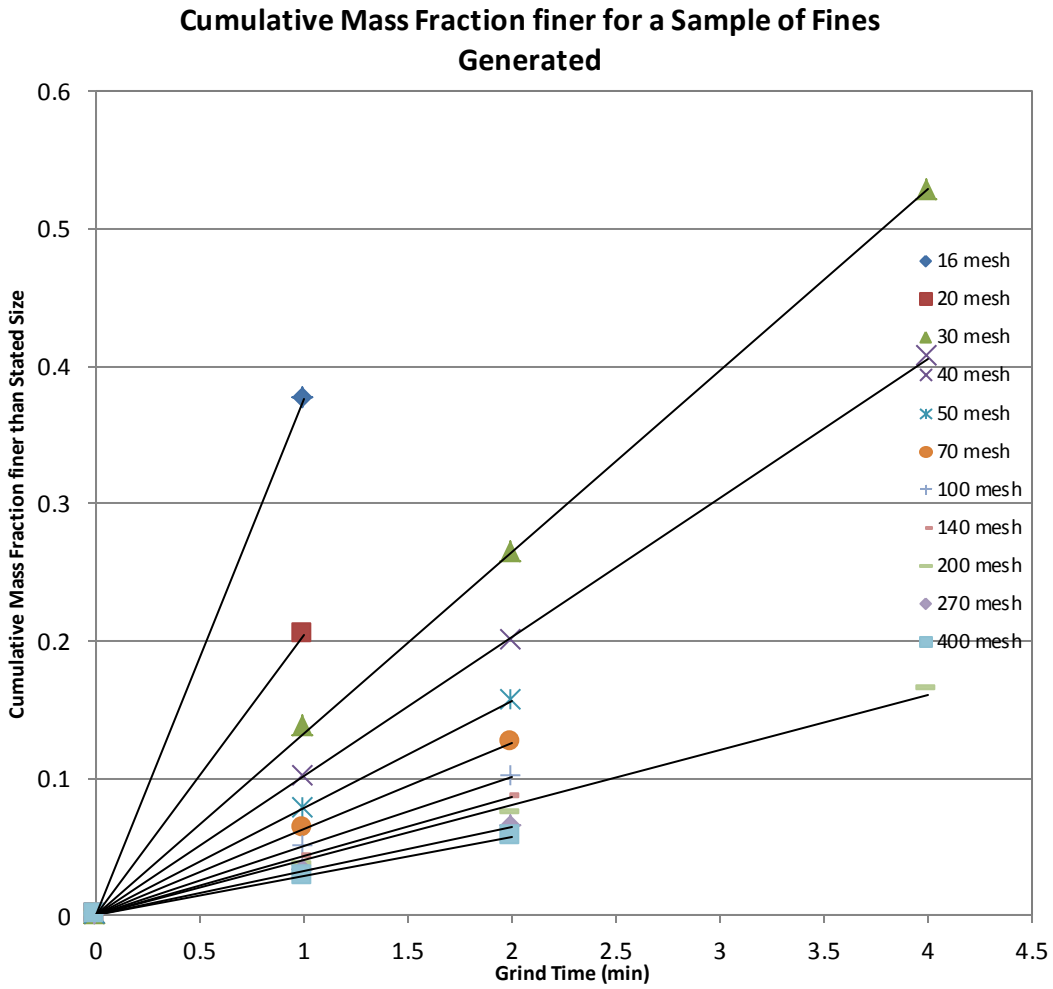

Figure 4.7.Sample of fines production plots over the entire product particle population for limestone ore.

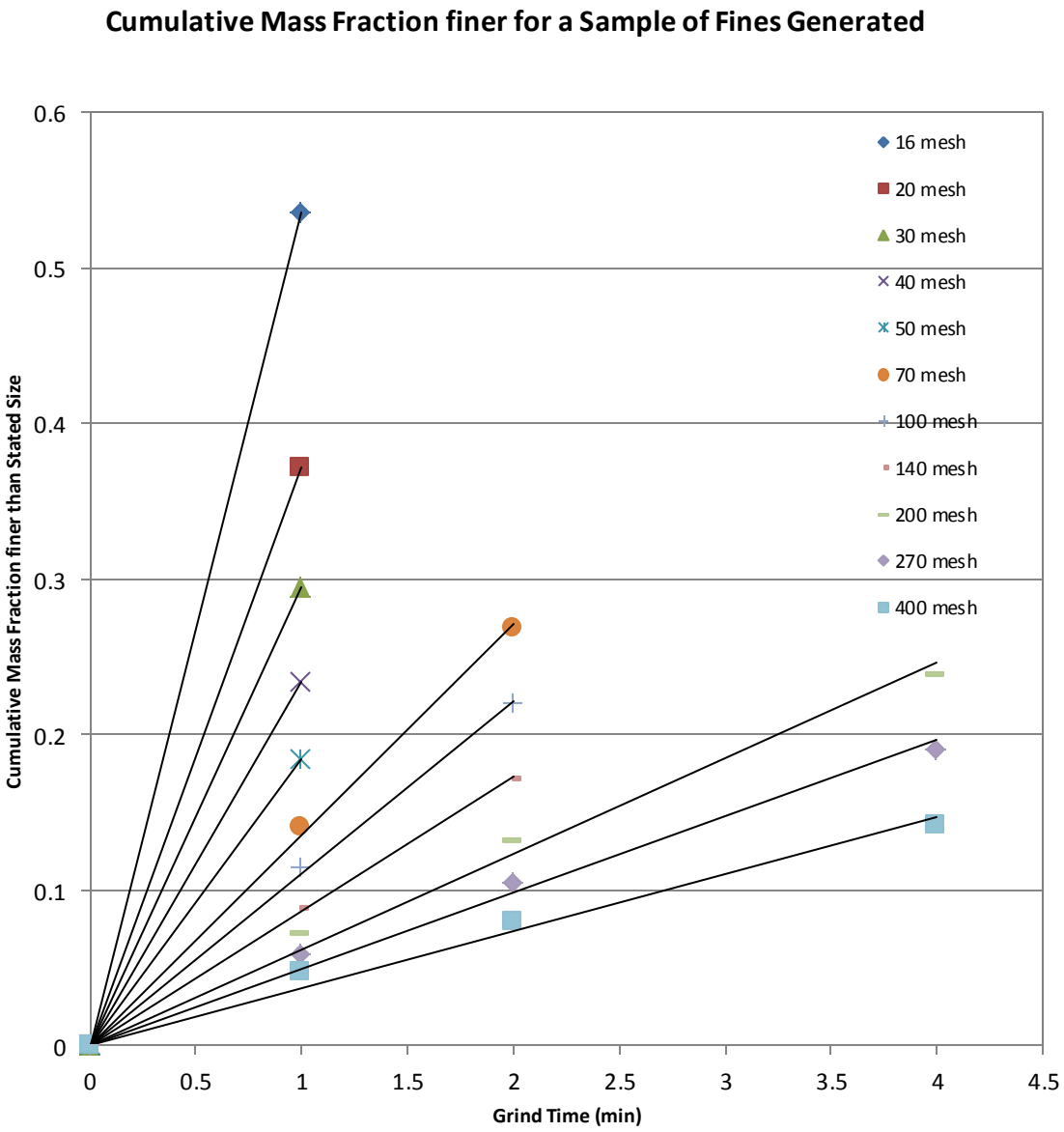

Figure 4.8.Sample of fines production plots over the entire product particle population for Quartzite ore.

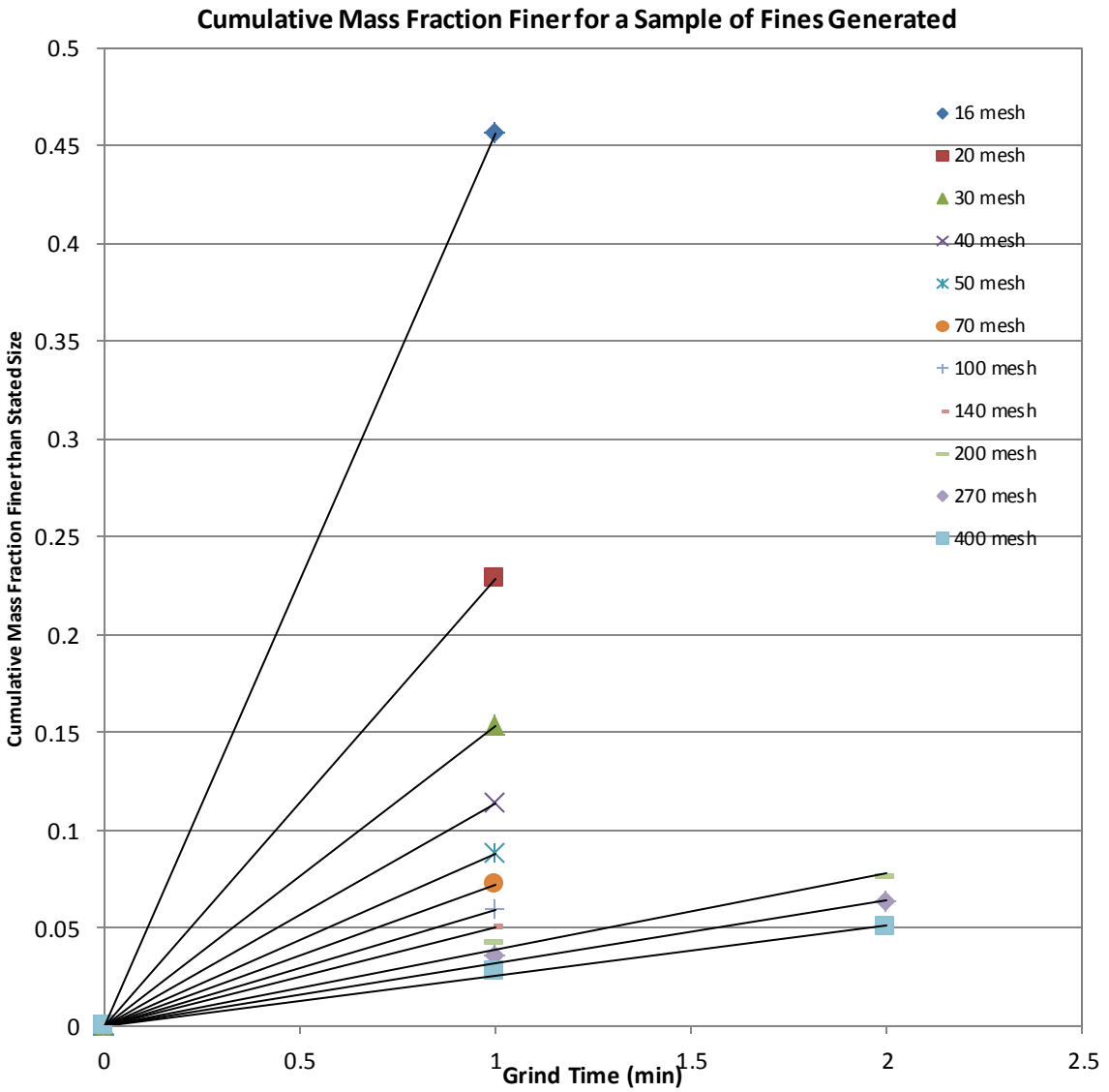

Figure 4.9.Sample of fines production plots over the entire product particle population for Gold ore.

Figures 4.10, 4.11, and 4.12 provide an insight into the distribution modulus α with plots of zero order rate production constant versus particle size for limestone, quartzite, and gold ore, respectively. α = 0.5426, 0.7539, and 0.6226 for limestone, quartzite, and gold ore, respectively. These parameters provide us with the initial estimates required for estimation of 1st and 2nd order breakage rates using ESTIMILL.

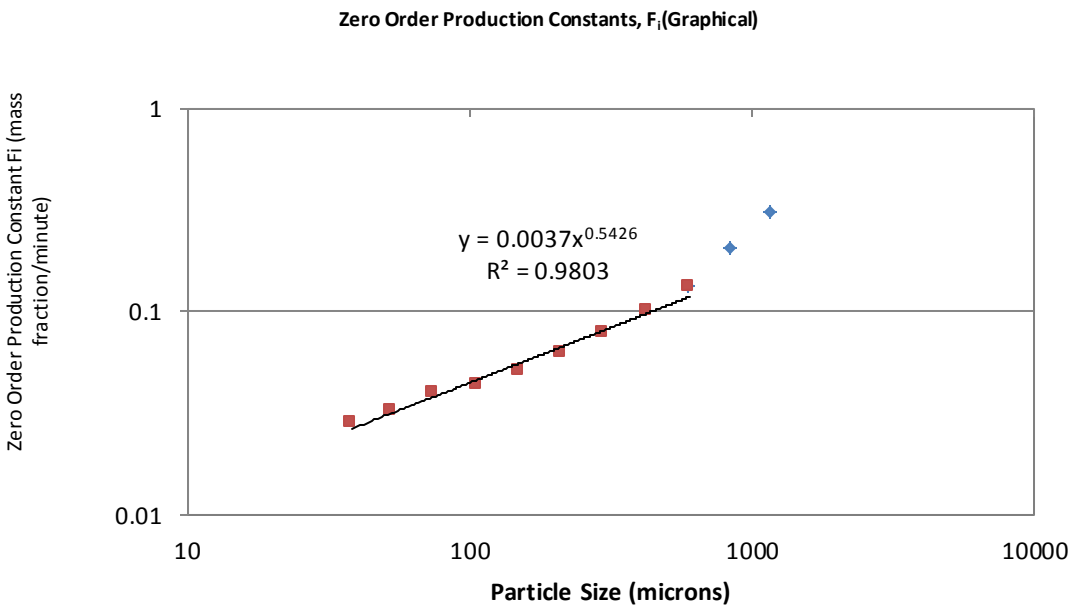

Figure 4.10.Plot of Zero Order Production Rate Constant versus Size X_i for limestone ore.

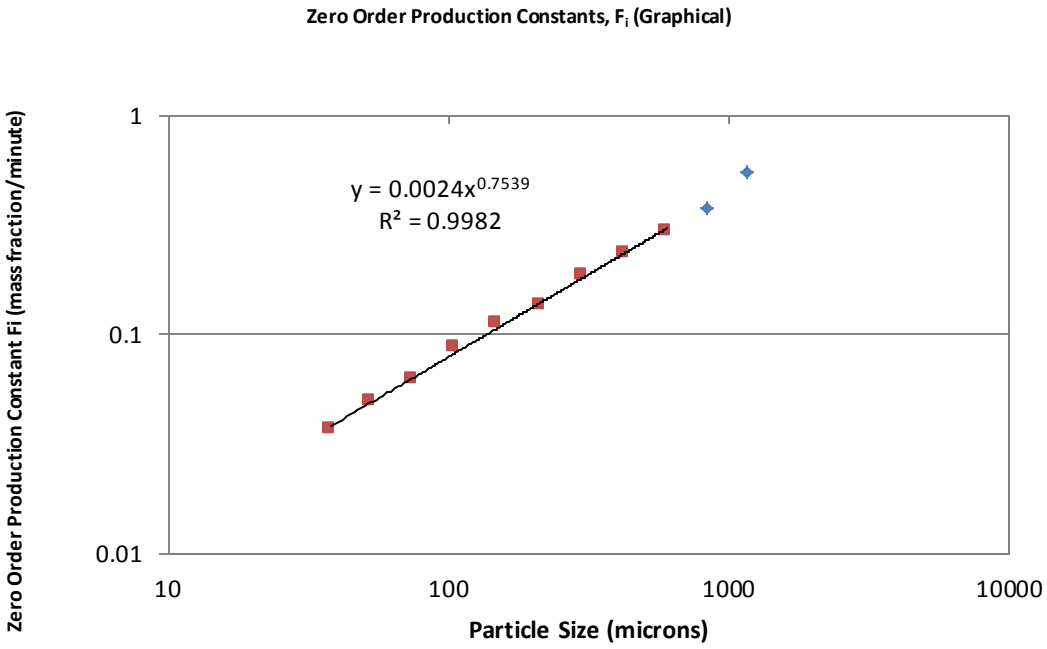

Figure 4.11.Plot of Zero Order Production Rate Constant versus Size X_i for quartzite ore.

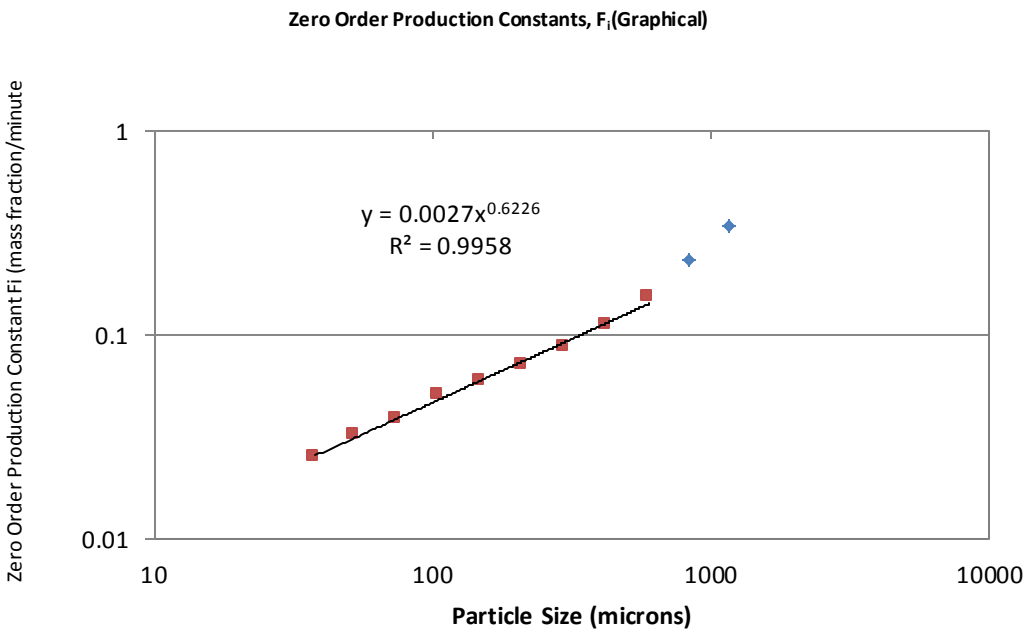

Figure 4.12.Plot of Zero Order Production Rate Constant versus Size X_i for Gold ore.

The functional form of the breakage function helps reduce the parameter set require for estimation, and also contributes to correlating the breakage rates and cumulative breakage function with the size intervals in the product particle population. The functional form does not have any explicit dependence on grind time or particle size distribution, and therefore, they are assumed to hold good for incremental durations of grind times, during which the breakage rates are presumed to be constant and uniform. This is the underlying rationale for predictive simulation and scale-up of larger mills, factoring in the concept of similar fineness of grind. The functional form of the cumulative breakage function is given as:

$$B_{ij} = \alpha_1 \left(\frac{x_i}{x_{j+1}}\right)^{\alpha_2} + (1-\alpha_1)\left(\frac{x_i}{x_{j+1}}\right)^{\alpha_3} \qquad \ldots 4.4$$

Equation 4.6 is a weighted sum of two individual normalizable Gaudin-Schumann distributions that yields a linear breakage function on a log-log plot, but shifts from linearity on approaching the coarser size fractions, that is, ($\frac{x_i}{x_{j+1}}$ → 1). Such a kind of functional form of the cumulative breakage function helps in reducing numerous parameters and helps in predictive simulation using ESTIMILL. For simulation using ESTIMILL, functional forms of parameter sets involve a set of 5 parameters for 2nd order estimation and predictive simulation. These are α_1, α_2, α_3, S_1 ξ_1, and ξ_2.

Mono-size wet grinding experiments help in determining top size selection and breakage functions, which, in turn, can be used to deduce initial estimates of α_1, α_2, and α_3. This is done by plotting a log-log graph of cumulative breakage values for each size fraction versus particle size. For this research, the initial estimates of these parameters coincided with the ones force-fitted using functional forms of the cumulative breakage functions, and thus, predictive simulation was performed based on estimation of selection functions only, keeping the breakage parameters constant. This was done to prevent force-fitting of selection and breakage functions simultaneously. Instead, this gave a veritable approach to predictive simulation, the results for which can be seen in the simulated plots. For fine size fractions, $\frac{x_i}{x_{j+1}}$ → 0, as $\alpha_3 > \alpha_2$. This causes Equation 4.4 to reduce to:

$$B_{ij} = \alpha_1 \left(\frac{x_i}{x_{j+1}} \right)^{\alpha_2} \qquad \text{... 4.5}$$

which gives the equation of a straight line with slope α_2 and an intercept of α_1 at ($\frac{x_i}{x_{j+1}}$ → 1). After determination of α_1 and α_2, α_3 can be determined by a log-log plot of the rearranged form of Equation 4.6. this equation is given by :

$$\frac{B_{ij} - \alpha_1 \left(x_i / x_{j+1}\right)^{\alpha_2}}{1 - \alpha_1} = \left(\frac{x_i}{x_{j+1}}\right)^{\alpha_3} \qquad \ldots 4.6$$

This is usually referred to as the slope of the coarser size fractions in the particle population ($\frac{x_i}{x_{j+1}} \rightarrow 1$). For our predictive simulation considerations, experimentally derived values were used for the functional form of selection and breakage parameters, as illustrated in Table 4.1.

Figures 4.13, 4.14, and 4.15 provide a comparison of experimentally derived cumulative breakage functions and the functional forms of these functions for limestone, quartzite, and gold ore, respectively. Table 4.1 provides initial estimates for the breakage parameters used for estimating 1st order and 2nd order breakage rates. Initial estimates of α_1, α_2, $\alpha 3$, S_1, and S_1^E have been derived from wet grinding experiments performed on the batch ball mill.

Table 4.1.Initial Estimates of Experimental Breakage Parameters

Initial Estimates of Experimental Breakage Parameters					
Ore	$\boldsymbol{\alpha_1}$	$\boldsymbol{\alpha_2}$	$\boldsymbol{\alpha_3}$	$\boldsymbol{S_1}$	$\boldsymbol{S_1^E}$
Limestone	0.459	0.5426	2.146	0.465	0.975
Quartzite	0.7536	0.7539	5.1355	0.877	1.9427
Gold Ore	0.512	0.6226	2.3874	0.538	1.2623

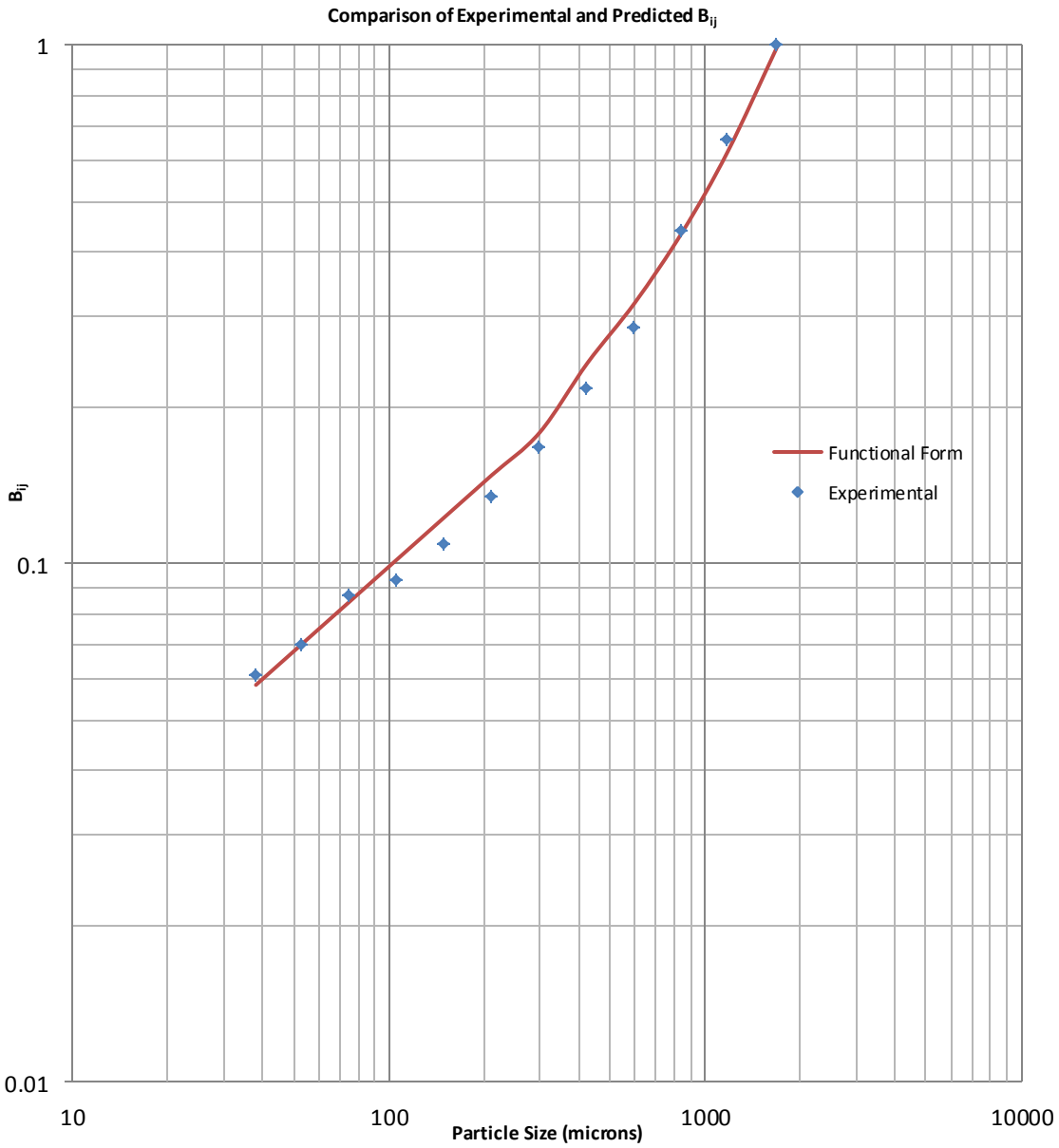

Figure 4.13.Comparison of experimentally derived cumulative breakage function and its functional form for limestone.

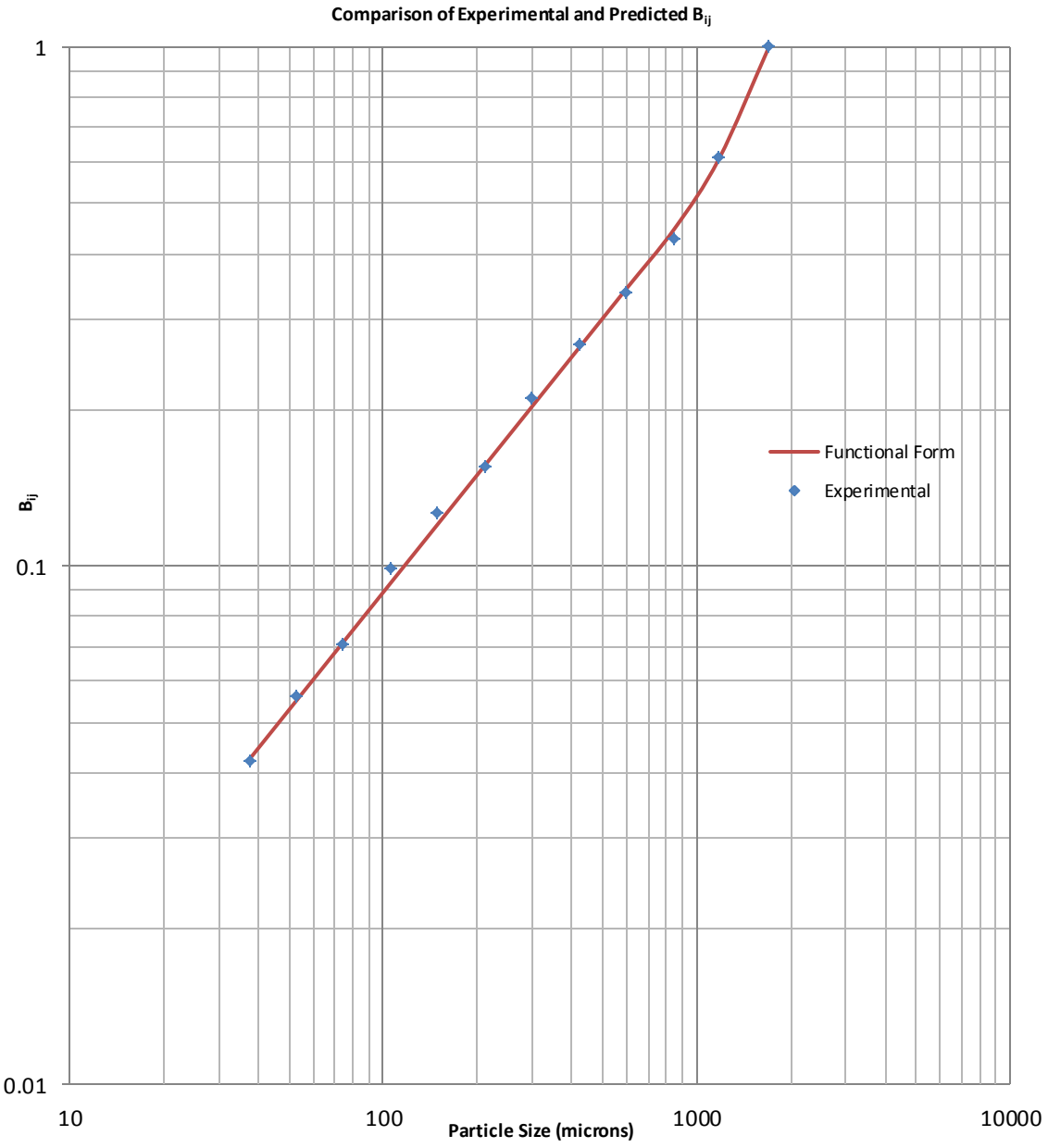

Figure 4.14.Comparison of experimentally derived cumulative breakage function and its functional form for quartzite.

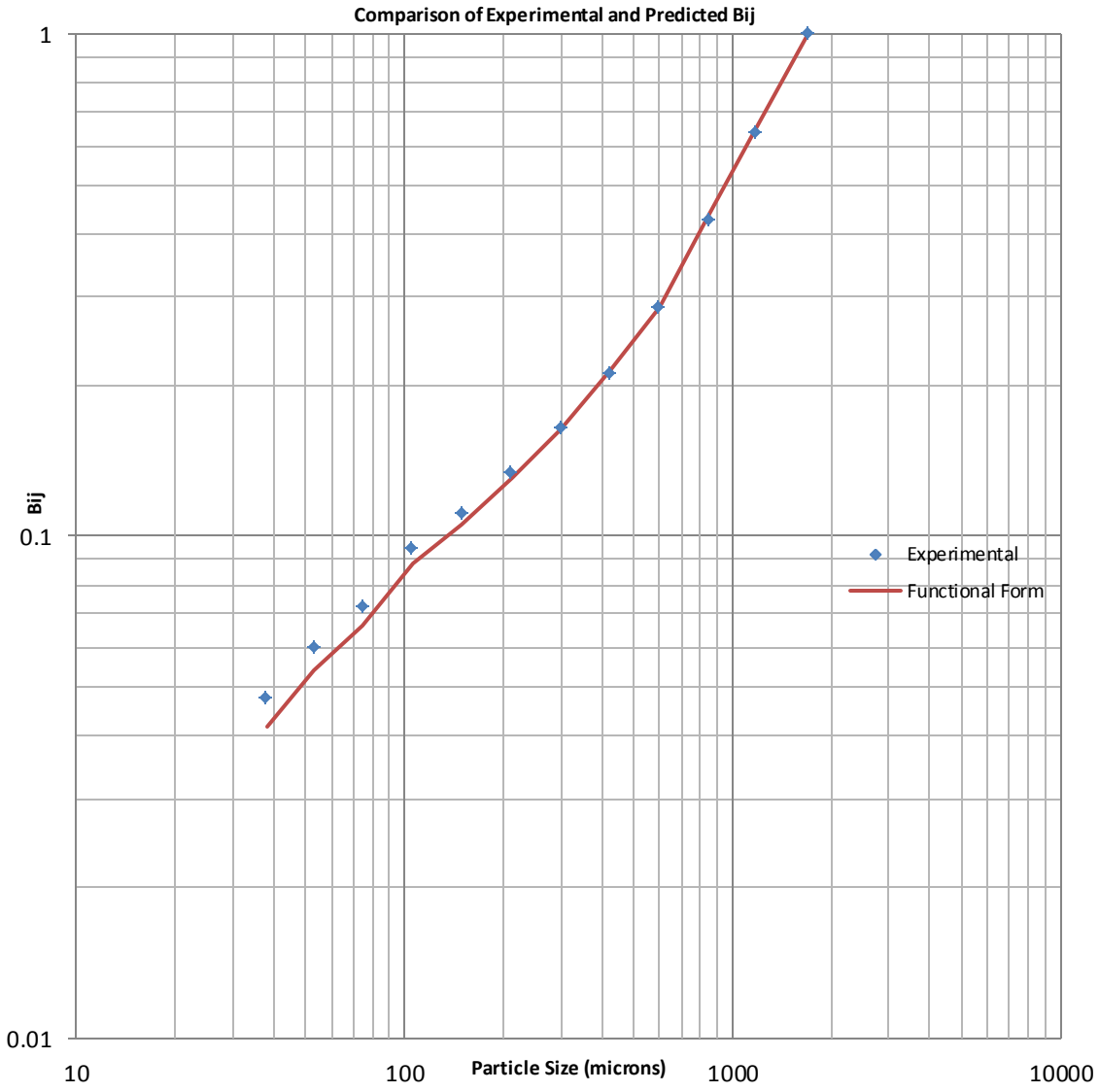

Figure 4.15.Comparison of experimentally derived cumulative breakage function and its functional form for gold ore.

Figures 4.13, 4.14, and 4.15 illustrate near-perfect compatibility of experimental cumulative breakage functions with respect to their functional forms. For predictive simulation reasons, experimental values of the breakage parameters were used to prevent force-fitting, but as will be observed in the following graphs, they give stupendous results. It is a well-known fact that all breakage parameters for the finer size fractions are

also required along with those for the coarser size fractions for effective simulation. Batch tests are the simplest way to determine parameters for breakage kinetics in an experimental fashion. Also, there is an added benefit of easier quantitative interpretation of results, as the complexities involving residence time distribution is negated completely [33]. An indirect approach, as formulated and mentioned earlier [40], involves a continuous time variable and a discretized size variable. Parameter estimation done using this procedure minimizes deviations obtained from predictive models and experimentally observed product size distributions.

Feed size selection function S_1 is evaluated from Equation 4.1. In addition to estimating feed size selection functions, the remaining selection functions are determined using the following expression:

$$S_i = S_1 \left(\frac{\sqrt{x_i x_{i+1}}}{\sqrt{x_1 x_2}} \right)^{\alpha} \qquad \ldots 4.7$$

α is the distribution modulus of the cumulative breakage function. The slope of the fine size fractions on a log-log plot of the cumulative breakage function versus the particle size provides the value for the distribution modulus. α = 0.5426, 0.7539, and 0.6226 for limestone, quartzite, and gold ore, respectively.

The specific breakage rate function is given as:

$$S_i^E = S_1^E \left(\frac{\sqrt{x_i x_{i+1}}}{\sqrt{x_1 x_2}} \right)^{\alpha} \qquad \ldots 4.8$$

The results derived are in strong consistency with those obtained from Equation 2.10. Estimation of breakage function is done on the fundamental and preliminary assumption that size-discretized breakage functions are normalizable, given by the expression [11]:

$$B_{ij} = B_{i-j+1,1} \quad \ldots 4.9$$

B_{ij} is obtained from a modified and rearranged form of Equation 4.3 given as:

$$B_{ij} S_j = F_i \quad \ldots 4.10$$

with S_j being derived from Equation 4.9, and F_i being the initial slope of the fines generation plot illustrated in Figures 4.7, 4.8, and 4.9. Parameter improvement for predictive simulation involves determination of parameters experimentally and comparison with values derived from the functional forms of these expressions. Equations 4.4 and 4.6 give a detailed overview of such functional forms for selection functions and cumulative breakage functions, respectively.

4.2. Linearized PBM Estimates of Breakage Rates

As mentioned before, wet grinding is inherently nonlinear in nature. This has a significant impact on the spatial distribution of material in the mill during wet grinding operations. In wet grinding systems, the fine particles tend to get suspended in the water whilst the coarse particles are apparently settled in the ball mass, thereby providing reason for an increased probability in the breakage of the coarse particles [12, 16]. This phenomenon, as mentioned before, is termed as "preferential breakage." With an increase in grind time, the amount of fines produced during the milling process increases, thereby leading to greater suspension of fine particles in the slurry. This leads to an increased rate of breakage for the coarser particles with a simultaneous decrease in the breakage of finer particles. Therefore, this strongly indicates that the selection function and the specific selection function are vehemently dependent on the size consist or particle size distribution in the mill. Figures 4.16 through 4.27 and Tables 4.2 through 4.13 depict this

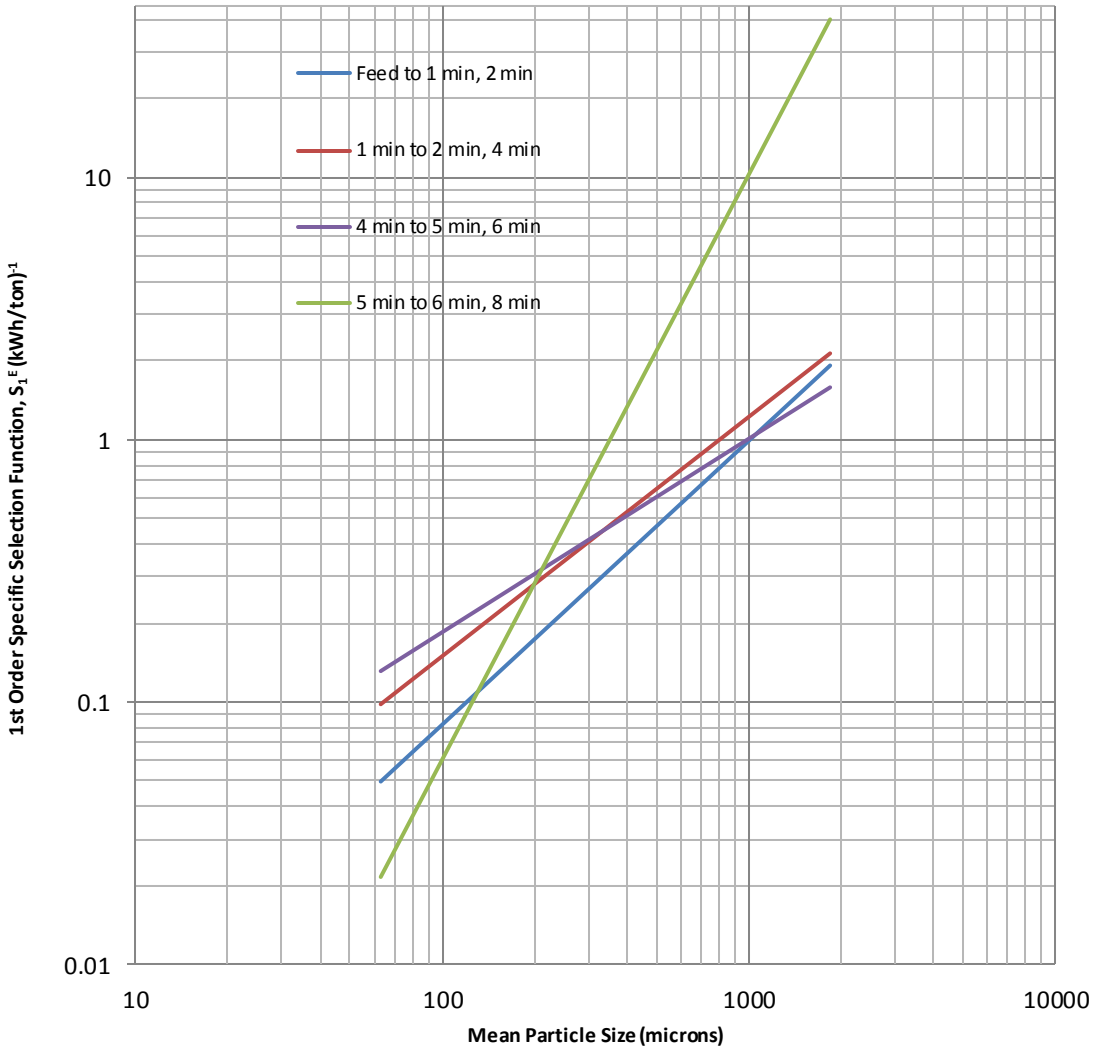

Figure 4.16.Dependence of specific selection functions on the particle size distribution in the ball mill, for -10 mesh feed (Limestone) in wet grinding at 65% solids and 100% slurry filling, showing pronounced nonlinearity.

Table 4.2.Converged Values of S_1^E and ζ_1 for Figure 4.16

Increment	S_1^E (kWh/ton)$^{-1}$	ζ_1
feed to 1,2 min	1.9191	1.0825
1 to 2,4 min	2.1348	0.9127
4 to 5,6 min	1.5836	0.738
5 to 6,8 min	40.0850	2.2305

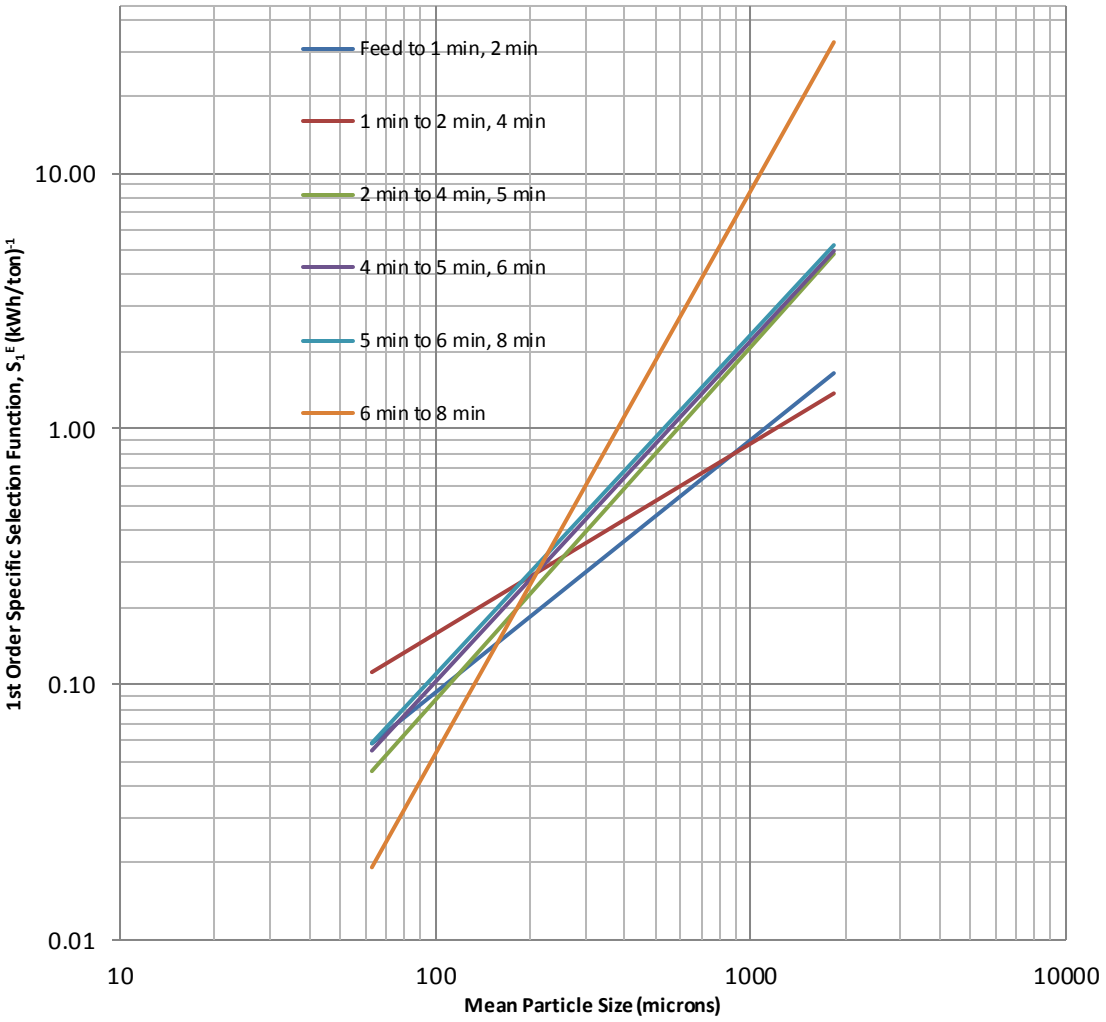

Figure 4.17.Dependence of specific selection functions on the particle size distribution in the ball mill, for -10 mesh feed (Limestone) in wet grinding at 72% solids and 100% slurry filling, showing pronounced nonlinearity.

Table 4.3.Converged Values of S_1^E and ζ_1 for Figure 4.17

Increment	S_1^E (kWh/ton)$^{-1}$	ζ_1
feed to 1,2 min	1.6501	0.9887
1 to 2,4 min	1.3754	0.7442
2 to 4,5 min	4.8343	1.3808
4 to 5,6 min	4.9643	1.3341
5 to 6,8 min	5.231	1.329
6 to 8 min	32.5736	2.2027

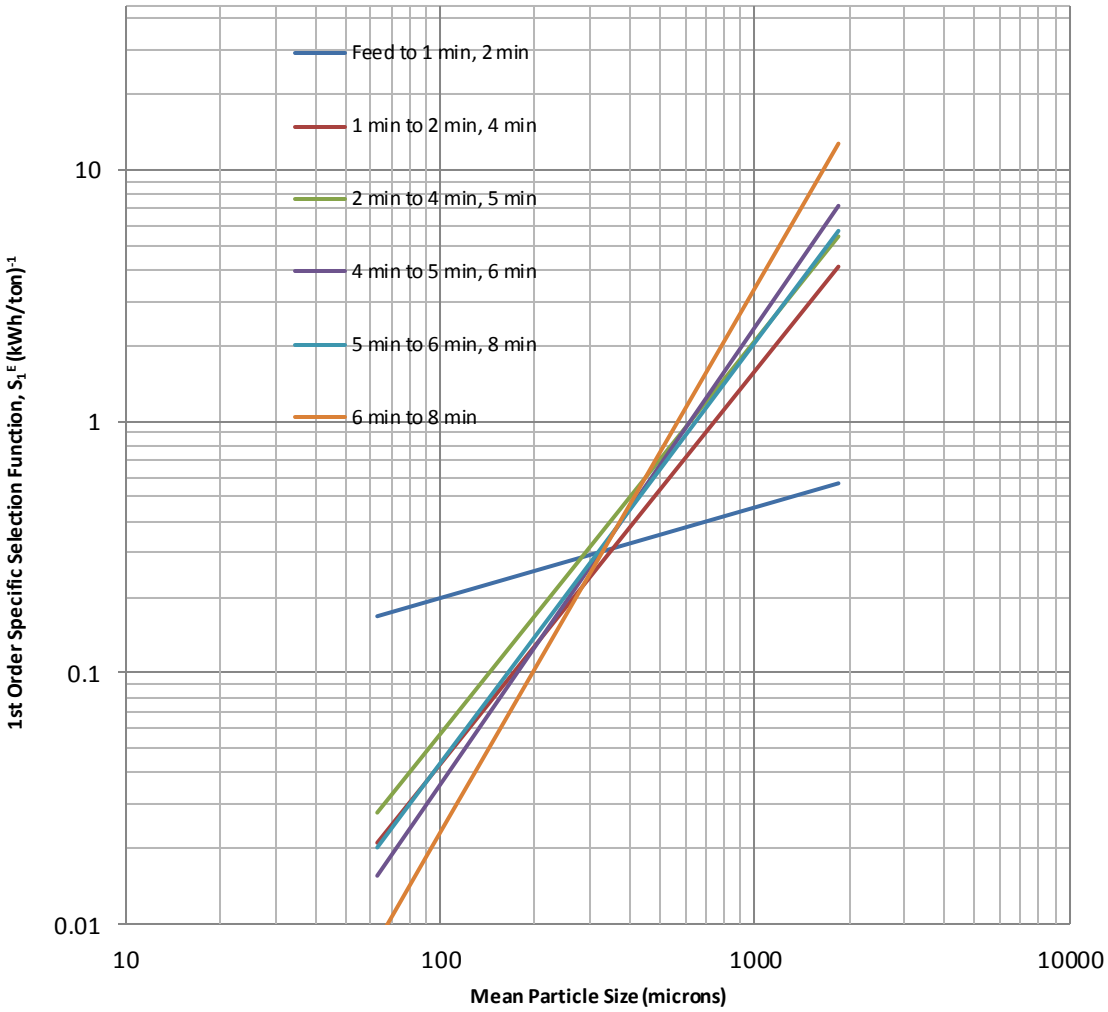

Figure 4.18.Dependence of specific selection functions on the particle size distribution in the ball mill, for -10 mesh feed (Limestone) in wet grinding at 65% solids and 260% slurry filling, showing pronounced nonlinearity.

Table 4.4.Converged Values of S_1^E and ζ_1 for Figure 4.18

Increment	S_1^E (kWh/ton)$^{-1}$	ζ_1
feed to 1,2 min	0.5665	0.3604
1 to 2,4 min	4.1183	1.5628
2 to 4,5 min	5.4312	1.563
4 to 5,6 min	7.1849	1.8175
5 to 6,8 min	5.7133	1.6721
6 to 8 min	12.6964	2.1635

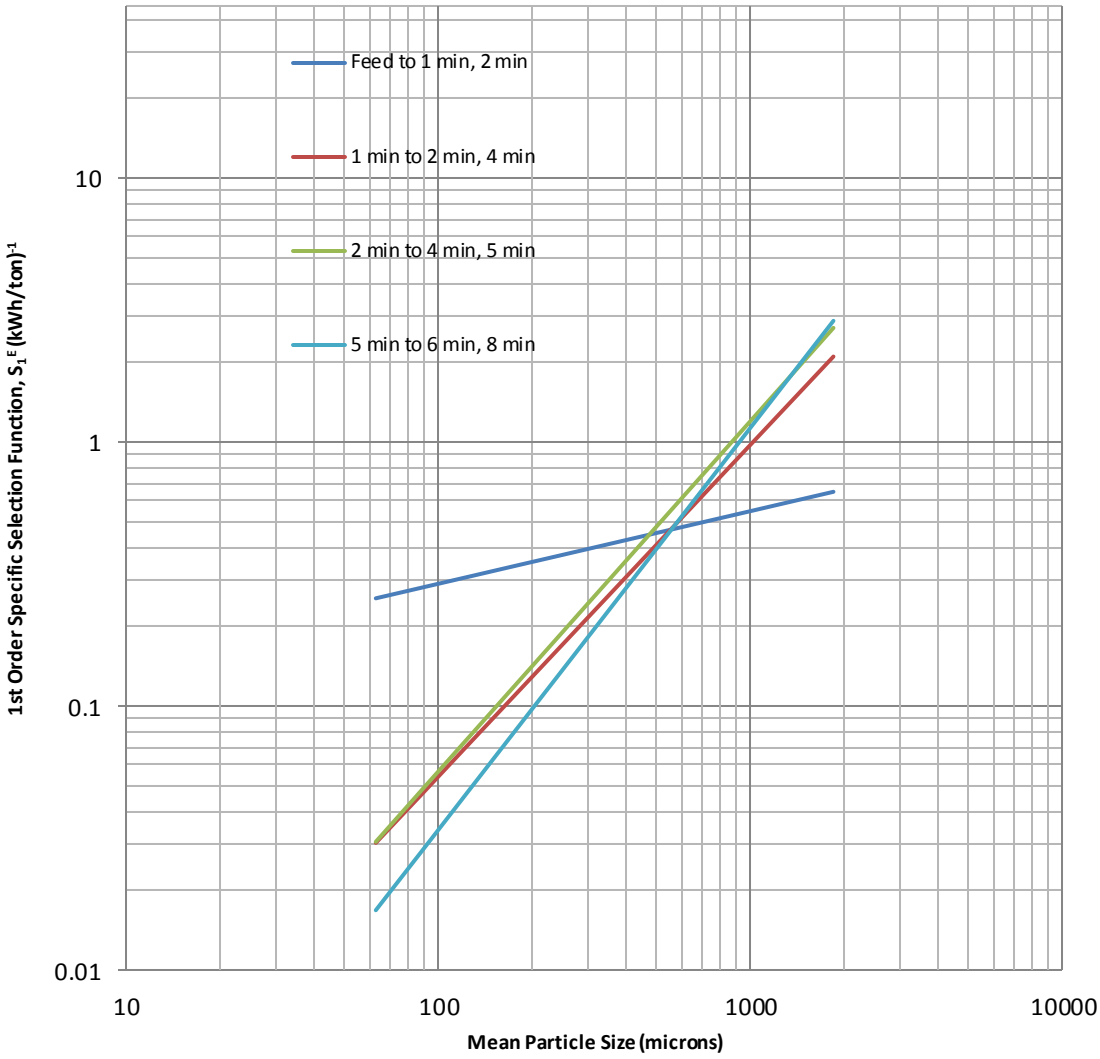

Figure 4.19.Dependence of specific selection functions on the particle size distribution in the ball mill, for -10 mesh feed (Limestone) in wet grinding at 72% solids and 260% slurry filling, showing pronounced nonlinearity.

Table 4.5.Converged Values of S_1^E and ζ_1 for Figure 4.19

Increment	S_1^E (kWh/ton)$^{-1}$	ζ_1
feed to 1,2 min	0.6494	0.2752
1 to 2,4 min	2.1124	1.2567
2 to 4,5 min	2.7122	1.3273
5 to 6,8 min	2.8847	1.5233

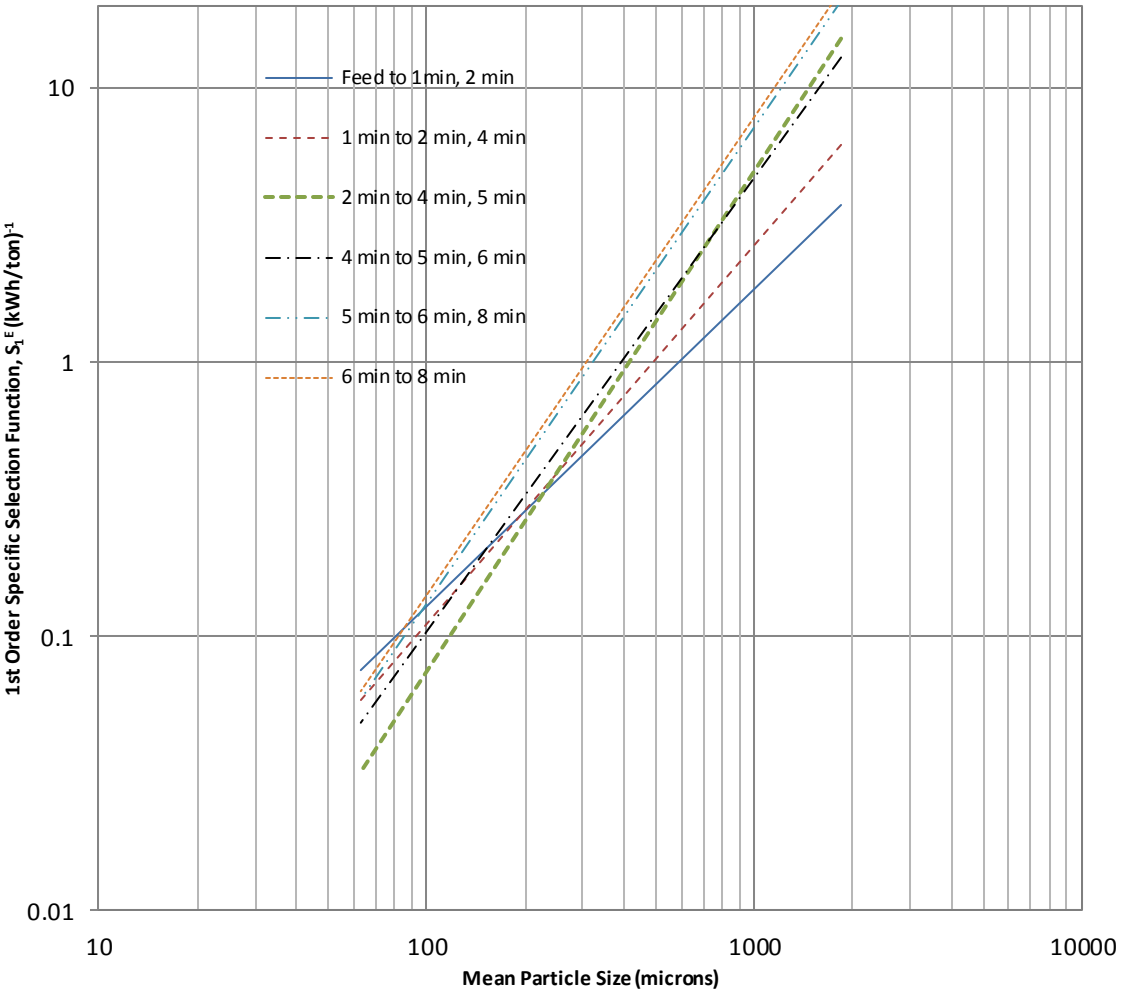

Figure 4.20.Dependence of specific selection functions on the particle size distribution in the ball mill, for -10 mesh feed (Quartzite) in wet grinding at 65% solids and 100% slurry filling, showing pronounced nonlinearity.

Table 4.6.Converged Values of S_1^E and ζ_1 for Figure 4.20

Increment	S_1^E (kWh/ton)$^{-1}$	ζ_1
feed to 1,2 min	3.7412	1.1566
1 to 2,4 min	6.1979	1.3808
2 to 4,5 min	15.1216	1.8235
4 to 5,6 min	12.9076	1.6543
5 to 6,8 min	20.7259	1.7364
6 to 8 min	22.6734	1.7427

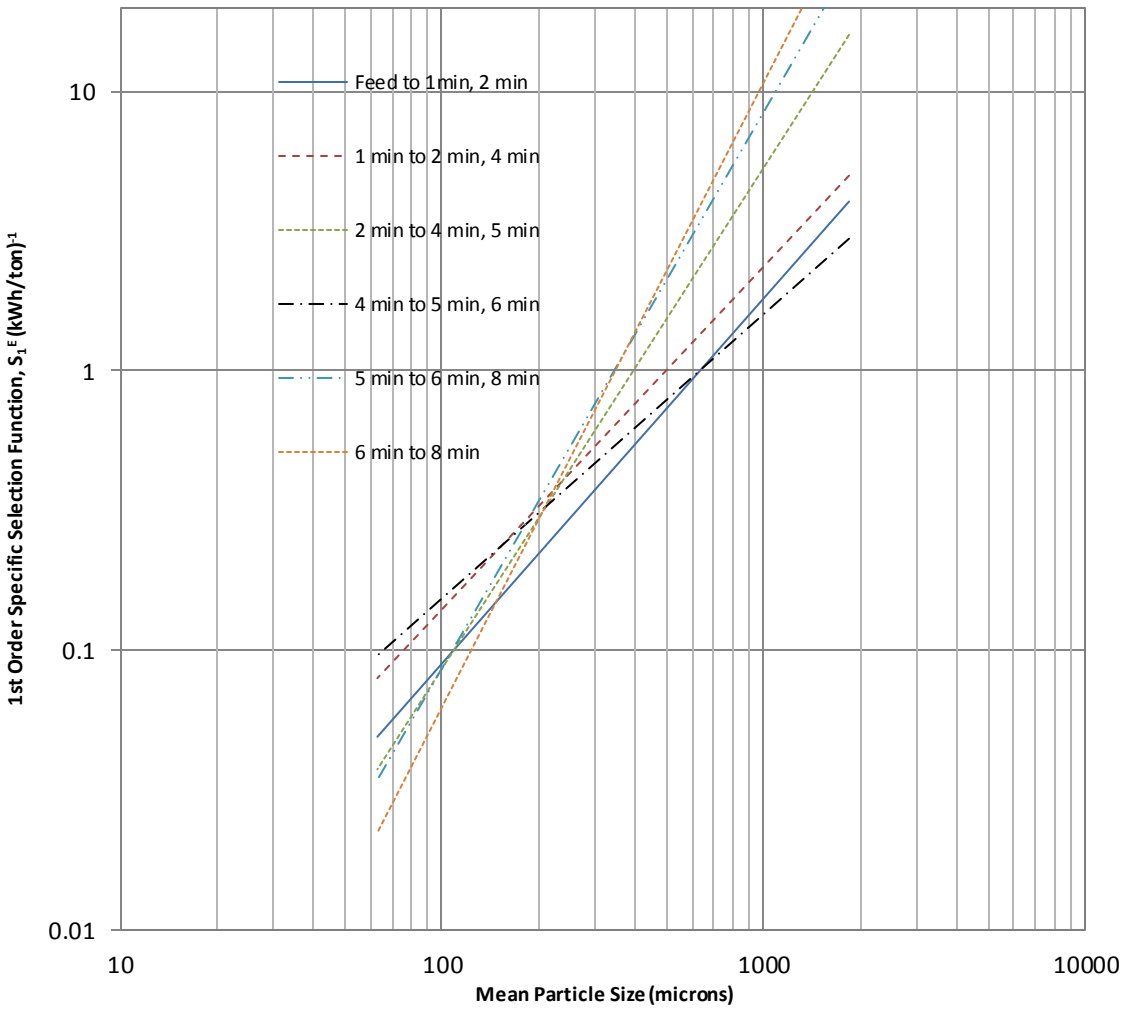

Figure 4.21.Dependence of specific selection functions on the particle size distribution in the ball mill, for -10 mesh feed (Quartzite) in wet grinding at 72% solids and 100% slurry filling, showing pronounced nonlinearity.

Table 4.7.Converged Values of S_1^E and ζ_1 for Figure 4.21

Increment	S_1^E (kWh/ton)$^{-1}$	ζ_1
feed to 1,2 min	4.0373	1.3074
1 to 2,4 min	4.9976	1.2275
2 to 4,5 min	15.9504	1.7936
4 to 5,6 min	2.9712	1.0174
5 to 6,8 min	28.4925	1.9917
6 to 8 min	42.2738	2.2368

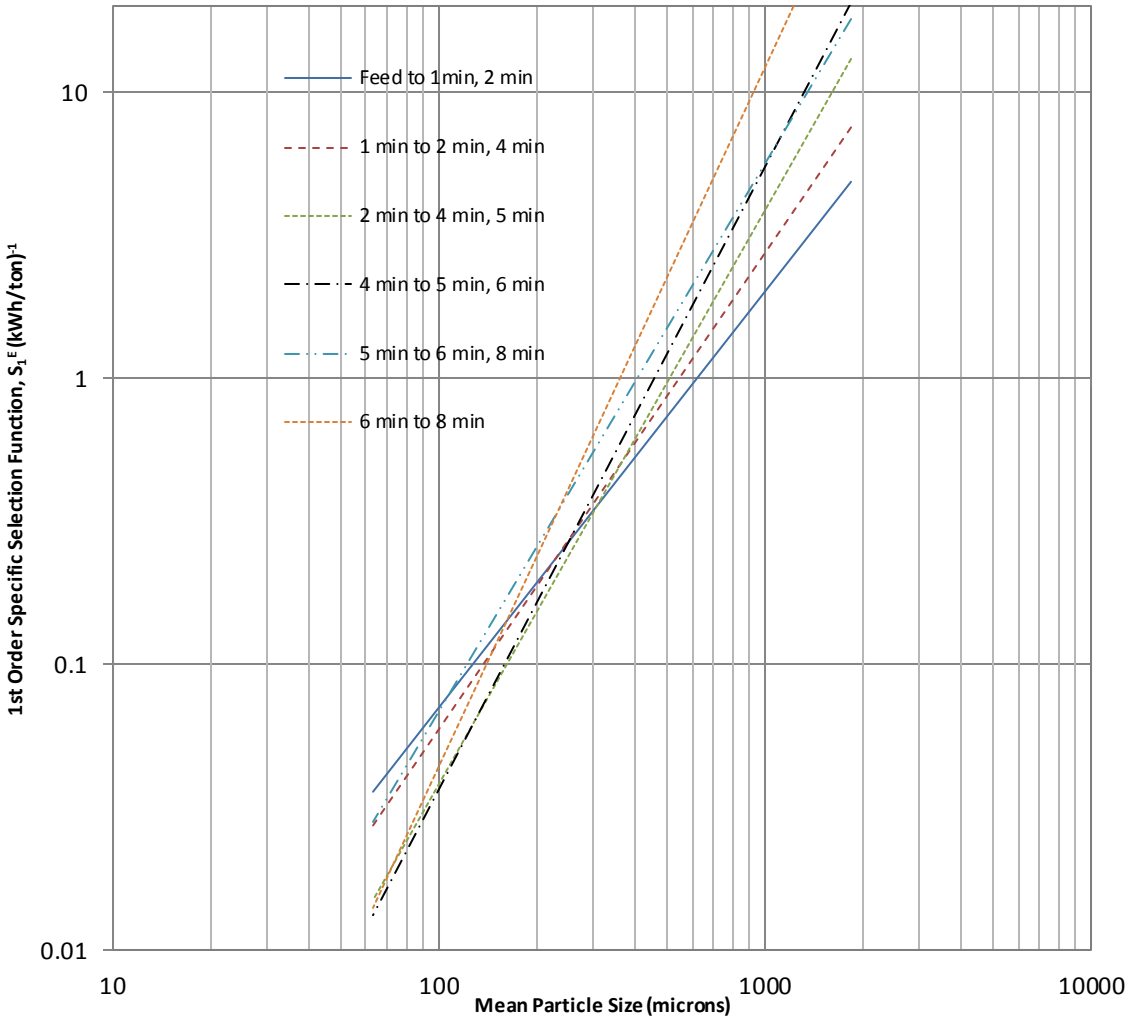

Figure 4.22.Dependence of specific selection functions on the particle size distribution in the ball mill, for -10 mesh feed (Quartzite) in wet grinding at 65% solids and 260% slurry filling, showing pronounced nonlinearity.

Table 4.8.Converged Values of S_1^E and ζ_1 for Figure 4.22

Increment	S_1^E (kWh/ton)$^{-1}$	ζ_1
feed to 1,2 min	4.8739	1.456
1 to 2,4 min	7.5572	1.6667
2 to 4,5 min	13.1192	2.0079
4 to 5,6 min	20.6522	2.179
5 to 6,8 min	18.0933	1.917
6 to 8 min	54.1475	2.4462

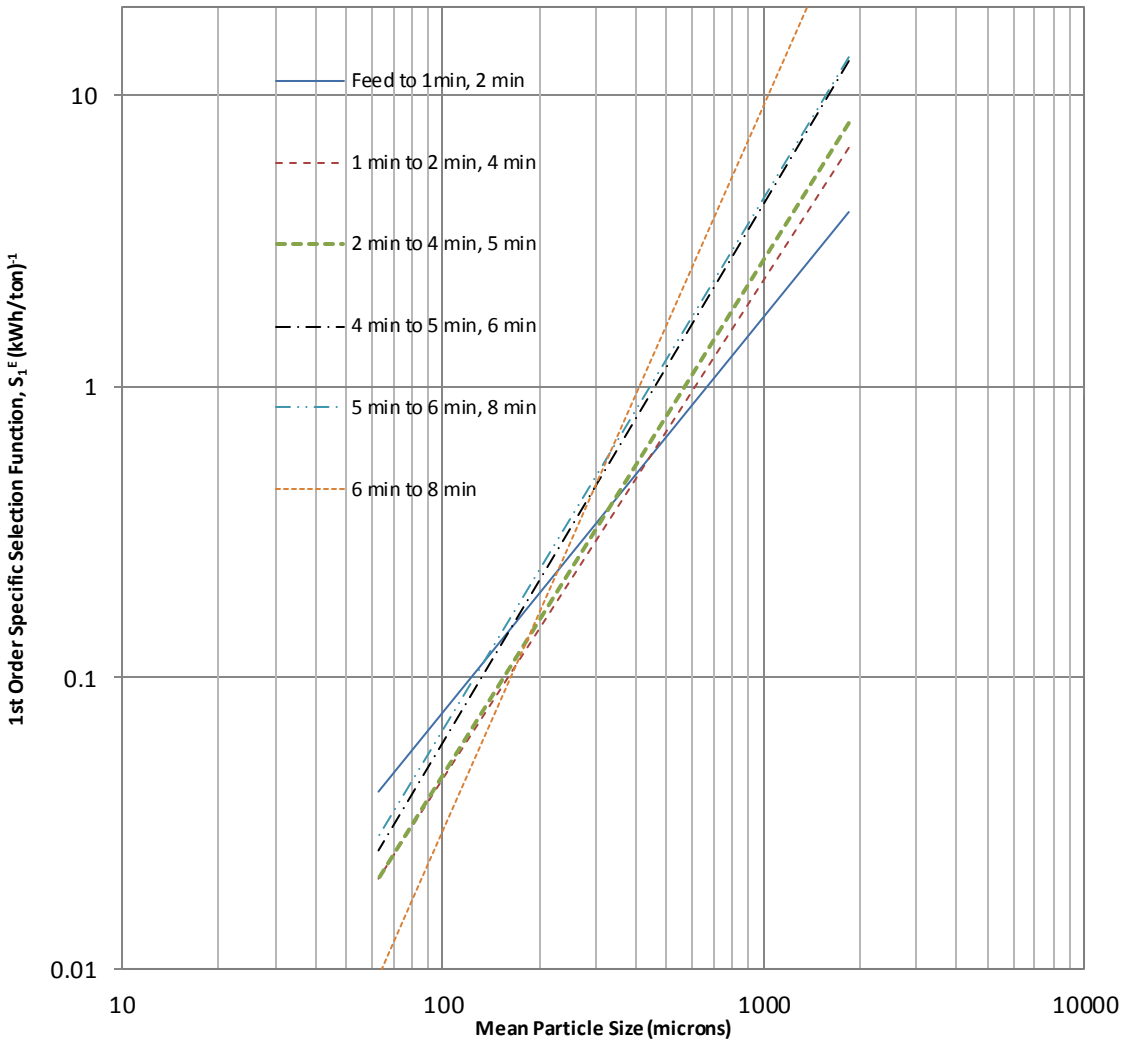

Figure 4.23.Dependence of specific selection functions on the particle size distribution in the ball mill, for -10 mesh feed (Quartzite) in wet grinding at 72% solids and 260% slurry filling, showing pronounced nonlinearity.

Table 4.9.Converged Values of S_1^E and ζ_1 for Figure 4.23

Increment	S_1^E (kWh/ton)$^{-1}$	ζ_1
feed to 1,2 min	3.9682	1.3574
1 to 2,4 min	6.5942	1.7121
2 to 4,5 min	8.0165	1.7694
4 to 5,6 min	13.0903	1.849
5 to 6,8 min	13.5009	1.8254
6 to 8 min	42.1548	2.4896

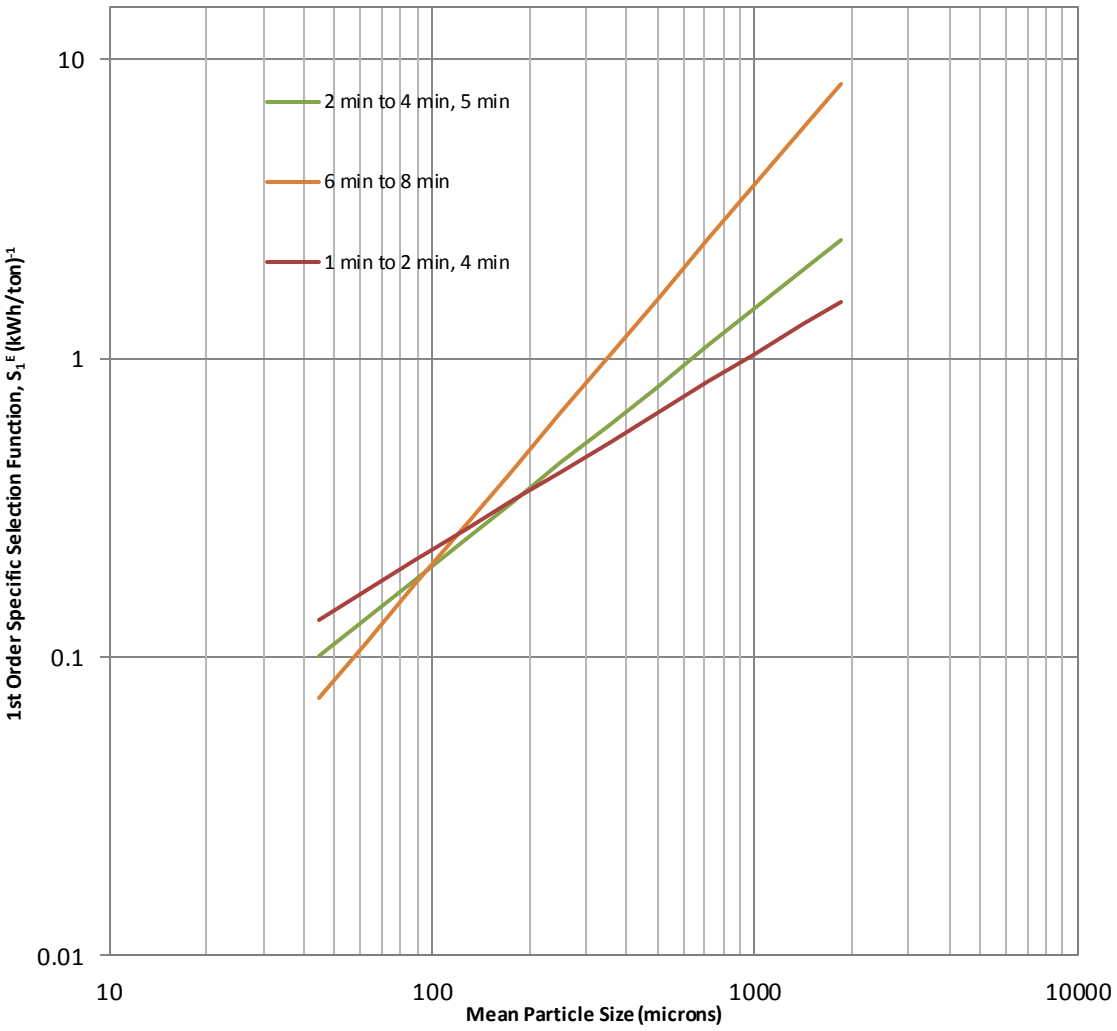

Figure 4.24.Dependence of specific selection functions on the particle size distribution in the ball mill, for -10 mesh feed (Gold Ore) in wet grinding at 65% solids and 100% slurry filling, showing pronounced nonlinearity.

Table 4.10.Converged Values of S_1^E and ζ_1 for Figure 4.24

Increment	S_1^E (kWh/ton)$^{-1}$	ζ_1
1 to 2,4 min	1.5566	0.6596
2 to 4,5 min	2.4945	0.8638
6 to 8 min	8.2963	1.272

.

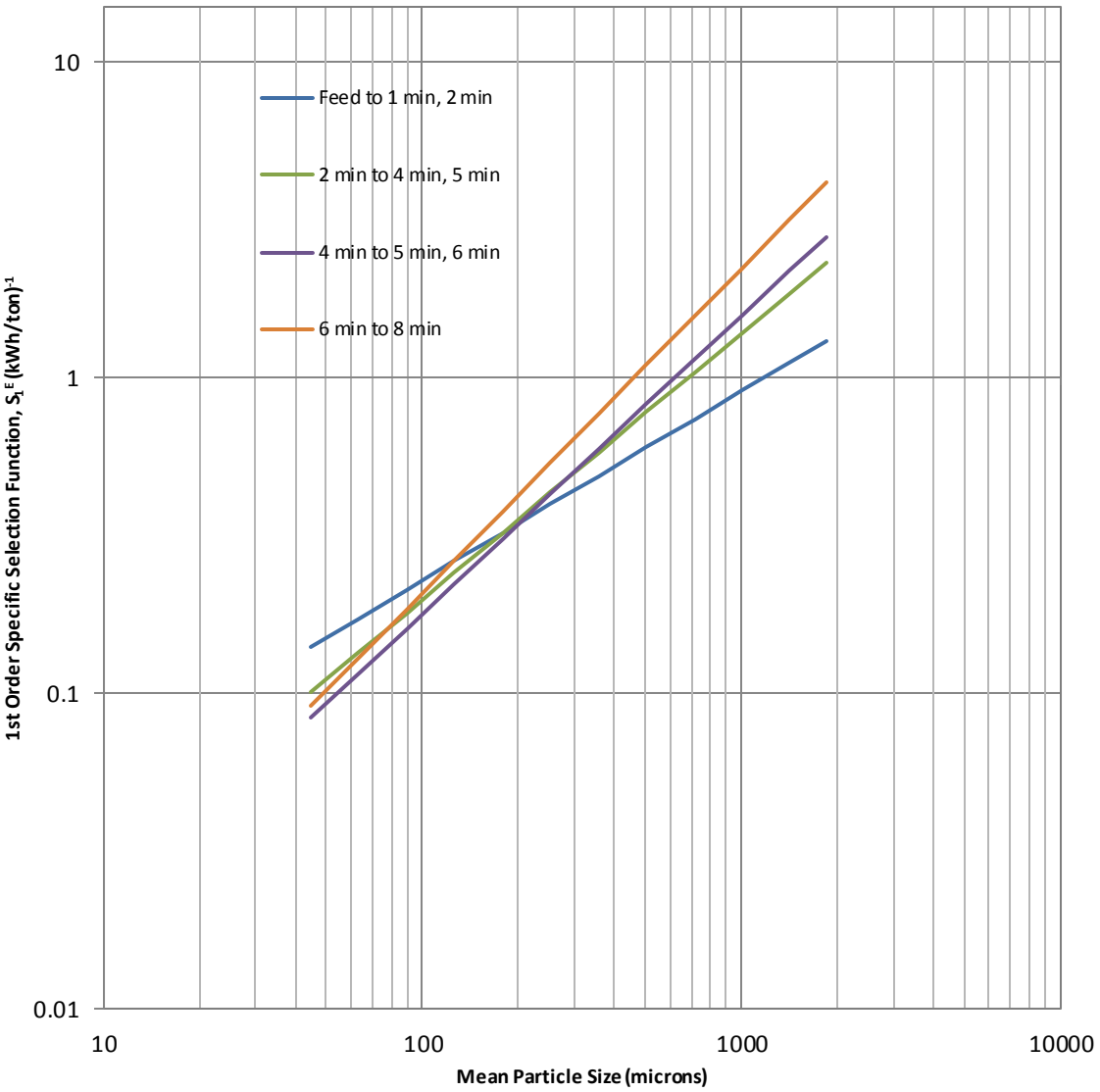

Figure 4.25.Dependence of specific selection functions on the particle size distribution in the ball mill, for -10 mesh feed (Gold Ore) in wet grinding at 72% solids and 100% slurry filling, showing pronounced nonlinearity.

Table 4.11.Converged Values of S_1^E and ζ_1 for Figure 4.25

Increment	S_1^E (kWh/ton)$^{-1}$	ζ_1
feed to 1,2 min	1.3076	0.983
2 to 4,5 min	2.3115	0.8433
4 to 5,6 min	2.7946	0.9451
6 to 8 min	4.1648	1.0289

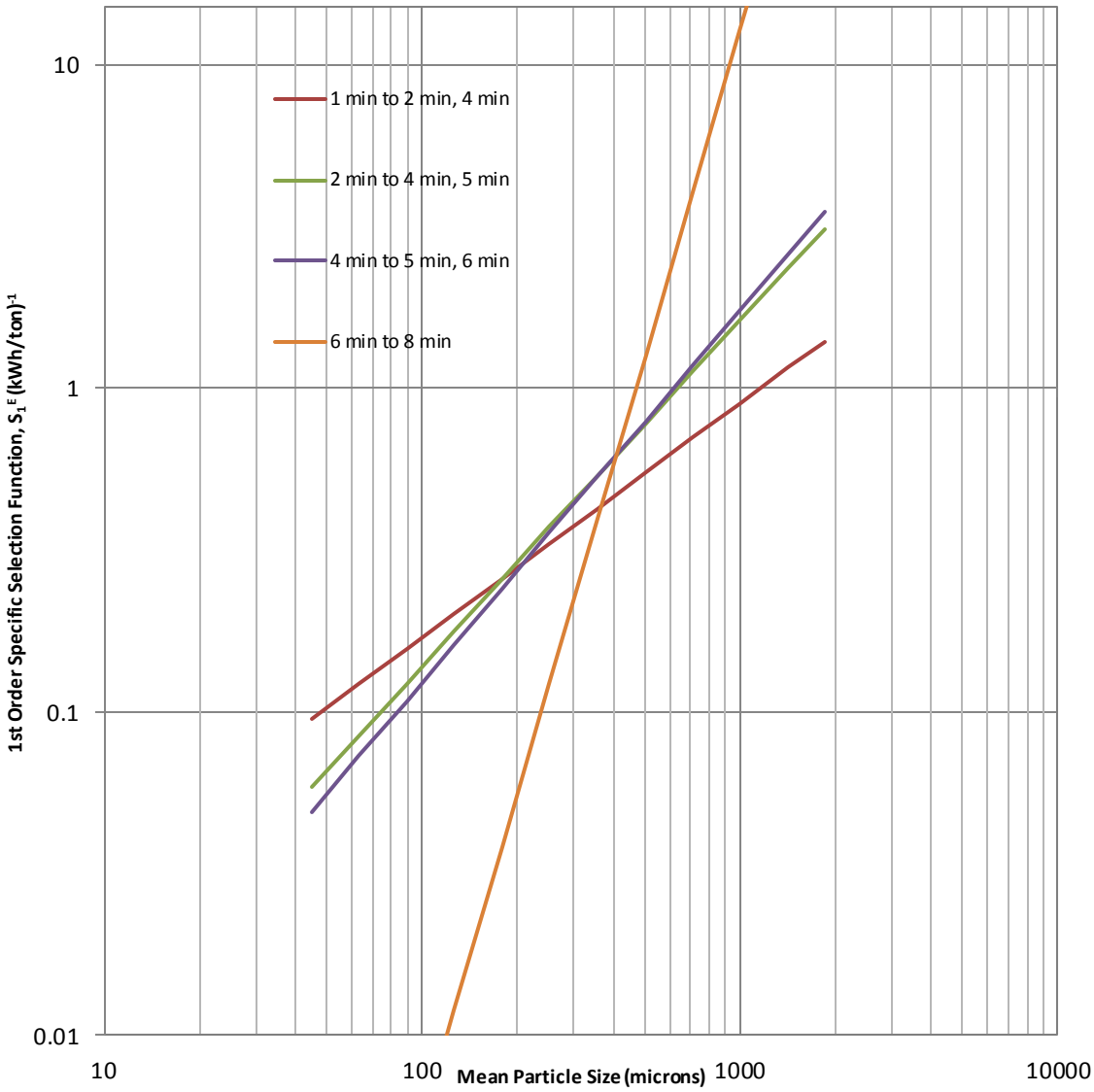

Figure 4.26.Dependence of specific selection functions on the particle size distribution in the ball mill, for -10 mesh feed (Gold Ore) in wet grinding at 65% solids and 260% slurry filling, showing pronounced nonlinearity.

Table 4.12.Converged Values of S_1^E and ζ_1 for Figure 4.26

Increment	S_1^E (kWh/ton)$^{-1}$	ζ_1
1 to 2,4 min	1.3981	0.7245
2 to 4,5 min	3.1115	1.0681
4 to 5,6 min	3.4929	1.1467
6 to 8 min	98.0436	3.3617

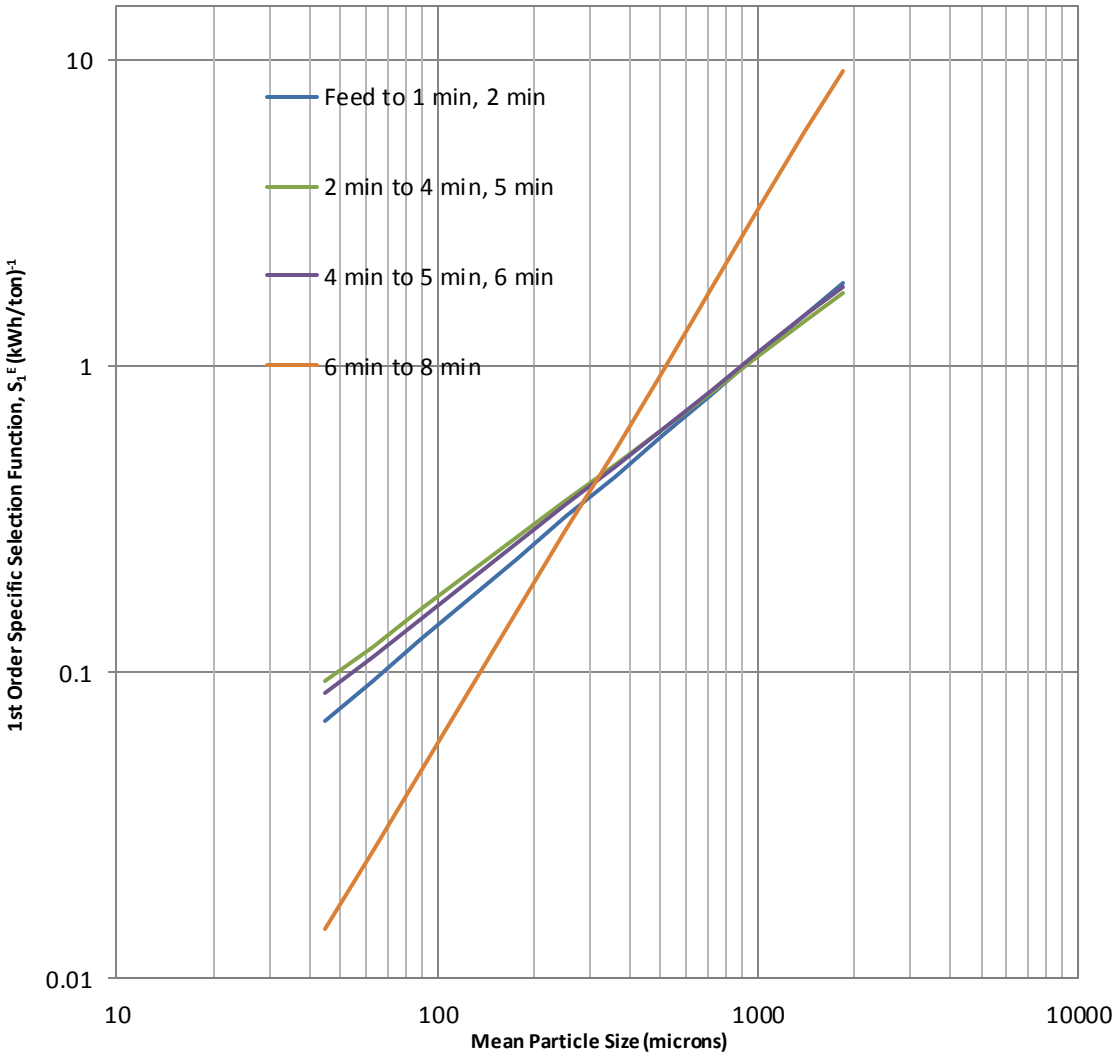

Figure 4.27.Dependence of specific selection functions on the particle size distribution in the ball mill, for -10 mesh feed (Gold Ore) in wet grinding at 72% solids and 260% slurry filling, showing pronounced nonlinearity.

Table 4.13.Converged Values of S_1^E and ζ_1 for Figure 4.27

Increment	S_1^E (kWh/ton)$^{-1}$	ζ_1
feed to 1,2 min	1.8742	0.886
2 to 4,5 min	1.7406	0.7868
4 to 5,6 min	1.8303	0.8256
6 to 8 min	9.2751	1.7396

effect of nonlinearity for various test conditions applied during wet grinding of limestone, quartzite, and gold ore, respectively. Tables associated with each figure detail incremental S_1^E and ζ_1 values. Tables 4.14, 4.15, and 4.16 illustrate the variation in mean particle size as a function of variation in percent solids and slurry filling. A nonlinear function fitting software code known as ESTIMILL was used to estimate 1st order specific selection

Table 4.14.Variation in Mean Particle Size as a Function of Percent Solids and Slurry Filling, Depicting Pronounced Nonlinearity (Limestone).

Percent Solids (%)	Percent Slurry Filling (%)	Mean Particle Size of Fulcrum (microns)
65	100	200
72	100	250
65	260	400
72	260	500

Table 4.15.Variation in Mean Particle Size as a Function of Percent Solids and Slurry Filling, Depicting Pronounced Nonlinearity (Quartzite).

Percent Solids (%)	Percent Slurry Filling (%)	Mean Particle Size of Fulcrum (microns)
65	100	180
72	100	220
65	260	300
72	260	390

Table 4.16.Variation in Mean Particle Size as a Function of Percent Solids and Slurry Filling, Depicting Pronounced Nonlinearity (Gold Ore).

Percent Solids (%)	Percent Slurry Filling (%)	Mean Particle Size of Fulcrum (microns)
65	100	150
72	100	180
65	260	250
72	260	300

functions in an incremental manner, over narrow ranges of specific energy input, thereby illustrating 1st order specific rates of breakage, along with the effect of fines content, particle size distribution in the mill, and inherent nonlinearity of the wet grinding process in a veritable manner. Incremental specific energy inputs ensured that the linear normalized population balance model was applicable in the narrow range of energy increment used in the specific selection function estimation process. These incremental inputs ensured the gradual yet marked increase in the breakage rates with extended grind times, as is witnessed in Figures 4.16 through 4.27. It is very closely observed that the breakage rates of coarser size fractions increases with an increase in grind time. Also, the quantity of fines being produced with each experimental run increases, thereby increasing the fines content in the average particle population. This directly supports the hypothesis that an increase in the fines content with extended grind times directly increases the breakage rates for the coarser size fractions. Reasons for this phenomenon have been discussed in the following pages. Variation in the breakage rates have been observed for all the three ore bodies incorporated in this study. Feed particle size distribution, percent solids, and slurry filling, slurry viscosity, fines content, and hardness are some of the factors that directly affect the nonlinearities in breakage rates of various materials. Effect of extended grind times have, therefore, been observed in close conjunction with the aforementioned reasons, and inferences have been drawn and discussed.

4.2.1. Factors Contributing to Nonlinearity

4.2.1.1 Preferential breakage of coarse particles. In stark contrast to dry grinding, wet grinding is inherently nonlinear, as discussed earlier. Also, it was discussed that the

nonlinearity is primarily due to "preferential breakage" of coarse particles which are prominently classified due to suspension of finer particles in the slurry, thereby leading to settling of coarser particles in the ball mass. This phenomenon augments the probability of breakage of coarser particles with a simultaneous decrease in the probability of breakage of finer particles. This kind of nonlinearity is profoundly illustrated in Figures 4.4, 4.5, and 4.6 for various ores where nonlinearity is present during mono-size wet grinding. It is observed that nonlinearity occurs when the fraction of feed size material remaining after each grind times goes below 0.1. For limestone and gold, this nonlinearity occurs after 4 minutes of wet grinding, whereas for quartzite which is a brittle material, this takes place just after 2 minutes of wet grinding. Figures 4.16 through 4.27 illustrate this effect in a very prominent manner. It is clearly enunciated that as the fineness of the particle population present in the mill increases, the top size selection function increases with a subsequent decrease in the fine size specific selection function. It is well known that breakage rates in wet batch grinding are time-dependent. This can be explained, loosely based on differential settling of particles in the slurry, thereby causing preferential breakage of the coarser particles. Austin and Tangsathitkulchai (1989) [42] proposed that breakage rates for coarser particles were either accelerated or decelerated as a function of mill loading conditions, slurry density, and feed size distribution.

4.2.1.2 Particle size distribution. It is known that a number of different breakage mechanisms are actively operative inside the mill during the milling process. Breakage may be caused due to impact fracture, chipping, or abrasion. But on a much broader perspective, the average breakage process remains the same and for wet grinding, it is the

shearing action between layers of ball mass. Dependence of breakage rate on the size distribution or particle size distribution of the particle population in the mill can be physically explained as follows. Consider two particle populations, one mono-size in nature comprised of coarse feed top size particles (10x14 mesh) only [41]. The second particle population is made up of natural feed size material, comprising both coarse and fine size particles. From an individualistic perspective, breakage rate of coarse particles is directly affected by two factors: firstly, the relative frequency of breakage events that the coarse particles encumber in relative preference to the fines, and secondly, the net energy per unit mass consumed by coarse particles during each breakage event. The breakage rate or the selection function/specific selection function can only increase when there is preferential occurrence of either or both of these events.

The frequency of such breakage events is directly influenced by preferential presence of coarse particles in the grinding zone. At any instant in a rotating ball mill, the grinding zone is generally assumed to be present mainly at the toe of ball mill charge. In comparison to a mono-size particle population, a natural size particle population will have coarse and fine size particles present in any independent breakage event. For a mono-size particle population, the impact energy will be shared by all particles coming in contact with all the balls. Natural size particle distribution has a pronounced amount of fines, which are really small in size, and hence a very small impact collision cross-section is presented during any collision event. The larger size of the coarser particles in a natural size particle distribution provides them with a much larger collision cross-section, thereby enabling them to absorb most or all of the impact energy. By virtue of their smaller mass fraction in a natural size particle distribution during wet grinding, coarser

particles absorb more impact energy per unit mass when compared to an augmented mass fraction of coarser particles present in a mono-size particle population. Another impending factor that contributes to this cause is the smaller collision cross-section of the finer particles in a natural size particle distribution, which makes them really difficult to break, and most of them are already in suspension in the slurry. Thus, during wet grinding operations of natural size particle distributions, there is always a mass of fine particles in suspension and in the material bed surrounding the coarser particles that simply transmit the impact energy to the coarser particles, thereby increasing the breakage rate of coarser particles. It is evident that coarser particles settle faster as compared to finer particles in a particle population, thereby causing preferential breakage. In any given particle population, the coarser particles are always subjected to maximum impact energy due to their size, irrespective of their mass fraction in the population. Therefore, the notion that the breakage rate of coarser particles increases with an increase in the amount of fines in the milling environment is supported, with subsequent decrease in the breakage rate of finer particles.

4.2.1.3 Viscosity. The viscosity of the slurry also plays a role in determining breakage rates during wet grinding experiments, since thick slurry will have a high tendency of absorbing the impact energy instead of transmitting it to the coarser particles in the particle bed, leading to nonlinearities at higher fulcrum values (refer to Tables 4.6, 4.11, and 4.16). The following expression relates slurry density to percent solids.

$$S_m = \frac{S_s * S_i}{S_s + C_w(S_i - S_s)} \qquad ..4.11$$

where S_m is the specific gravity of the slurry, S_i is the specific gravity of the liquid phase, S_s is the specific gravity of the solids phase, and C_w is the concentration of solids by

weight. Particle flow through the interstices of ball charge is directly dependent on the size distribution of the particle population and the viscosity of the slurry in the milling environment.

4.2.1.4 Percent solids. Percent solids also play a role in determining the breakage rates during wet grinding, since the size distribution of the particle population is directly varied as a function of percent solids, thereby causing a variation in the particulate environment present in the mill during wet grinding. Percent slurry filling also affects the breakage rates, as the amount of water added for wet-batch grinding experiments directly alters slurry densities as a function of time, that is, the slurry density is assumed to increase with an increase in grind time, due to greater mass fraction of fines present in suspension in the slurry. It is very clearly observed from Tables 4.6, 4.11, and 4.16 that percent solids and slurry filling have a profound effect on the nonlinearity of breakage rates. In each of the tables, it is noticed that with an increase in percent solids, the mass fraction of material present in each size interval is varied. As the amount of water decreases with an increase in percent solids, the slurry viscosity is increased comparatively, due to an increase in the mass fraction of fines present in the particle population. This varies breakage kinetics in a way that nonlinearity is attained at a greater mean particle size, as compared to that attained at a lower percent solids. Also, variations are noticed in the mean particle size (fulcrums) beyond which nonlinearities in breakage rates are observed in each ore under varying test conditions.

4.2.1.5 Ore hardness. Ore hardness variation is in the ascending order of limestone, quartzite, and gold ore. Therefore, the mean particle size below which nonlinearity in the breakage rates of various size fractions in the particle population

occurs during wet grinding is in the increasing order of gold ore, quartzite, limestone. Thus, it can be hypothesized that the hardness of an ore inversely affects the mean particle size below which nonlinearities in the breakage rates may occur, under the same test conditions. A softer ore will always produce a lot of fines, and the average particle size in the particle population will be such that nonlinearity in breakage rates will be attained at greater particle sizes, as in the case of limestone. For a hard yet brittle ore like quartzite, the average particle population will have a mass fraction of fines, such that energy from impact collisions would cause them to fracture further and create finer particles, thereby forcing the mean particle size to go down, along with coarser particles fracturing and generating more progeny particles which will be subjected to further breakage. This causes the nonlinearities at reduced mean particle sizes for a particle population subjected to wet grinding. In the case of gold ore, the feed material is made up of extremely hard rock, and though the average breakage event remains invariant, interparticle abrasions and chipping events between particles will also play a role. Although the rate of breakage for coarser size fractions increases rapidly, the energy-specific breakage rates for the finer size fractions decreases very gradually, indicating that hardness is factoring into determining the mean particle size for the population. Hence, since the average particle population is largely prone to fracture, and due to their extremely hard nature, transmission of energy solely to coarser size fractions is somewhat limited, leading to mean particle size being forced even lower than those of quartzite. This is directly illustrated in the figures and tables depicting the incremental first order breakage rates and the mean particle size for the three ore bodies respectively (limestone, quartzite, and gold ore).

4.2.2. Implications of Incremental Inputs of Specific Energy on the Nonlinearities Observed in 2nd Order Breakage Rates

As is known, selection functions are determined from fundamental breakage characteristics of particles. Selection function can be described as the probability that a particular particle will be fractured on impact during an independent time-discretized breakage event. Variation of the specific rate of breakage and the breakage function can be adequately accounted for by enunciating the variation of these functions with the specific power input. This assumption is equivalent to the fact that the degree of breakage occurring inside the mill is directly proportional to the amount of energy being expended during that stipulated grind time. Since the average breakage event for the entire particle population during wet grinding remains invariant, this rationale can be implemented for predictive simulation and scale-up. Equilibrium ball charge distribution directly varies s_1^E values and this impending factor is imperative for predictive simulation for pilot mills and industrial-scale mills with similar ball charge distribution.

Functional form for selection functions during wet grinding conditions can be given as:

$$S_i = S_1 exp\left(\sum_{j=1}^{n} \xi_j \left[\ln \frac{\sqrt{x_i x_{i+1}}}{\sqrt{x_1 x_2}}\right]^j\right) \quad \text{n} = 1,2,3 \qquad \ldots 4.12$$

Breakage rate and energy-specific rate of breakage can both be defined by this equation, as a power series of the natural logarithm of the particle size. Usually, two series in the term are considered appropriate to describe the nature of the breakage rate. The parameter ξ_2 is used to determine the sharpness of the maximum in the plot of energy-specific selection function versus mean particle size. It should always be a negative number. For

our experimental study, the value of ξ_2 was initially assumed to be -0.05. ESTIMILL was used to predict 2nd order energy-specific breakage rates in an incremental manner, with narrow inputs of specific energy according to corresponding grind times. The nonlinearity observed in the breakage rates is pretty consistent with predetermined experimental data and literature. This also helps deduce actual experimental selection functions that can provide an overview of particle behavior during milling operations in wet grinding systems.

$$S_i = S_1 \exp[\{\xi_1 \left(\ln \frac{\sqrt{x_i x_{i+1}}}{\sqrt{x_1 x_2}}\right) + \xi_2 \left(\ln \frac{\sqrt{x_i x_{i+1}}}{\sqrt{x_1 x_2}}\right)^2 + \dots \dots\}] \qquad \dots 4.13$$

As specific selection functions during wet grinding are only dependent on the particle size distribution of the particle population in the mill, the energy-specific PBM expression can be directly drawn from Equation 2.10. The expression is as follows:

$$\frac{dm_i}{d\bar{E}} = -S_i^E(\underline{m})m_i + \sum_{j=1}^{i-1} b_{ij} S_j^E(\underline{m})m_j \qquad \dots 4.14$$

Figures 4.28 through 4.36 give a detailed overview of actual experimental energy-specific selection functions for limestone, quartzite and gold ore under varying test conditions. Tables 4.17 through 4.25 associated with each figure provide incremental S_1^E, ζ_1, and ζ_2 values.

Figures 4.28 and 4.29 depict incremental 2nd order specific selection functions. The nature of these graphs hint directly toward the already established notion that as the amount of fines in a particle population increases during wet grinding, the specific rate of breakage for coarser particles increases with a simultaneous decrease in the energy-specific breakage rates for the finer size fractions in the population. For a much harder and extremely brittle ore like quartzite, the trends noticed in the 2nd order energy-specific

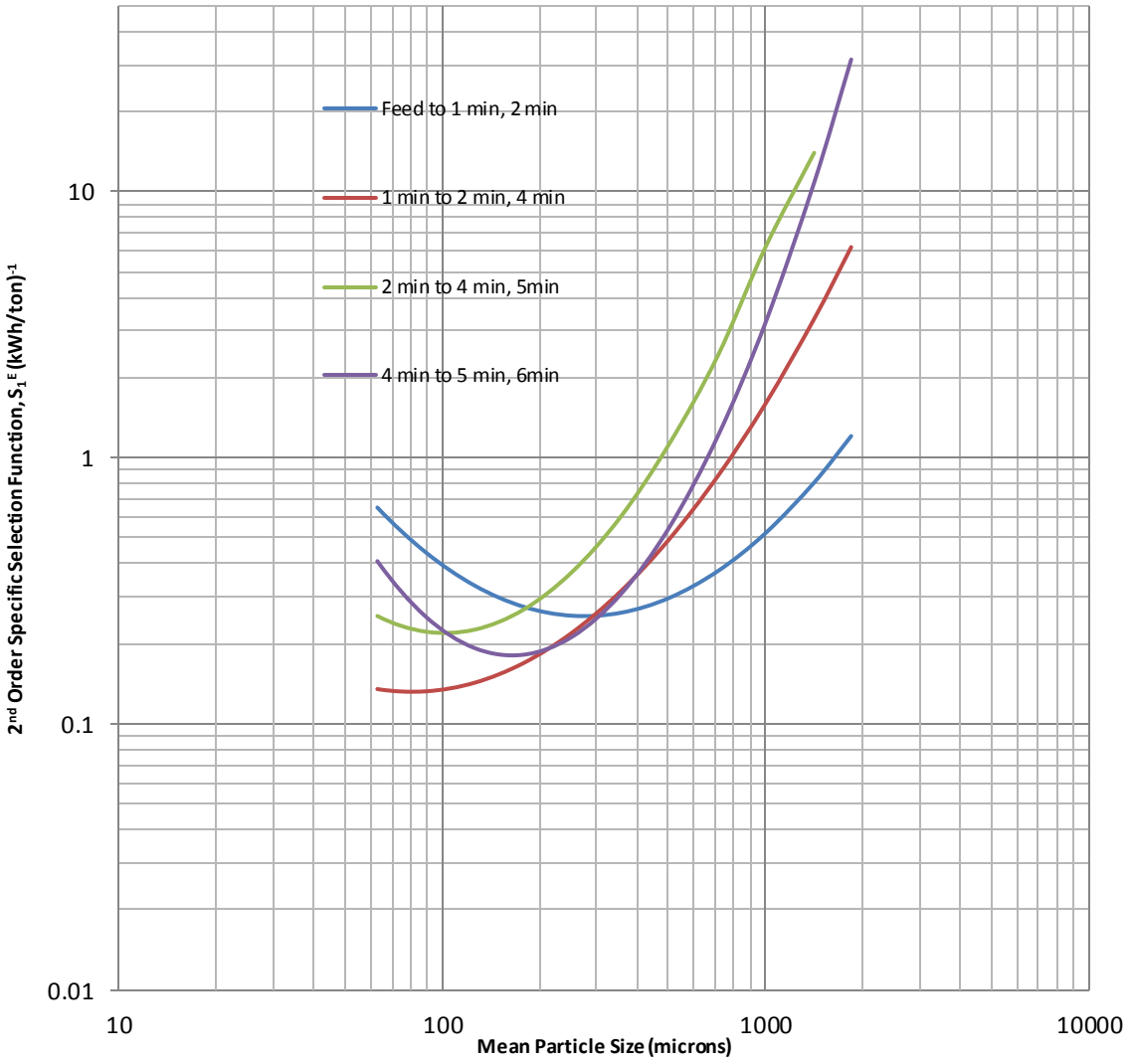

Figure 4.28.Dependence of 2nd order specific selection functions on the particle size distribution in the ball mill, for -10 mesh feed (Limestone) in wet grinding at 65% solids and 260% slurry filling, showing pronounced nonlinearity.

Table 4.17.Converged Values of S_1^E, ζ_1 and ζ_2 for Figure 4.28

Increment	S_1^E (kWh/ton)$^{-1}$	ζ_1	ζ_2
feed to 1,2 min	1.2065	1.6406	0.4317
1 to 2,4 min	6.1888	2.4595	0.3929
2 to 4,5 min	13.9947	3.2598	0.6392
4 to 5,6 min	31.4021	4.2713	0.8843

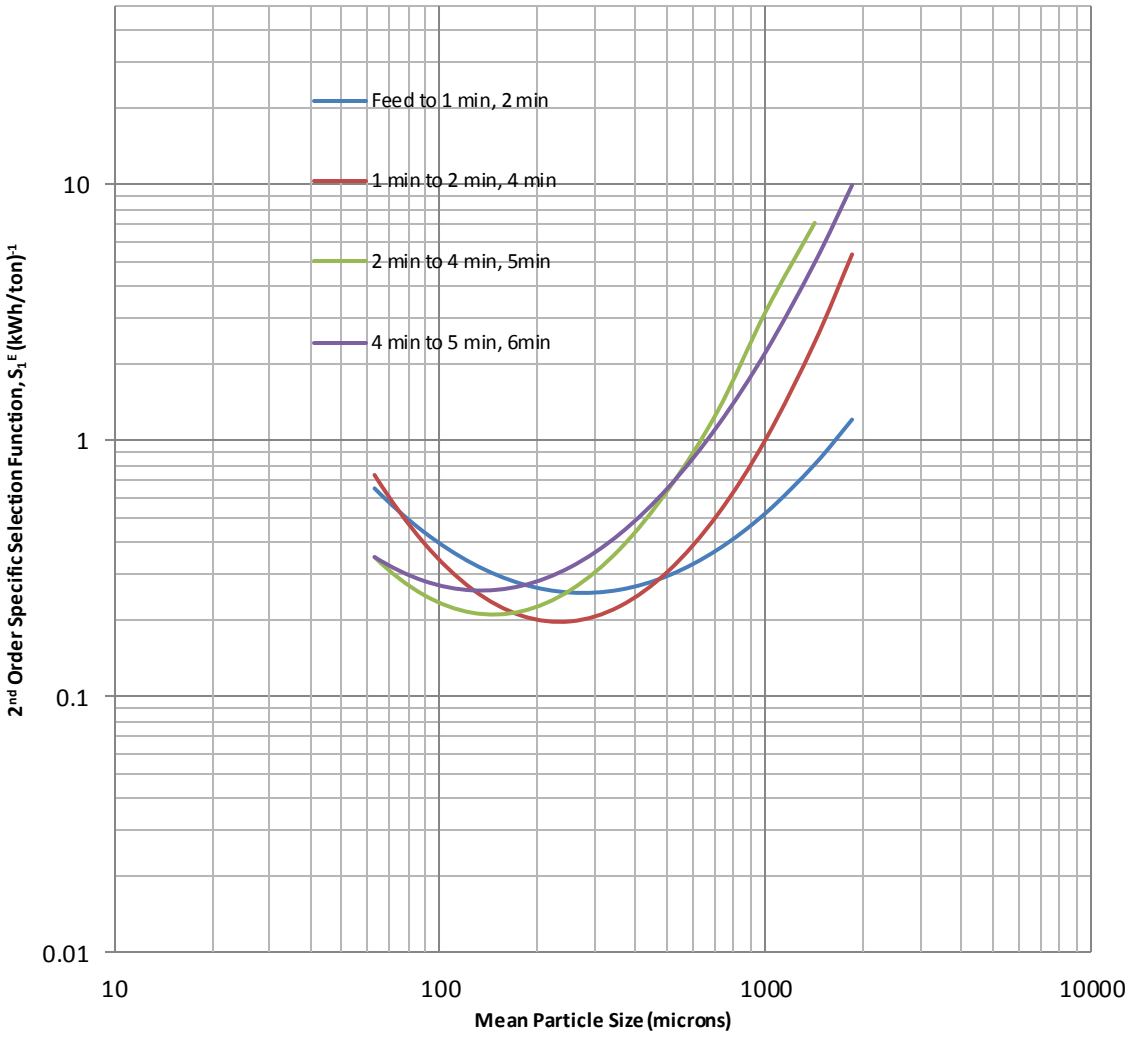

Figure 4.29.Dependence of 2nd order specific selection functions on the particle size distribution in the ball mill, for -10 mesh feed (Limestone) in wet grinding at 72% solids and 260% slurry filling, showing pronounced nonlinearity.

Table 4.18.Converged Values of S_1^E, ζ_1 and ζ_2 for Figure 4.29

Increment	S_1^E (kWh/ton)$^{-1}$	ζ_1	ζ_2
feed to 1,2 min	0.6488	0.2737	-0.0005
1 to 2,4 min	5.3269	3.1951	0.7725
2 to 4,5 min	7.0697	3.215	0.7339
4 to 5,6 min	9.9247	2.7803	0.5302

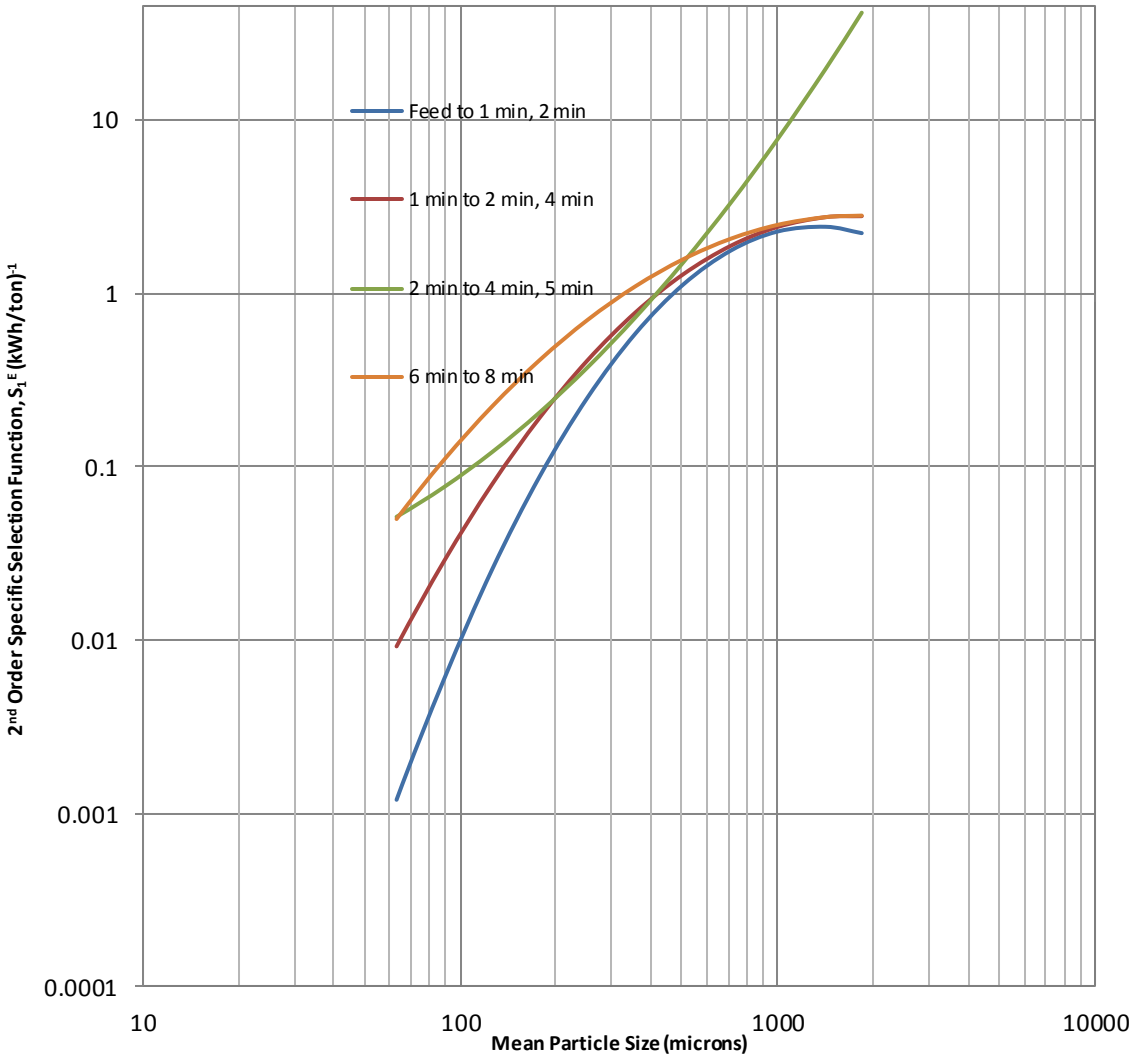

Figure 4.30.Dependence of 2nd order specific selection functions on the particle size distribution in the ball mill, for -10 mesh feed (Quartzite) in wet grinding at 65% solids and 100% slurry filling, showing pronounced nonlinearity.

Table 4.19.Converged Values of S_1^E, ζ_1 and ζ_2 for Figure 4.30

Increment	S_1^E $(kWh/ton)^{-1}$	ζ_1	ζ_2
feed to 1,2 min	2.2195	-0.5368	-0.8209
1 to 2,4 min	2.7805	-0.0876	-0.5273
2 to 4,5 min	41.4397	2.9186	0.2774
6 to 8 min	2.8017	-0.0175	-0.3586

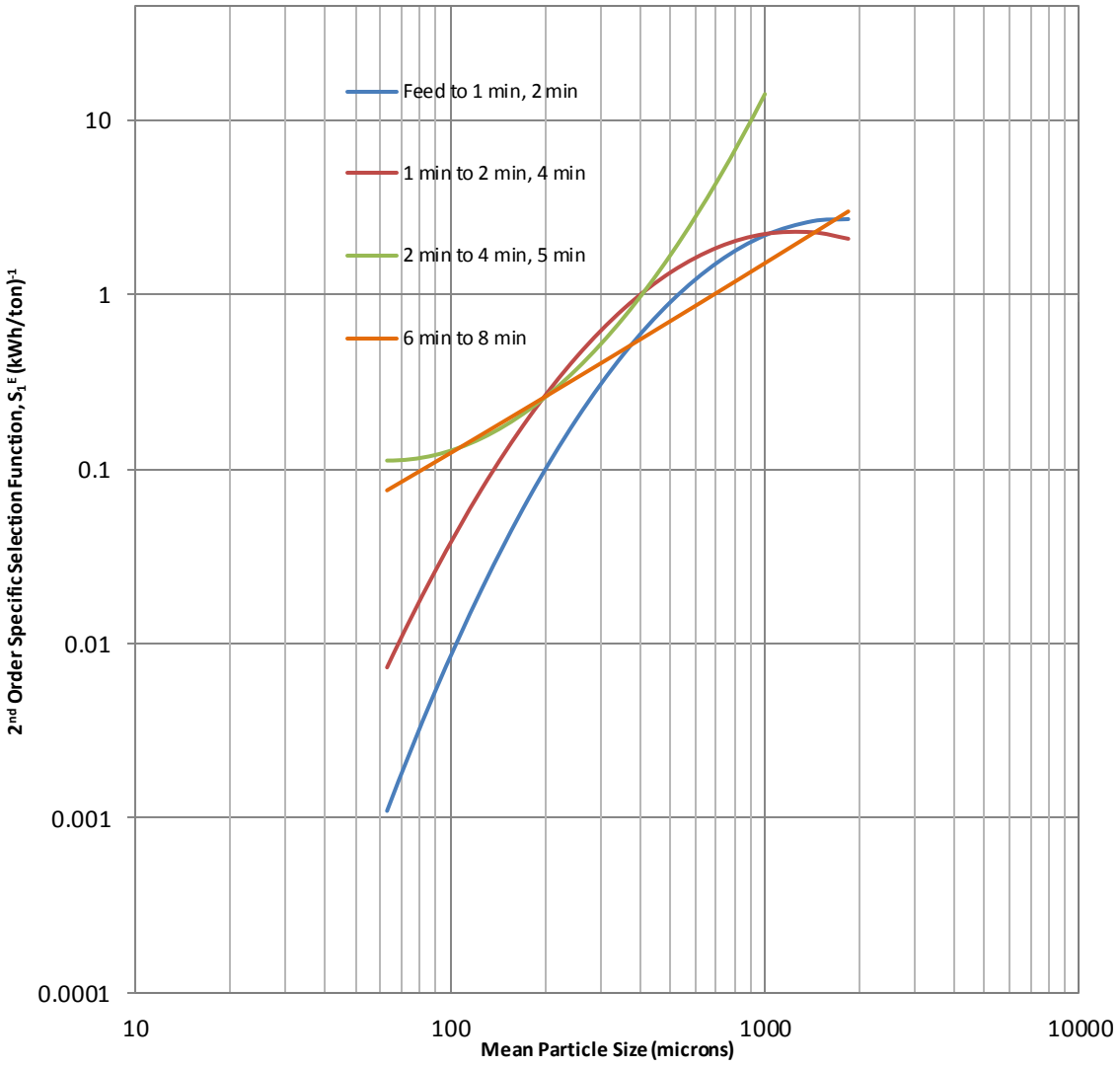

Figure 4.31.Dependence of 2nd order specific selection functions on the particle size distribution in the ball mill, for -10 mesh feed (Quartzite) in wet grinding at 72% solids and 100% slurry filling, showing pronounced nonlinearity.

Table 4.20.Converged Values of S_1^E, ζ_1 and ζ_2 for Figure 4.31

Increment	S_1^E $(kWh/ton)^{-1}$	ζ_1	ζ_2
feed to 1,2 min	2.6965	-0.0815	-0.7081
1 to 2,4 min	2.0815	-0.4961	-0.6435
2 to 4,5 min	47.4972	4.2908	0.6379
6 to 8 min	2.9844	1.124	0.0101

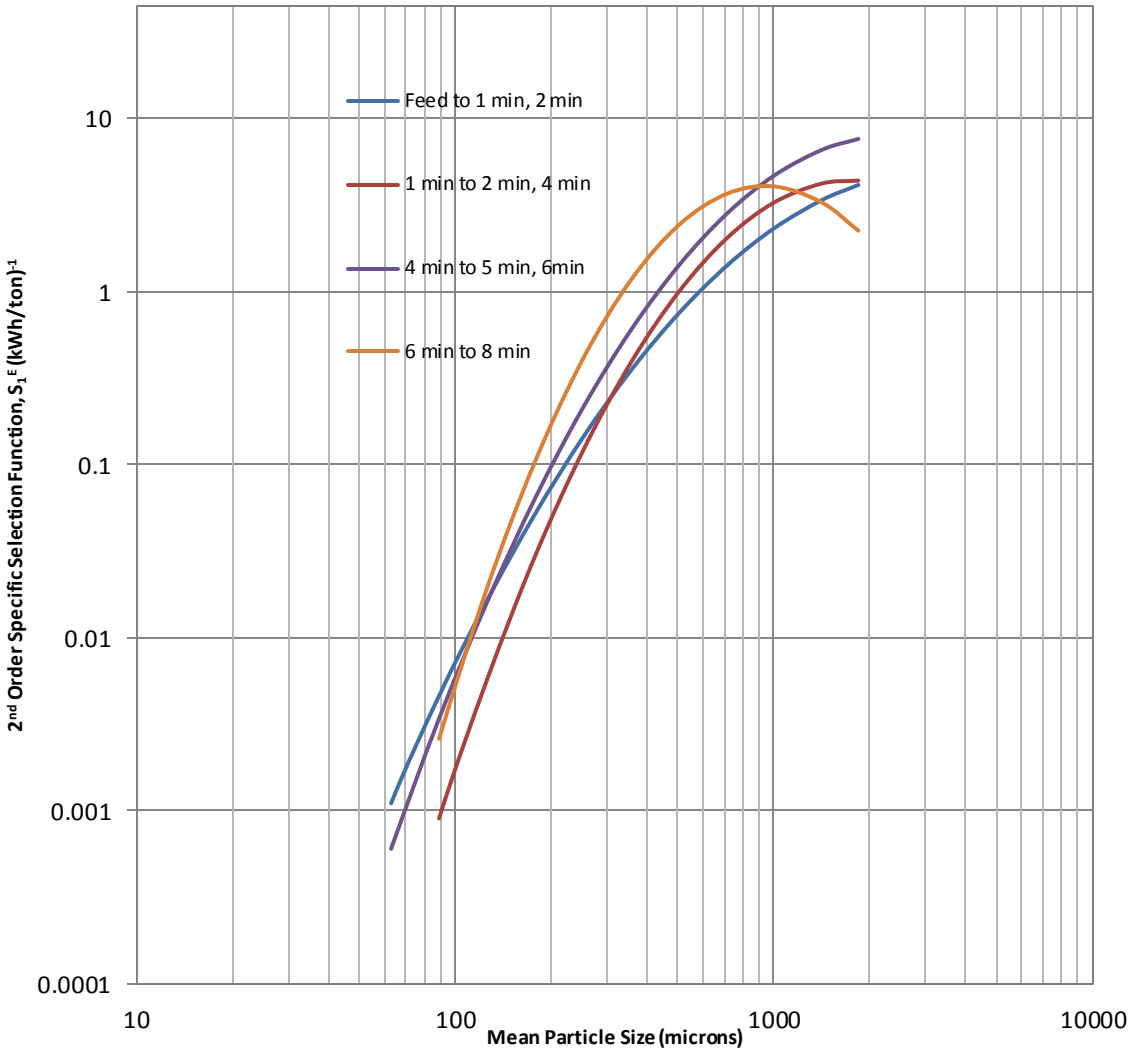

Figure 4.32.Dependence of 2nd order specific selection functions on the particle size distribution in the ball mill, for -10 mesh feed (Quartzite) in wet grinding at 65% solids and 260% slurry filling, showing pronounced nonlinearity.

Table 4.21.Converged Values of S_1^E, ζ_1 and ζ_2 for Figure 4.32

Increment	S_1^E $(kWh/ton)^{-1}$	ζ_1	ζ_2
feed to 1,2 min	4.1437	0.6205	-0.5372
1 to 2,4 min	4.3915	-0.1074	-0.9629
4 to 5,6 min	7.6523	0.3621	-0.7225
6 to 8 min	2.2544	-1.7743	-1.3233

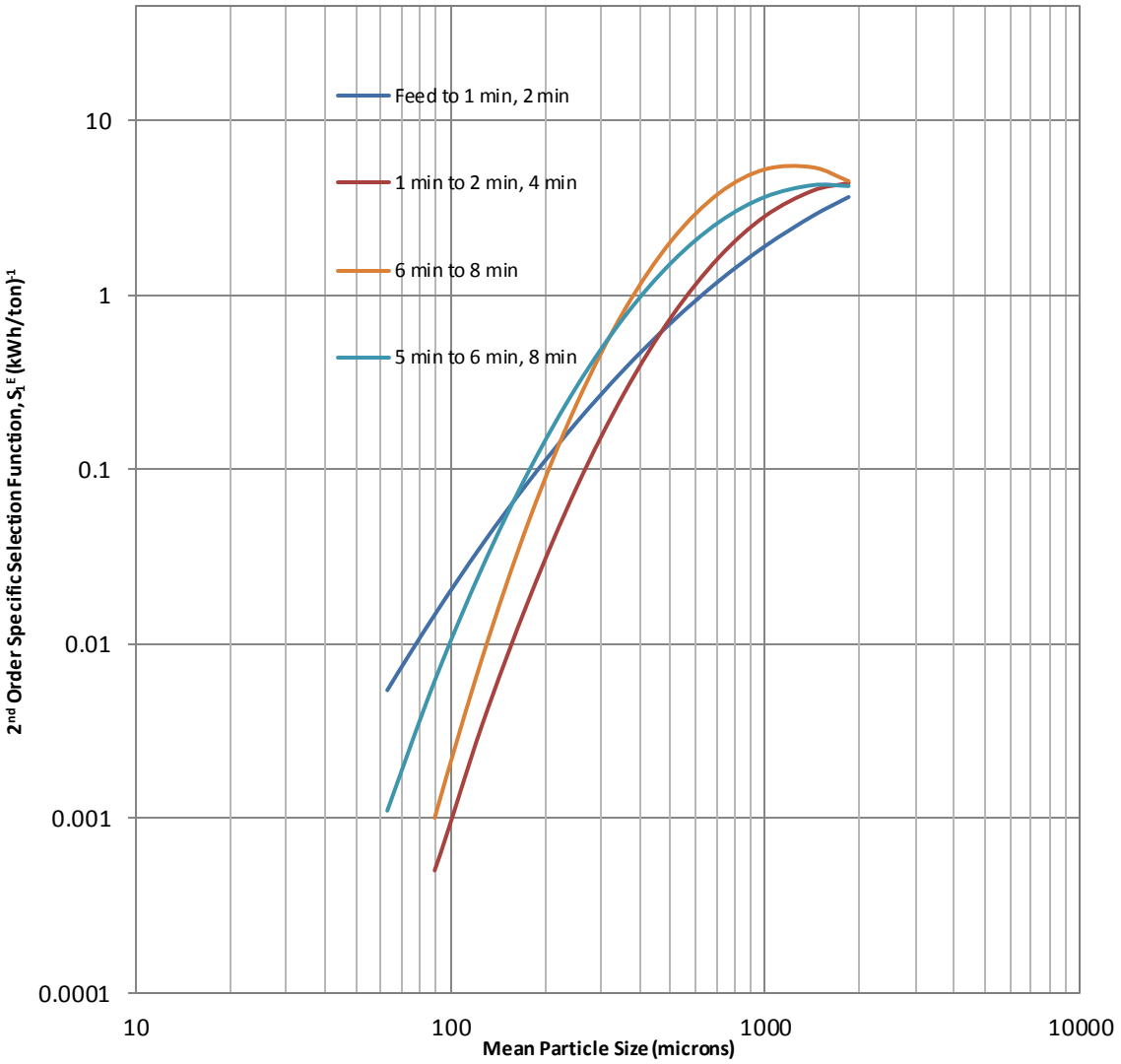

Figure 4.33.Dependence of 2nd order specific selection functions on the particle size distribution in the ball mill, for -10 mesh feed (Quartzite) in wet grinding at 72% solids and 260% slurry filling, showing pronounced nonlinearity.

Table 4.22.Converged Values of S_1^E, ζ_1 and ζ_2 for Figure 4.33

Increment	S_1^E $(kWh/ton)^{-1}$	ζ_1	ζ_2
feed to 1,2 min	3.6341	0.869	-0.3143
1 to 2,4 min	4.3701	0.136	-0.9459
5 to 6,8 min	4.2012	-0.2511	-0.7945
6 to 8 min	4.4791	-1.0254	-1.2578

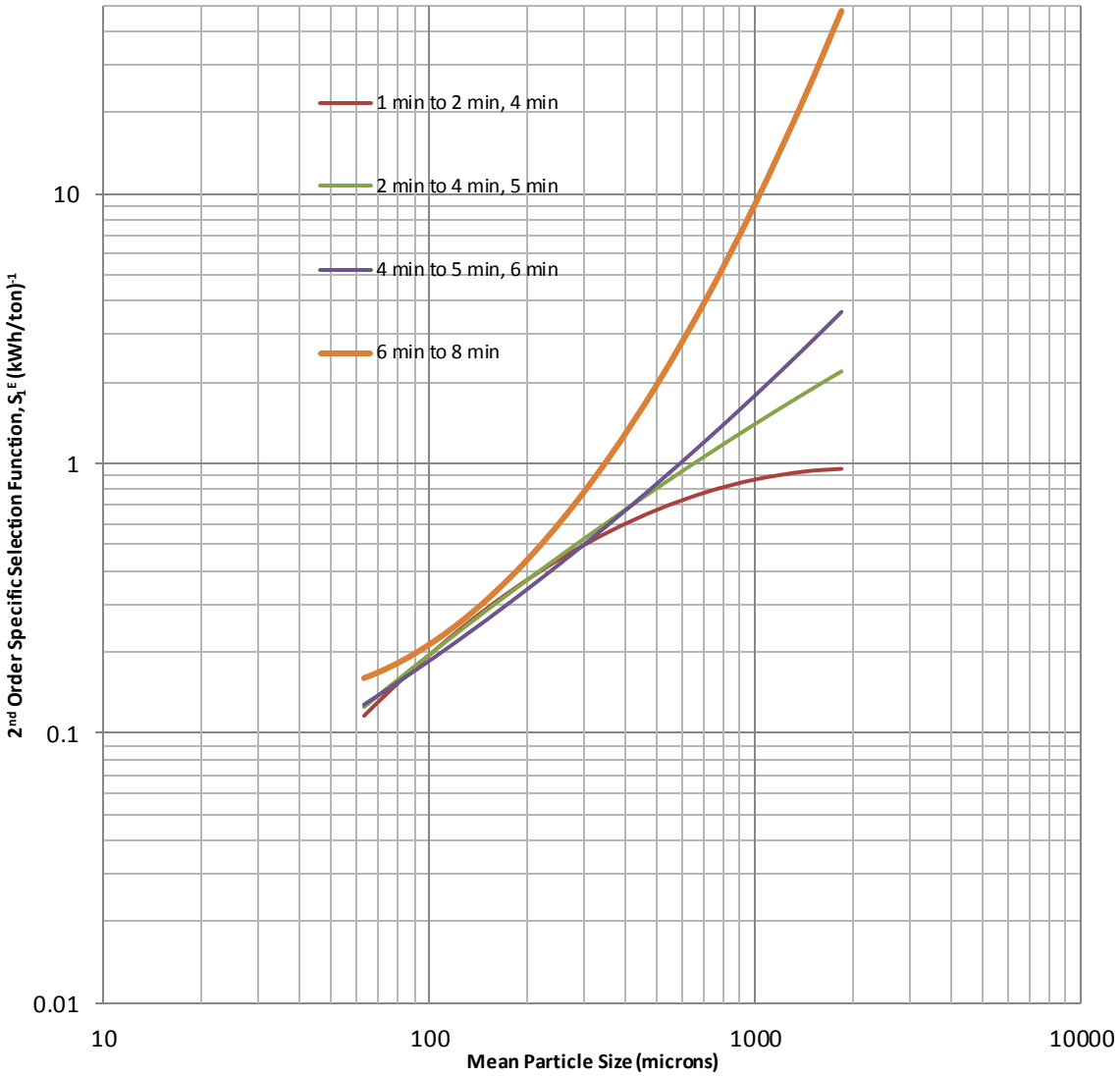

Figure 4.34.Dependence of 2nd order specific selection functions on the particle size distribution in the ball mill, for -10 mesh feed (Gold) in wet grinding at 65% solids and 100% slurry filling, showing pronounced nonlinearity.

Table 4.23.Converged Values of S_1^E, ζ_1 and ζ_2 for Figure 4.34

Increment	S_1^E (kWh/ton)$^{-1}$	ζ_1	ζ_2
1 to 2,4 min	0.9551	0.0441	-0.172
2 to 4,5 min	2.194	0.7104	-0.041
4 to 5,6 min	3.6428	1.2046	0.0628
6 to 8 min	47.5635	2.92	0.3653

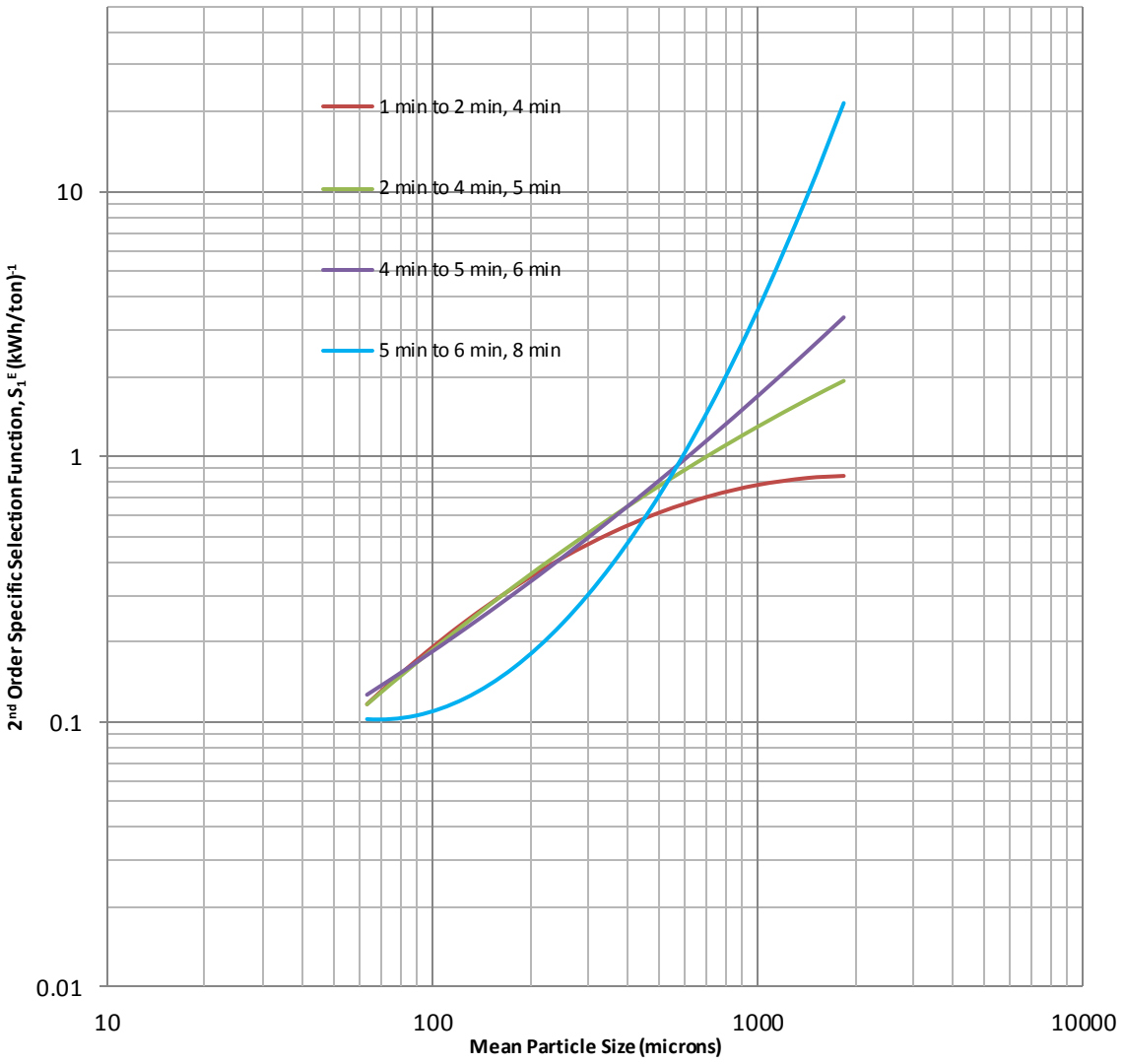

Figure 4.35.Dependence of 2nd order specific selection functions on the particle size distribution in the ball mill, for -10 mesh feed (Gold) in wet grinding at 72% solids and 100% slurry filling, showing pronounced nonlinearity.

Table 4.24.Converged Values of S_1^E, ζ_1 and ζ_2 for Figure 4.35

Increment	S_1^E (kWh/ton)$^{-1}$	ζ_1	ζ_2
1 to 2,4 min	0.8462	0.0275	-0.1658
2 to 4,5 min	1.9318	0.6139	-0.0646
4 to 5,6 min	3.3522	1.1557	0.0548
5 to 6,8 min	0.7981	-0.041	-0.1794

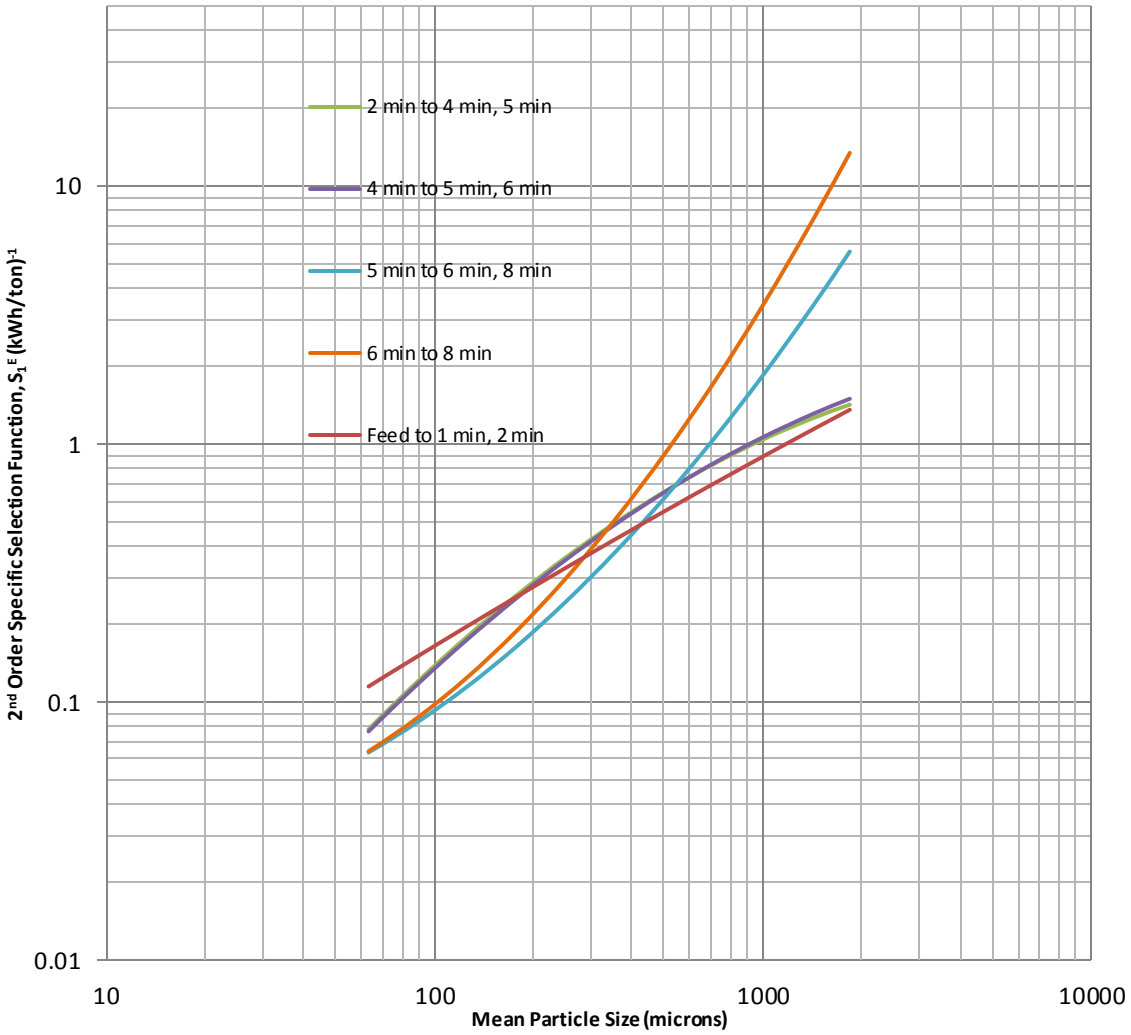

Figure 4.36.Dependence of 2nd order specific selection functions on the particle size distribution in the ball mill, for -10 mesh feed (Gold) in wet grinding at 65% solids and 260% slurry filling, showing pronounced nonlinearity.

Table 4.25.Converged Values of S_1^E, ζ_1 and ζ_2 for Figure 4.36

Increment	S_1^E (kWh/ton)$^{-1}$	ζ_1	ζ_2
feed to 1,2 min	4.6751	1.7165	0.17
2 to 4,5 min	2.3124	0.5584	-0.1848
4 to 5,6 min	2.7452	0.7602	-0.1335
5 to 6,8 min	21.5474	3.2524	0.4941
6 to 8 min	1.9889	1.1657	0.0712

breakage rates are quite different than those of limestone. Figures 4.30 and 4.31 illustrate that at constant slurry filling of 100%, the energy-specific breakage rates for coarser size fractions in the particle population increase as established, but in a gradual fashion, whereas the breakage rates for the finer particles decrease rapidly. This is also somewhat noticed in Figures 4.29 and 4.30 at a constant slurry filling of 260%. Also, with an increase in grind time, as the amount of fines in the slurry increases, the breakage rates for coarser particles tend to decrease significantly, as is shown in Figures 4.30 through 4.33 for the incremental input of specific energy at 6 minutes through 8 minutes. This can be directly attributed to the extreme brittle nature of quartzite, wherein the average particle population is readily being impacted and fractured during the milling process. This leads to an increase in the amount of fines leading to generation of a fines medium, thereby increasing slurry viscosity slightly, but still comprised largely of particles that, when subjected to impact collisions will fracture and generate finer progeny particles. Thus, energy is not entirely transmitted to coarser fractions in the particle population.

For gold ore, the energy-specific breakage rates for the coarser size fractions increase rapidly and are augmented by chipping and abrasion breakage events along with impact fracture, due to the extreme hardness of the material. An increase in grind time propagates production of fines in the particle population, and even though the breakage rates for the coarser size fractions follow the generic trend of increasing with increase in the amount of fines, the breakage rates for the finer fractions in the population decrease gradually due to the hard nature of the material. This is vehemently observed in Figures 4.34, 4.35, and 4.36. Thus, the variation in 2^{nd} order breakage rates for limestone, quartzite, and gold ore can be fully realized in these graphical illustrations.

4.2.3. Implications of Nonlinearity in Breakage Rates on Parameter Estimation

Breakage functions derived from experimental data have proven to be independent of mill diameter and ball load. A scale-up scheme entirely dependent on specific energy input will be a feasible solution for parameter estimation. The estimation capability of the linear normalized model (Equation 4.6) can be validated and implemented for narrow ranges of specific energy input where the breakage kinetics would be "nearly linear" and be fitted accordingly. Also, incremental inputs of specific energy in the "near neighborhood" of actual experimental data provide for simulation and better prediction of breakage rates. Thus, simulation with parameter estimates derived from wet grinding experiments done in the 10-inch mill with accurate similar fineness of grind will provide for veritable scale-up, and with strong agreement to experimental product particle size distributions. Preferential breakage of coarser particles in comparison to finer size fractions is the fundamental and singular reason for such classification action, as this causes suspension of fines in the slurry and settling of coarser particles in the ball mass. This directly hints toward the dependence of selection function with variation in the milling environment, as is depicted in Figures 4.16 through 4.27 and Figures 4.28 through 4.36. Observed nonlinearity takes place below 0.1 for all ores of varying hardness, as is illustrated in Figures 4.4, 4.5, and 4.6. Figures 4.16 through 4.27 illustrate variation in breakage rates with incremental variations in grind times and specific energy inputs, indicating 1st order breakage kinetics, with breakage parameters obtained in the 'nearly linear' region (coarse particle grind). The effects of this will be observed in the following graphs which give a veritable comparison between the two

methods used for predictive simulation of experimental product particle size distributions obtained from wet grinding experiments.

Method I, as mentioned, will take into account initial parameter estimates (from coarser size fractions) derived from experimental data and try to estimate product size distributions, in a cumulative fashion, that is, a one-time input for all parameter estimates, and deriving subsequent product size distributions. In other words, the breakage rate parameters are estimated just one time from all of the product size distributions, measured in a particular grinding experiment. This method inherently neglects the nonlinearities observed in the finer size fractions with extended grinding times. Breakage rate parameters will also be obtained from this method. This method will be compared with an alternative procedure known as Method II.

Method II takes into account incremental inputs of specific energy, to calculate individual 2^{nd} order selection functions (Figures 4.28 through 4.36), thereby encompassing nonlinearity factors in a way that the breakage kinetics are in the proximity or "near neighborhood" of the subsequent experimental product size distributions, thereby rendering the linear model pretty consistent and valid for predictive simulations of the finer size fractions. Successive inputs of S_1^E, ζ_1, and ζ_2 will be used for the same. The variation in the results obtained from both these methods will be hugely distinguished by the variation in RMS values (Root Mean Square of Residuals) obtained at the end of each simulation. Also, the closeness or the degree of proximity for the "near neighborhood" criterion will be decided by incremental inputs of specific energy, and the product size distributions will be calculated on an incremental basis, with variations in 2^{nd} order top-size selection functions in the foregoing simulation acting as input for the

immediately succeeding simulation. This helps maintain the "near neighborhood" criterion.

The accuracy of this logic is ratified by the RMS values derived after each simulation, which, in turn, hints toward the efficiency of the convergence criteria followed by ESTIMILL to produce such predictions in the first place. Replacing *m* with *m** provides a reference set of mass fractions that directly reiterates the concept of the "near neighborhood" criterion with the logic of "similar fineness of grind," and makes them similar. In this context, ESTIMILL uses the convergence criteria to bridge and shorten the gap between *m* and *m** through numerous iterations, varying breakage rates over all size fractions. The simulation is complete only after the RMS values have been minimized from the 1^{st} iteration and get their least value at the n^{th} iteration, which actually illustrates that the reference set of mass fractions *m** has been varied according to varying breakage rates at each size fraction, thereby improving convergence at the end of each iteration. The number of iterations set in both the methods has been kept constant at ten. This is fully illustrated in the lower values obtained from Method II, as compared to those obtained from Method I. Figures 4.37 through 4.48 provide a graphical insight into the product size distributions, obtained from wet grinding experiments, Method I and Method II. The difference in the product particle size distributions obtained from the three different ways has been discussed and the reasons for such discrepancies have also been hypothesized. Inferences have been drawn to indicate the causes for such discrepancies and the best suited method for parameter estimation is selected out of the two methods. The following graphical illustrations will provide an in-depth insight into the particle size distributions obtained from the three different ways.

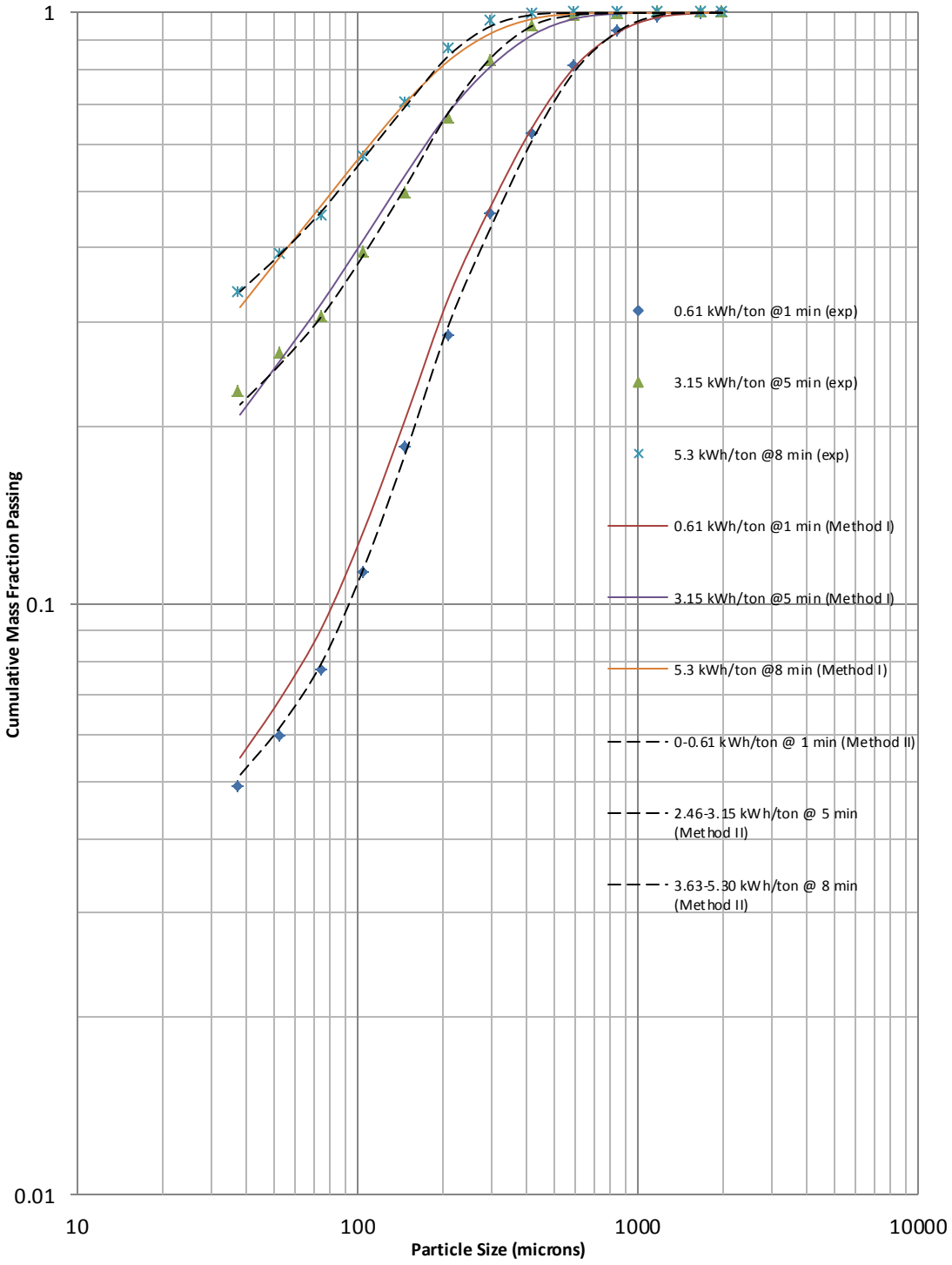

Figure 4.37.Comparison of Product Size Distributions obtained from Experimental Data, Method I and Method II (Limestone Ore, 65% solids – 100% slurry filling).

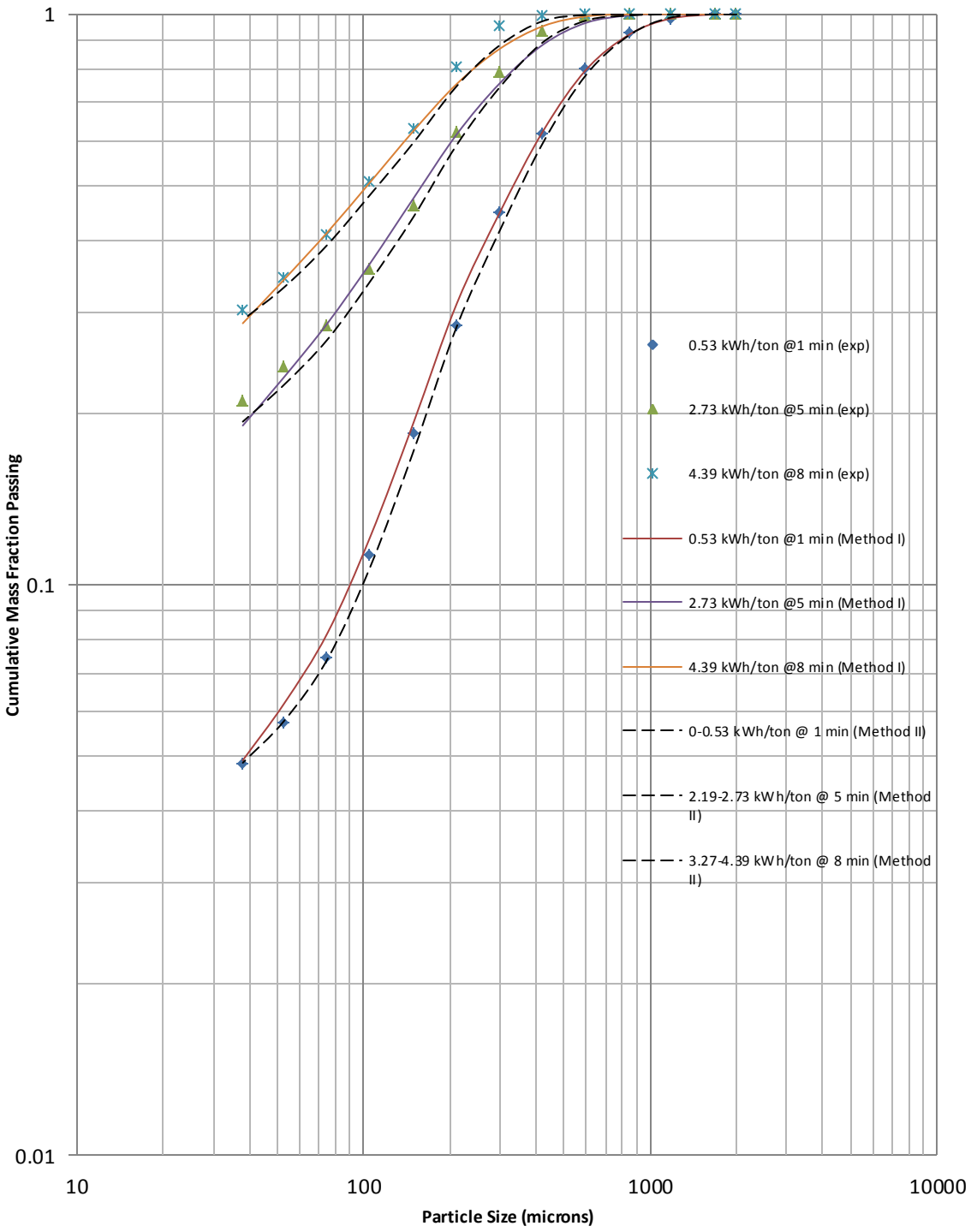

Figure 4.38.Comparison of Product Size Distributions obtained from Experimental Data, Method I and Method II (Limestone Ore, 72% solids – 100% slurry filling).

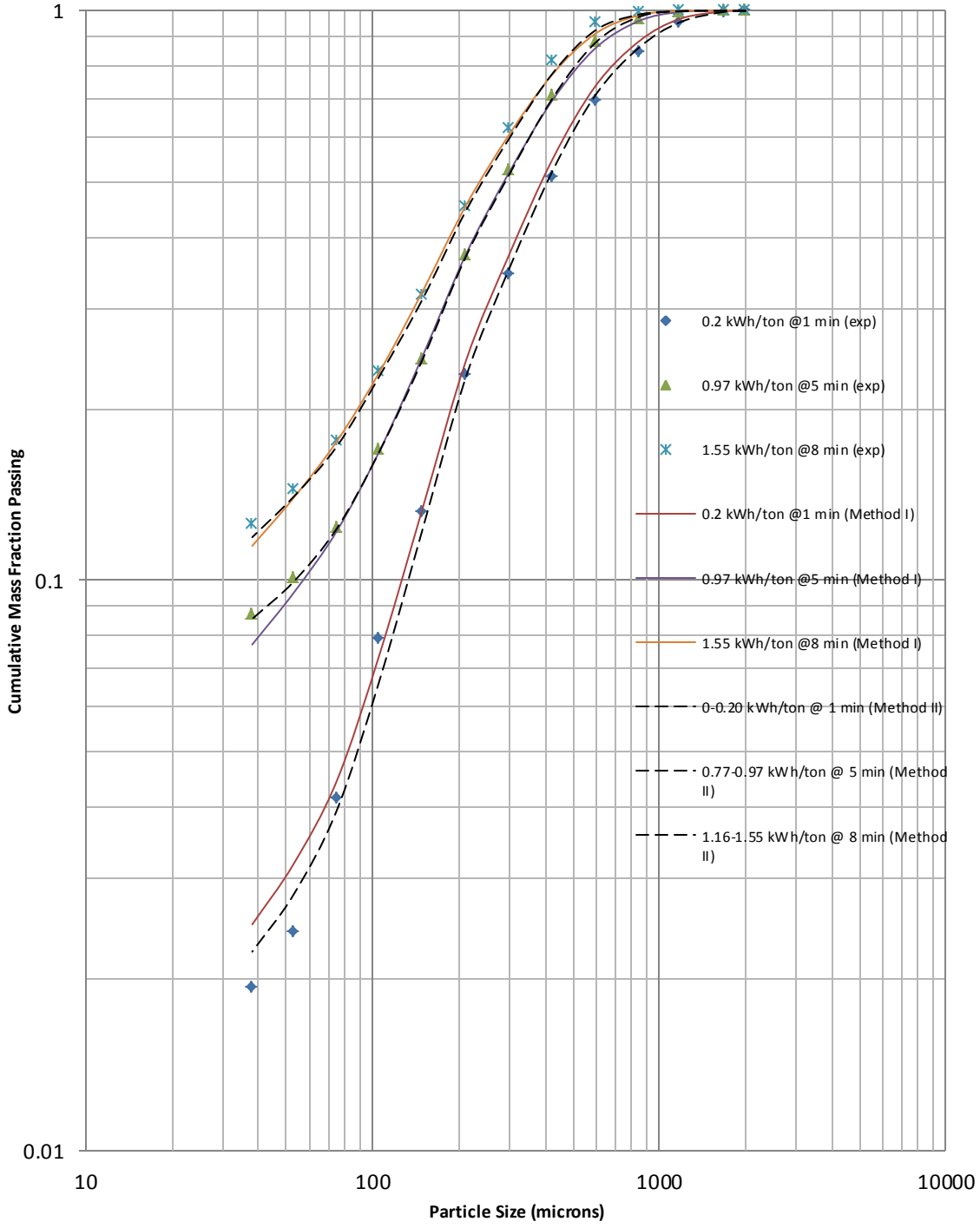

Figure 4.39.Comparison of Product Size Distributions obtained from Experimental Data, Method I and Method II (Limestone Ore, 65% solids – 260% slurry filling).

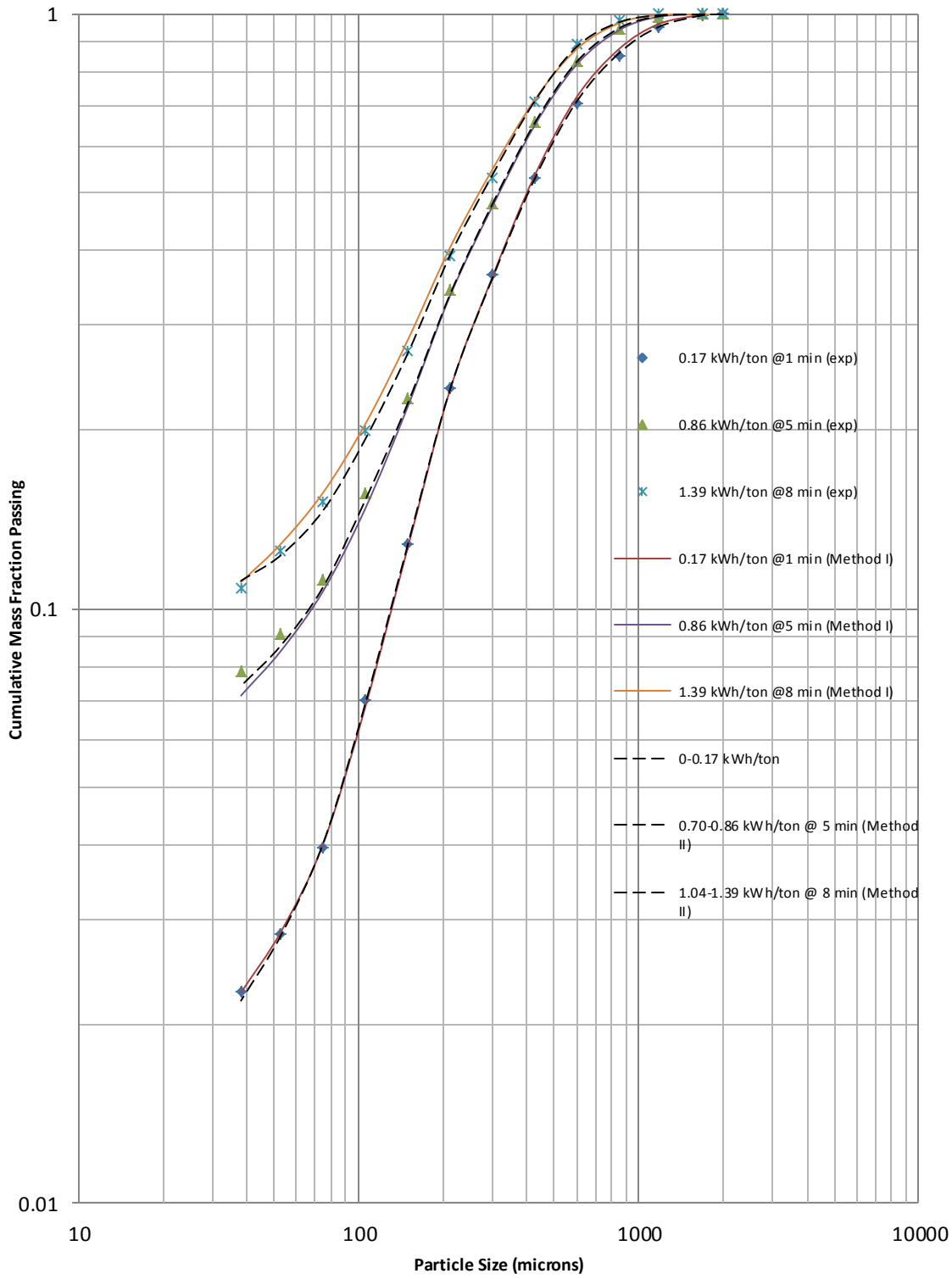

Figure 4.40.Comparison of Product Size Distributions obtained from Experimental Data, Method I and Method II (Limestone Ore, 72% solids – 260% slurry filling).

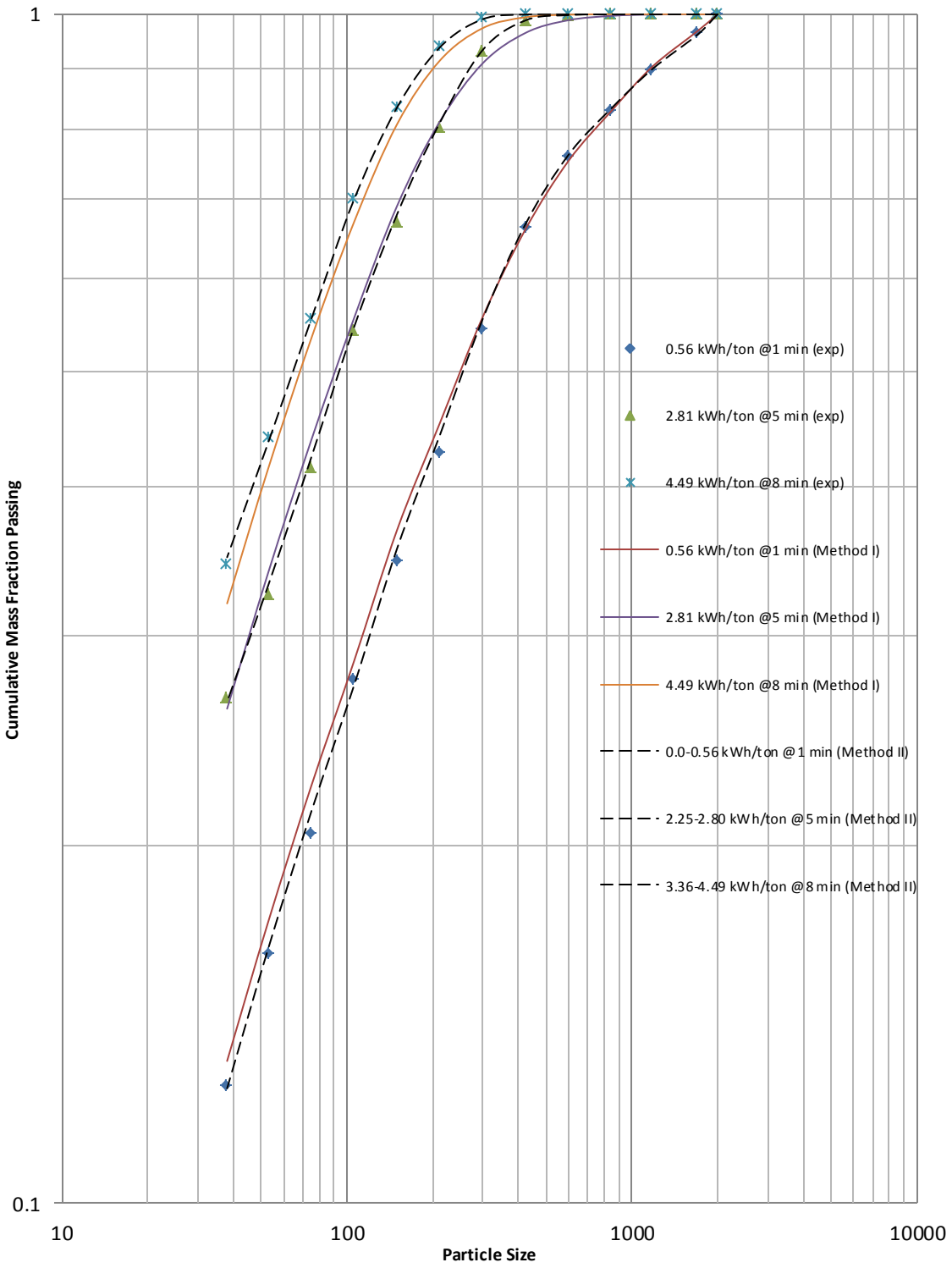

Figure 4.41.Comparison of Product Size Distributions obtained from Experimental Data, Method I and Method II (Quartzite Ore, 65% solids – 100% slurry filling).

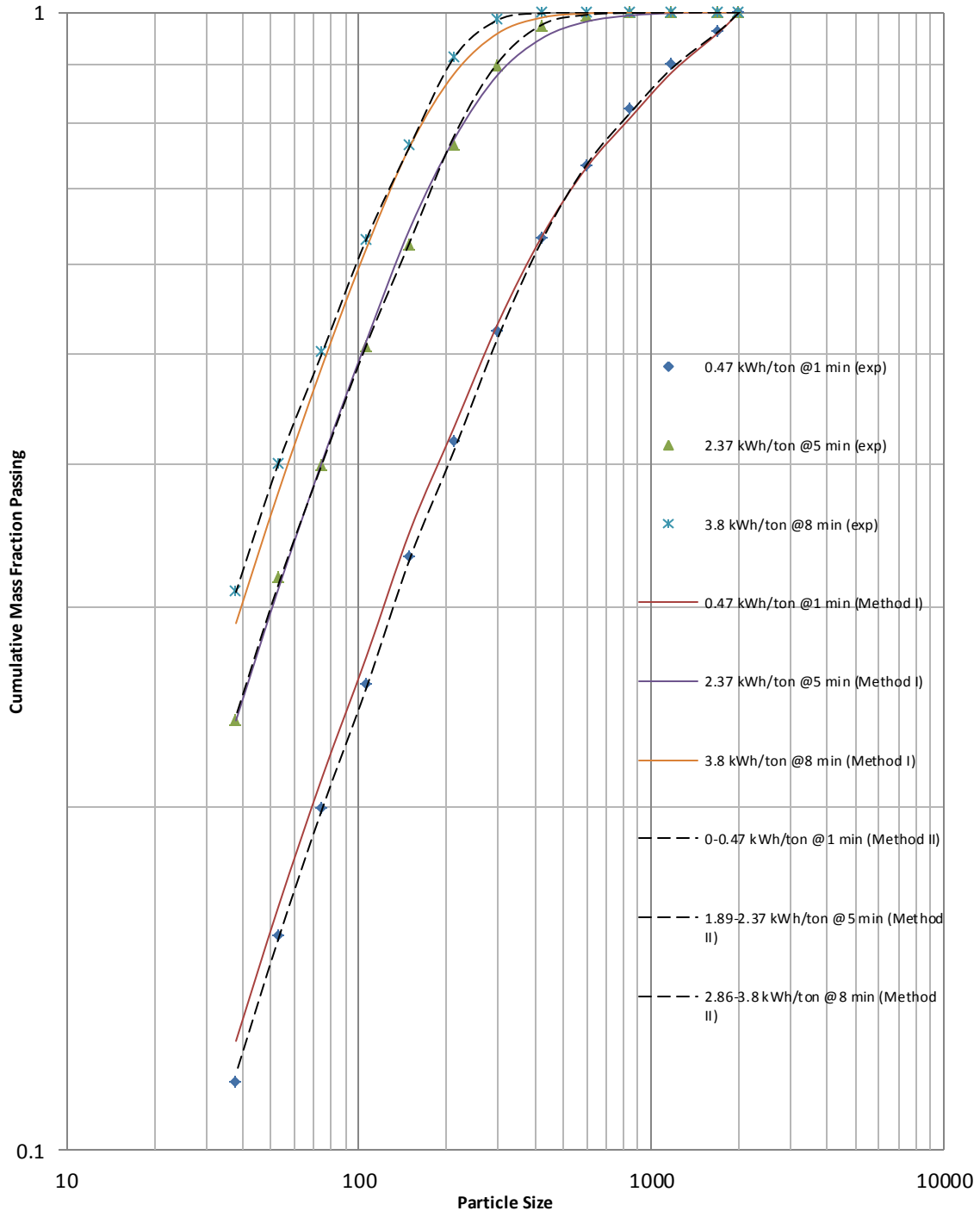

Figure 4.42.Comparison of Product Size Distributions obtained from Experimental Data, Method I and Method II (Quartzite Ore, 72% solids – 100% slurry filling).

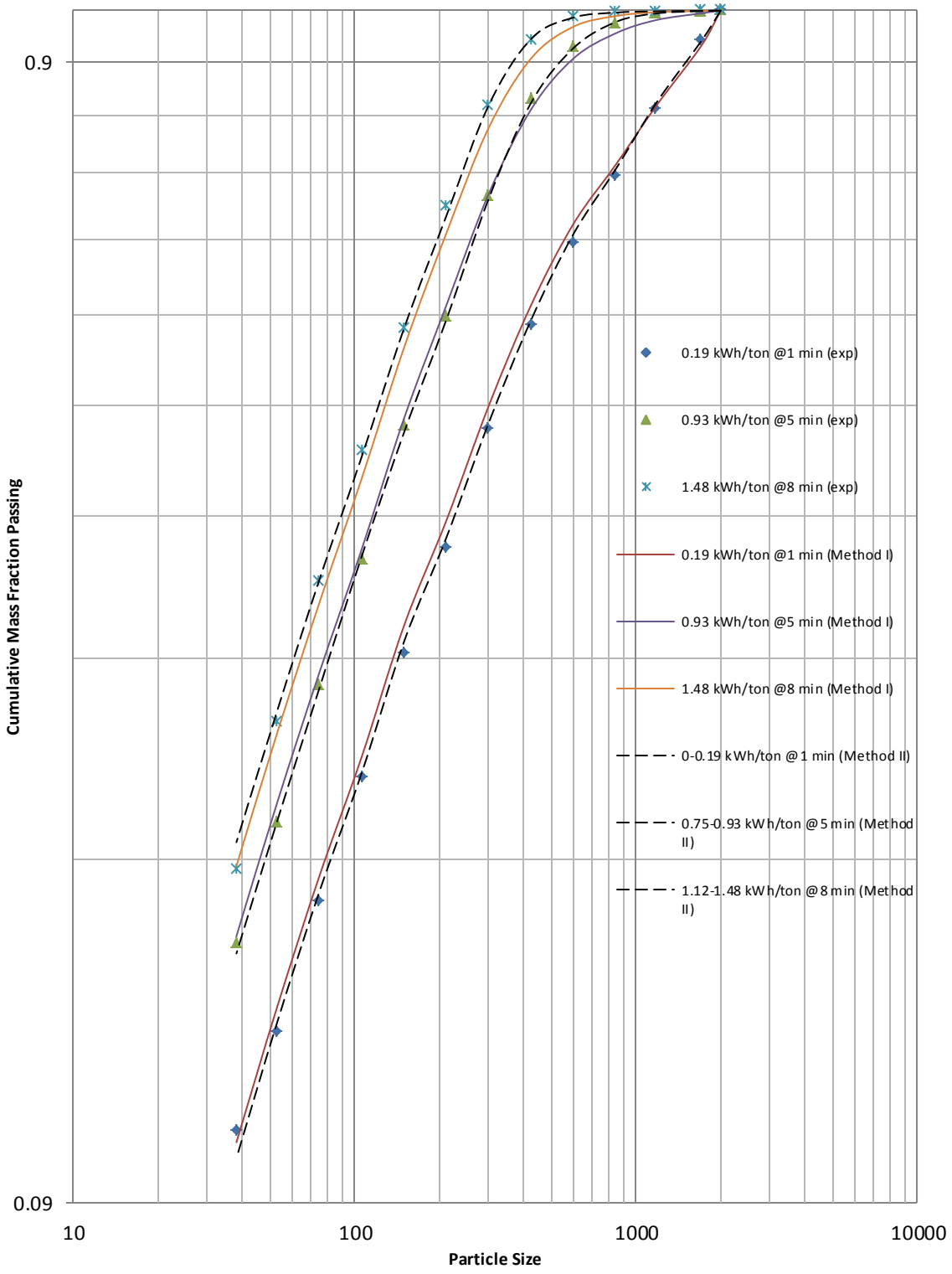

Figure 4.43.Comparison of Product Size Distributions obtained from Experimental Data, Method I and Method II (Quartzite Ore, 65% solids – 260% slurry filling).

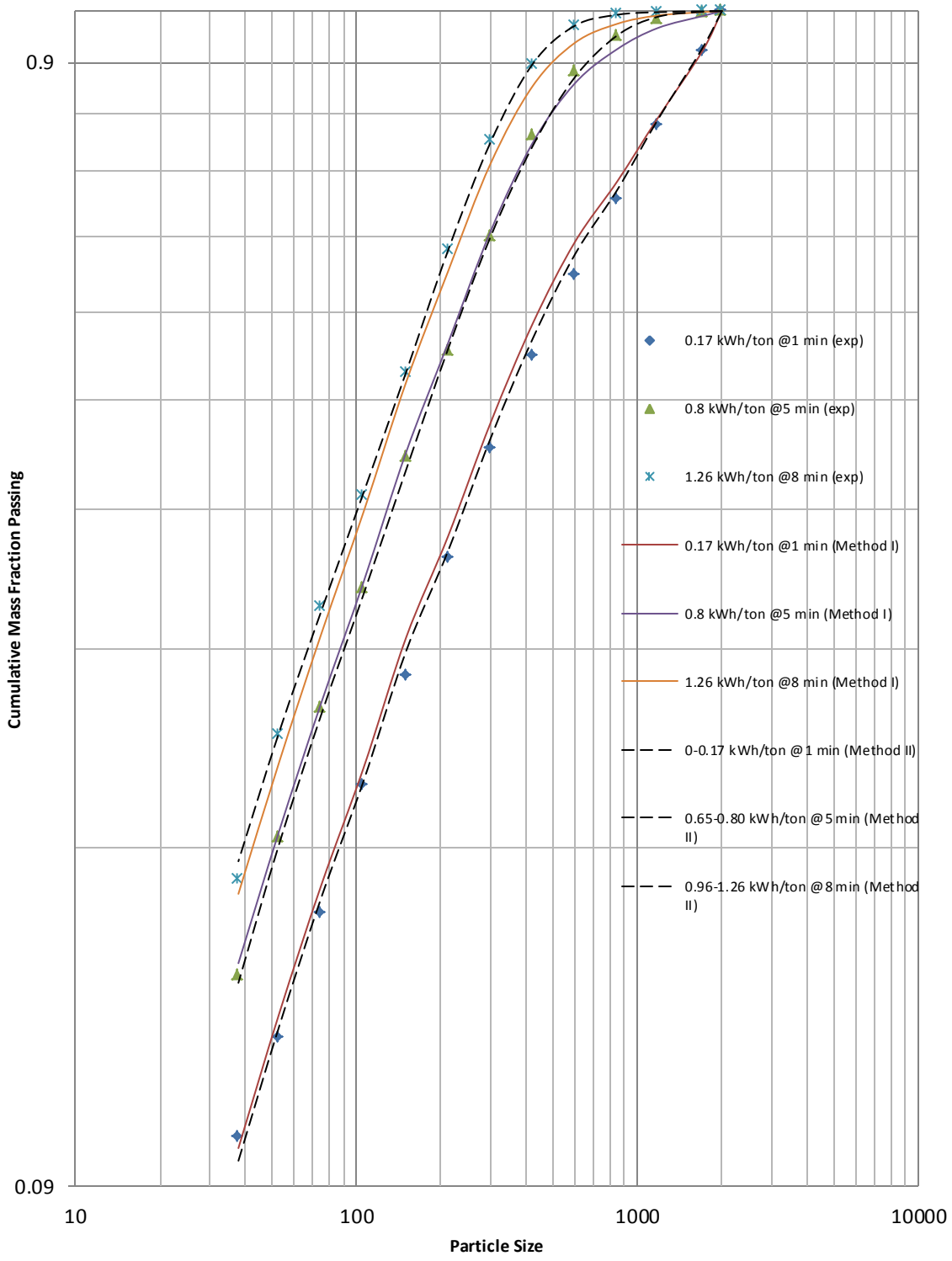

Figure 4.44.Comparison of Product Size Distributions obtained from Experimental Data, Method I and Method II (Quartzite Ore, 72% solids – 260% slurry filling).

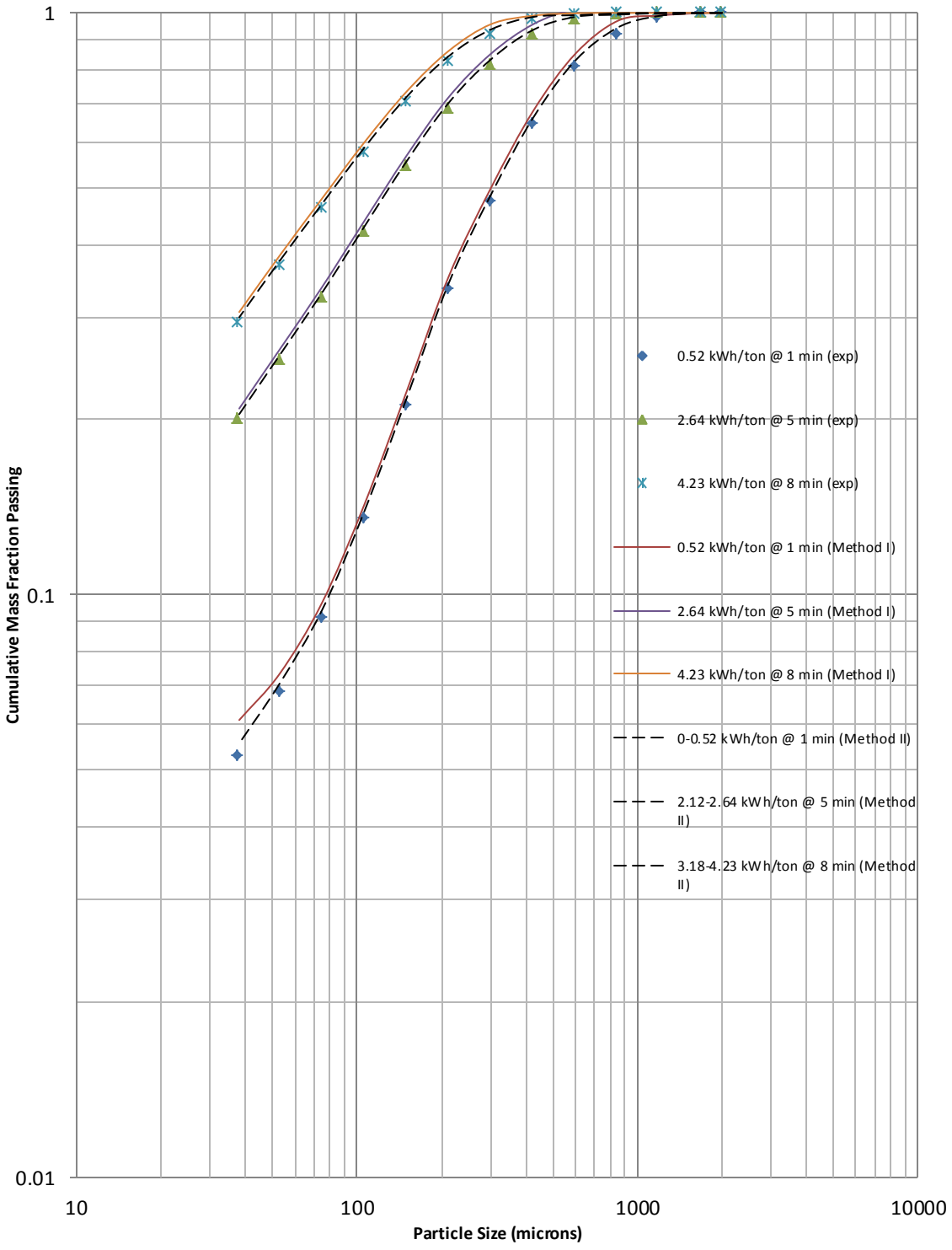

Figure 4.45.Comparison of Product Size Distributions obtained from Experimental Data, Method I and Method II (Gold Ore, 65% solids – 100% slurry filling).

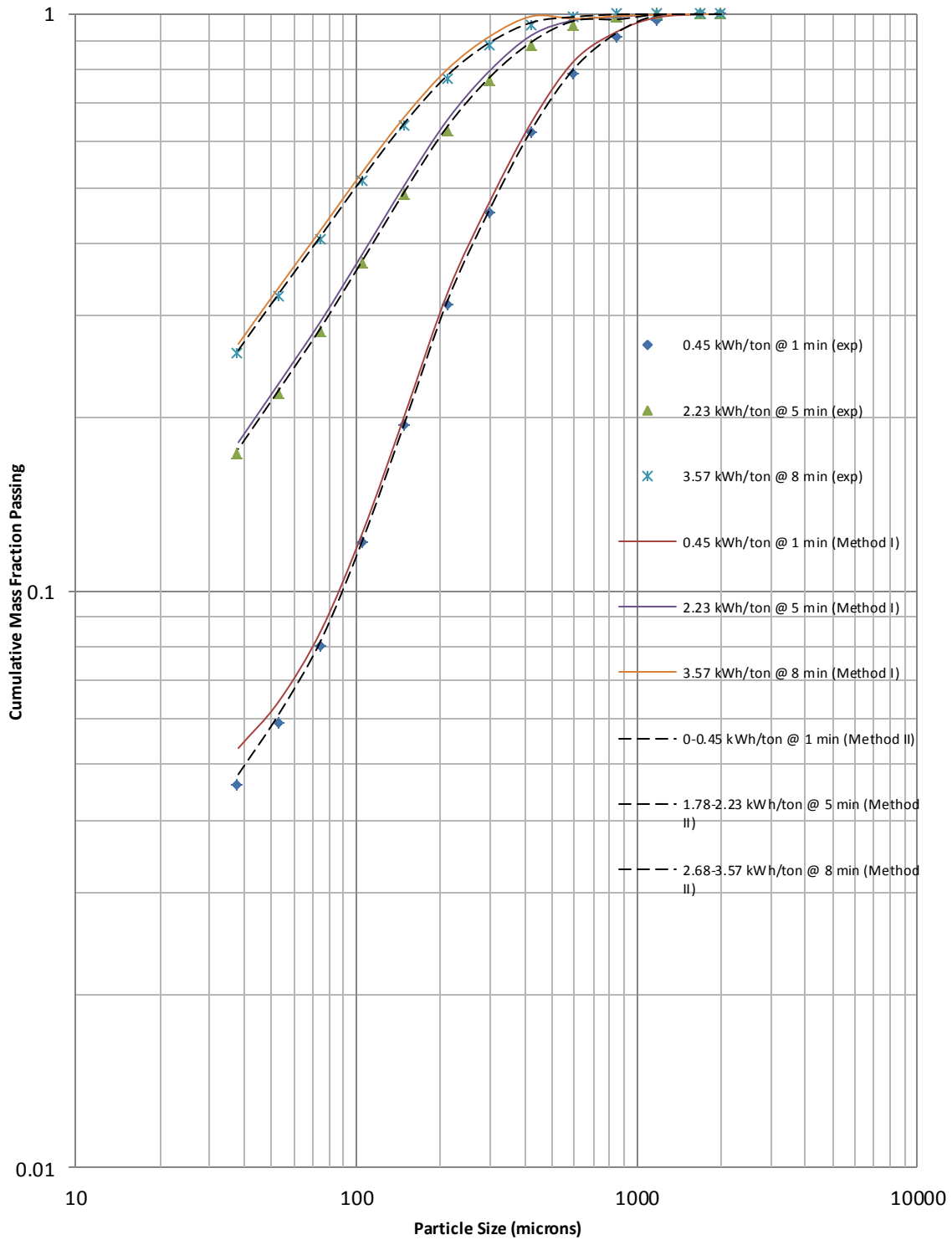

Figure 4.46.Comparison of Product Size Distributions obtained from Experimental Data, Method I and Method II (Gold Ore, 72% solids – 100% slurry filling).

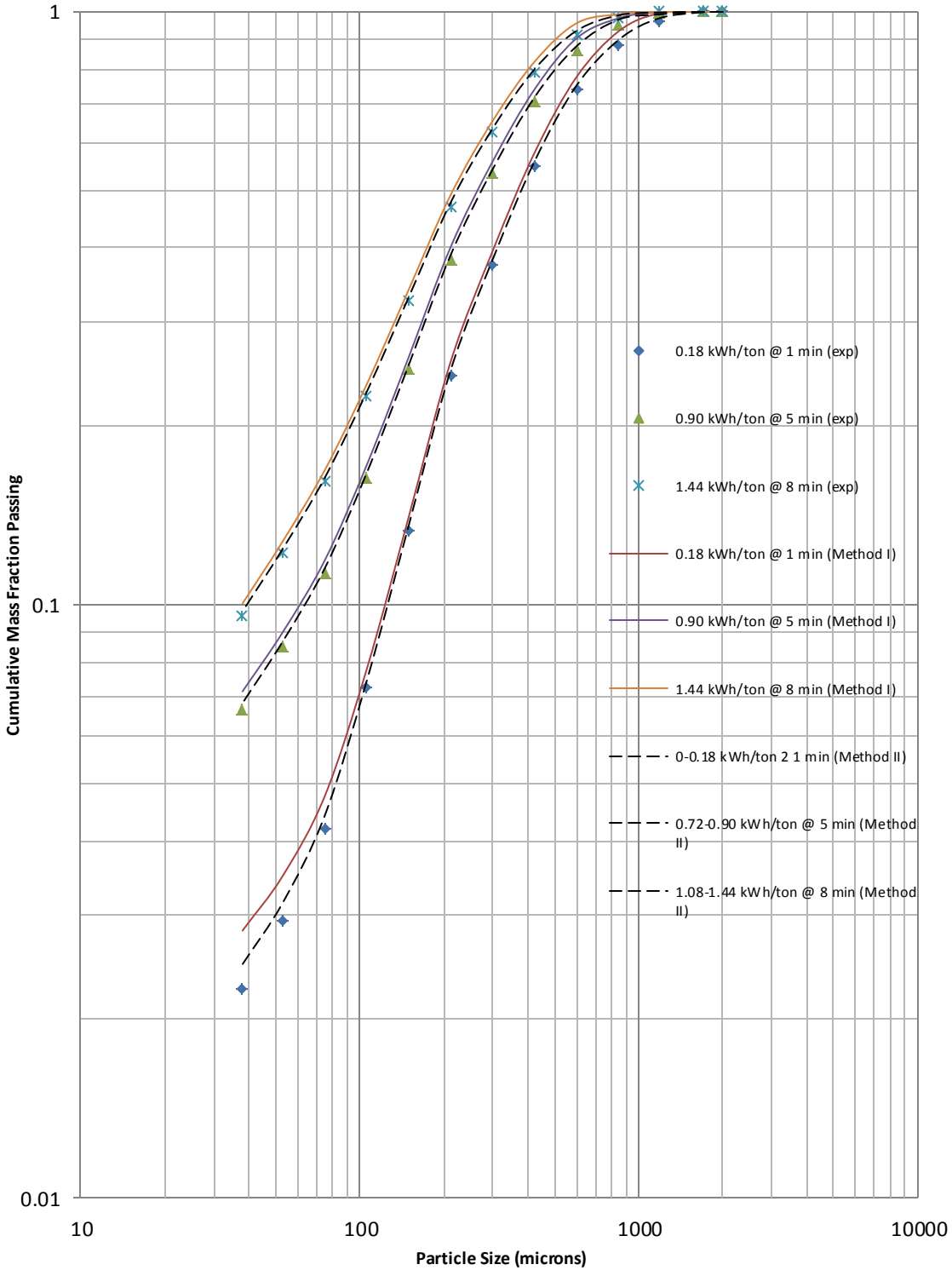

Figure 4.47.Comparison of Product Size Distributions obtained from Experimental Data, Method I and Method II (Gold Ore, 65% solids – 260% slurry filling).

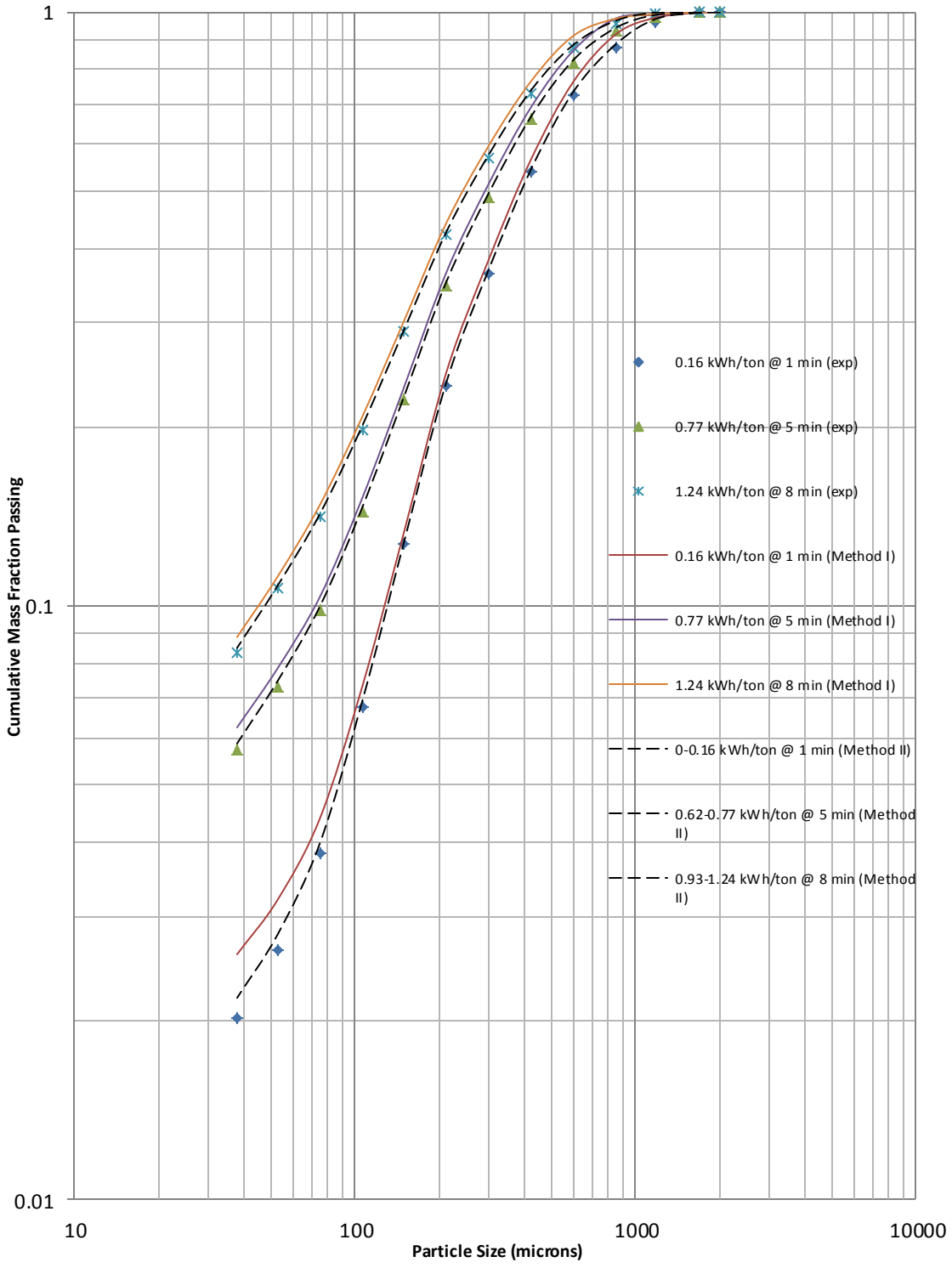

Figure 4.48.Comparison of Product Size Distributions obtained from Experimental Data, Method I and Method II (Gold Ore, 72% solids – 260% slurry filling).

4.3 Summary

Figures 4.37 through 4.48 depict trends for Method I and Method II, and as is observed, Method I is consistently failing to predictively simulate the finer size fractions in the product size distributions. As the breakage parameter estimates used as input are in the "nearly linear" region for the coarser fractions of the particle size distribution, the inability of the model to effective predict and simulate finer size fractions is evident from the plots. On the contrary, Method II, with its "near neighborhood" regime, consistently predicts product size distributions in close agreement with experimentally derived product size distributions. The effectiveness of such a method is visible in the plots, and the process of breakage rates being reiterated for each size fraction helps make convergence much more practically applicable, leading to precise predictive simulations. Such a method can be used to further scale-up and design of pilot mills and industrial mills. Table 4.5 gives a detailed insight into the RMS values derived from the predictive simulations (Method I and Method II).

Table 4.5.RMS Values Depicting the Effectiveness of Method II over Method I During Predictive Simulation.

Ore	Percent Solids (%)	Percent Slurry Filling (%)	Method I	Method II					
			Feed → 1, 2, 4, 5, 6, 8 min	Feed → 1 , 2 min	1 → 2 , 4 min	2 → 4 , 5 min	4 → 5 , 6 min	5 → 6, 8 min	6 → 8 min
Limestone	65	100	0.015	0.0083	0.0078	0.0028	0.0034	0.0051	0.0016
	72	100	0.013	0.0097	0.0022	0.0078	0.0042	0.0045	0.0021
	65	260	0.016	0.0066	0.0045	0.0038	0.0039	0.0043	0.0077
	72	260	0.0098	0.0035	0.003	0.0073	0.0027	0.008	0.0043
Quartzite	65	100	0.0151	0.0069	0.0086	0.0044	0.0048	0.0032	0.0023
	72	100	0.0164	0.0052	0.0099	0.0069	0.0056	0.0086	0.0049
	65	260	0.0149	0.0064	0.0062	0.0056	0.0043	0.0081	0.0079
	72	260	0.0157	0.0096	0.0044	0.0091	0.0058	0.0074	0.0024
Gold Ore	65	100	0.0172	0.0048	0.0059	0.0054	0.0084	0.0036	0.002
	72	100	0.0135	0.0025	0.0066	0.0077	0.0054	0.0087	0.0069
	65	260	0.0112	0.0023	0.0085	0.0059	0.0086	0.0071	0.0042
	72	260	0.0137	0.0081	0.0065	0.0046	0.0068	0.0019	0.0031

CHAPTER 5

SUMMARY AND CONCLUSIONS

This chapter provides an insight into various inferences and conclusions derived from detailed investigations in wet grinding systems, primarily to determine the dependence of breakage rates of ores of varying hardness on the fines content and milling environment, and subsequently its implications on linear and energy normalized population balance models during predictive simulations. A 10-inch batch ball mill was used for experimental study, with operating conditions being $N^{*}= 0.683$, $M^{*}_{B} = 0.3$ being constant for all wet grinding experiments. Table 3.2 summarizes the skeletal framework for all wet grinding experiments performed on natural size and mono-size materials. Table 3.1 summarizes the equilibrium ball charge distribution used during experimental work with the top ball size being 1 ½ inch. The materials used for this study were limestone, quartzite, and gold ore. The order of hardness for these ores follows in increasing order of limestone, quartzite, and gold ore. This was done to demonstrate the effect of hardness on the variation in breakage rates.

Experimental data obtained from wet grinding experiments were analyzed with respect to the batch grinding model. It was observed that hardness and brittleness of material played a substantial role in the fractional rate of breakage of various particle sizes, as is illustrated in Figures 4.4, 4.5, and 4.6. In the figures, quartzite

was observed to have the highest fractional rate of breakage due to it its extremely hard and brittle nature. Gold, being comprised primarily of granitic and gneissic rock, was the hardest material of all three, but was not as brittle as quartzite. The fractional rate of breakage for gold proved to be lower than that of quartzite. Limestone, being the softest ore of all three, had a low fractional rate of breakage, compared to other materials. Parameters like percent solids and interstitial void filling (slurry filling) also played a role in determining energy-specific breakage rates. The cumulative breakage functions were assumed to be invariant for all three materials, irrespective of variations in test conditions. The predictive simulations done later are in close agreement with experimentally derived particle size distributions for natural size and mono-size experiments.

Specific selection functions ($S_i^E = S_i$ (P/H) were also observed to be independent of ball load and mill speed. The breakage distribution modulus were also calculated for each material, providing an overview on the average particle distribution for the finer size fractions in the form of a slope of the cumulative breakage function versus the particle size on a log-log plot. This plot was also used to evaluate α_1, α_2, and α_3 in the form of cumulative breakage functions.

The prime focus of this research was to observe the inherent nonlinearities in breakage rates during wet grinding of various materials, and trying to correlate their dependence on the fines content, milling environment, size consist, and other such parameters like percent solids and slurry filling in a cause-effect manner. The variation in breakage rates as a function of size consist in the mill was investigated in the study. The conclusions from this research have been summarized as follows:

1. For wet grinding systems, the breakage functions for various materials are assumed to be invariant with respect to mill operating conditions. B_{ij} was estimated using a graphical procedure (refer Section 4.1). Mono-size wet grinding experiments were performed and α_1, α_2, and α_3 were determined.
2. The selection functions were strongly proportional and dependent on the specific energy input to the mill. The specific selection functions based on specific energy input were inherently dependent on the particle size distribution or size consist in the mill. 1^{st} order specific selection functions were estimated using initial estimates of S_1^E from mono-size experiments and ζ_1 from the slope of the zero order production constants. Thereafter, S_1^E and ζ_1 outputs obtained incrementally were used for estimation. This showed nonlinearity trends for varying test conditions (percent solids and slurry filling) for all three materials in context of the mean particle size or fulcrum below which nonlinearities were observed.
3. Fulcrum values were explained for all the three ores in context of percent solids and slurry filling. It was hypothesized that varying the percent solids with respect to constant slurry filling and vice versa reported variation in the magnitude of the fulcrum values, thereby indicating their effects on the breakage rates. An increase in the percent solids tended to increase the slurry viscosity. This, in turn, increased the fulcrum value, which consequently caused nonlinearity trends at higher values of the mean particle size. Therefore, it is hypothesized that variation in percent solids varied slurry viscosity (refer to Tables 4.6, 4.11, 4.16).
4. Hardness of gold ore caused rapid incremental increases in energy-specific breakage rates, whilst the breakage rates of subsequent finer size fractions

decreased gradually due to the hardness factor. Quartzite, though a hard ore, depicted its brittle nature with a rapid decrease in breakage rates for its finer size fractions and subsequent increase in the coarser size fractions, but with extended grind times, energy-specific breakage rates for the coarser size fractions started decreasing. This phenomenon can be attributed to an excessive amount of fines produced, which caused a rapid increase in the number of contact points receiving the impact energy. Limestone, being the softest ore of all three, depicted breakage properties in accordance with previously established literature: breakage rates of coarser size fractions increase with an increase in the amount of fines, with a subsequent decrease in the breakage rates for the finer size fractions.

5. 2^{nd} order specific selection functions based on incremental inputs of specific energy displayed inherent nonlinearities in the wet grinding process in realtime. The plots showed that an increase in grind time only caused an increase in the amount of fines in the particle population, thereby causing more contact points to occur for energy to be transmitted to coarser size fractions in the mill, due to their great collision cross-section in comparison to the finer size fractions.
6. Two distinct methods were used to describe the effect of such nonlinearities. The first model considered breakage parameters in the "nearly linear" region. Simulations were not performed in an incremental manner, but rather in a cumulative fashion, which caused the nonlinearities to show up with extended grind times, thereby rendering the estimating capabilities of this model limited. The estimated output of this model was limited as the coarser size fractions of experimental data were simulated to a great extent, but the finer size fractions

were not simulated correctly, due to nonconsideration of the preferential breakage phenomenon in this scheme.

7. The 2nd method used an incremental scheme of input for specific energy, which took into consideration an iterative mechanism creating reference mass fractions, and applying the convergence criteria against experimentally derived product size distributions, modifying the energy-specific breakage rates with each iteration, until the RMS values were reduced to a minimum. This rendered the 2nd method more apt at predicting such experimental data, taking into consideration the inherent nonlinearities observed in wet grinding systems. This also illustrated that the breakage rates are varied with the size consist in the mill. This is the essential finding or conclusion of this research work.

APPENDIX A

EXPERIMENTAL PRODUCT SIZE DISTRIBUTIONS

Table A-1 (Limestone)						
Mill Size: 10"		Medium: Wet		Feed Size: -10 mesh (Natural)		
M^*_B = 0.3	Average Power (kW) = 0.0724			Mass Holdup (tons) = 0.001925		
Percent Solids (%) = 65			Percent Slurry Filling (%) = 100			
Mill Speed (rpm) = 61.8	Grind Time (min)					
Size	1	2	4	5	6	8
	Energy (kWh/ton)					
(Mesh)	0.6061	1.2828	2.4573	3.1514	3.6364	5.3044
-9	1.0000	1.0000	1.0000	1.0000	1.0000	1.0000
-10	0.9989	0.9986	0.9998	1.0000	1.0000	1.0000
-14	0.9821	0.9865	0.9990	0.9996	1.0000	1.0000
-20	0.9326	0.9503	0.9968	0.9982	0.9996	1.0000
-28	0.8148	0.8683	0.9872	0.9917	0.9983	0.9998
-35	0.6254	0.7091	0.9379	0.9518	0.9853	0.9970
-48	0.4554	0.5275	0.8005	0.8314	0.9133	0.9704
-65	0.2845	0.3783	0.6233	0.6632	0.7679	0.8708
-100	0.1834	0.2575	0.4499	0.4965	0.5921	0.7066
-150	0.1131	0.1851	0.3364	0.3933	0.4640	0.5716
-200	0.0773	0.1401	0.2621	0.3050	0.3705	0.4523
-270	0.0596	0.1161	0.2179	0.2645	0.3147	0.3916
-400	0.0490	0.0999	0.1881	0.2282	0.2765	0.3374

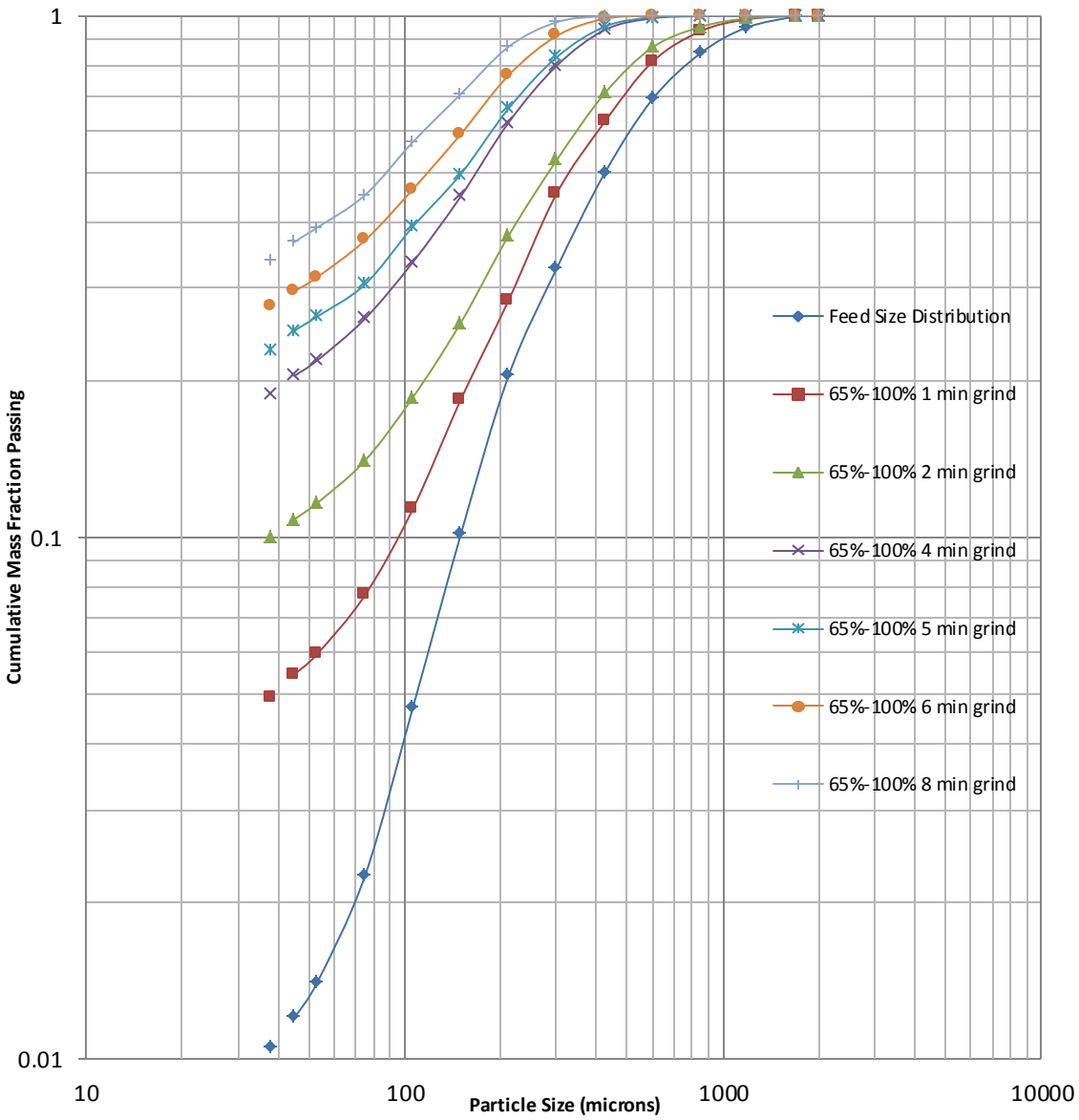

Figure A-1: Experimentally Derived Product Size Distribution (65% solids-100% slurry filling) for Limestone (-10 mesh natural size).

Table A-2 (Limestone)						
Mill Size: 10"		Medium: Wet		Feed Size: -10 mesh (Natural)		
M^*_B = 0.3	Average Power (kW) = 0.0732			Mass Holdup (tons) = 0.00225		
Percent Solids (%) = 72			Percent Slurry Filling (%) = 100			
Mill Speed (rpm) = 61.7	Grind Time (min)					
Size	1	2	4	5	6	8
	Energy (kWh/ton)					
(Mesh)	0.5339	1.0689	2.1902	2.7267	3.2657	4.3858
-9	1.0000	1.0000	1.0000	1.0000	1.0000	1.0000
-10	0.9988	0.9992	1.0000	1.0000	1.0000	1.0000
-14	0.9804	0.9863	0.9986	0.9996	1.0000	1.0000
-20	0.9270	0.9403	0.9925	0.9978	0.9991	0.9998
-28	0.8022	0.8354	0.9664	0.9884	0.9941	0.9996
-35	0.6139	0.6584	0.8675	0.9334	0.9563	0.9948
-48	0.4484	0.4817	0.6988	0.7889	0.8301	0.9495
-65	0.2828	0.3451	0.5364	0.6189	0.6696	0.8054
-100	0.1832	0.2301	0.3888	0.4598	0.5075	0.6277
-150	0.1121	0.1638	0.2956	0.3571	0.4037	0.5080
-200	0.0741	0.1222	0.2320	0.2844	0.3271	0.4088
-270	0.0571	0.1003	0.1948	0.2397	0.2778	0.3448
-400	0.0483	0.0867	0.1696	0.2099	0.2478	0.3025

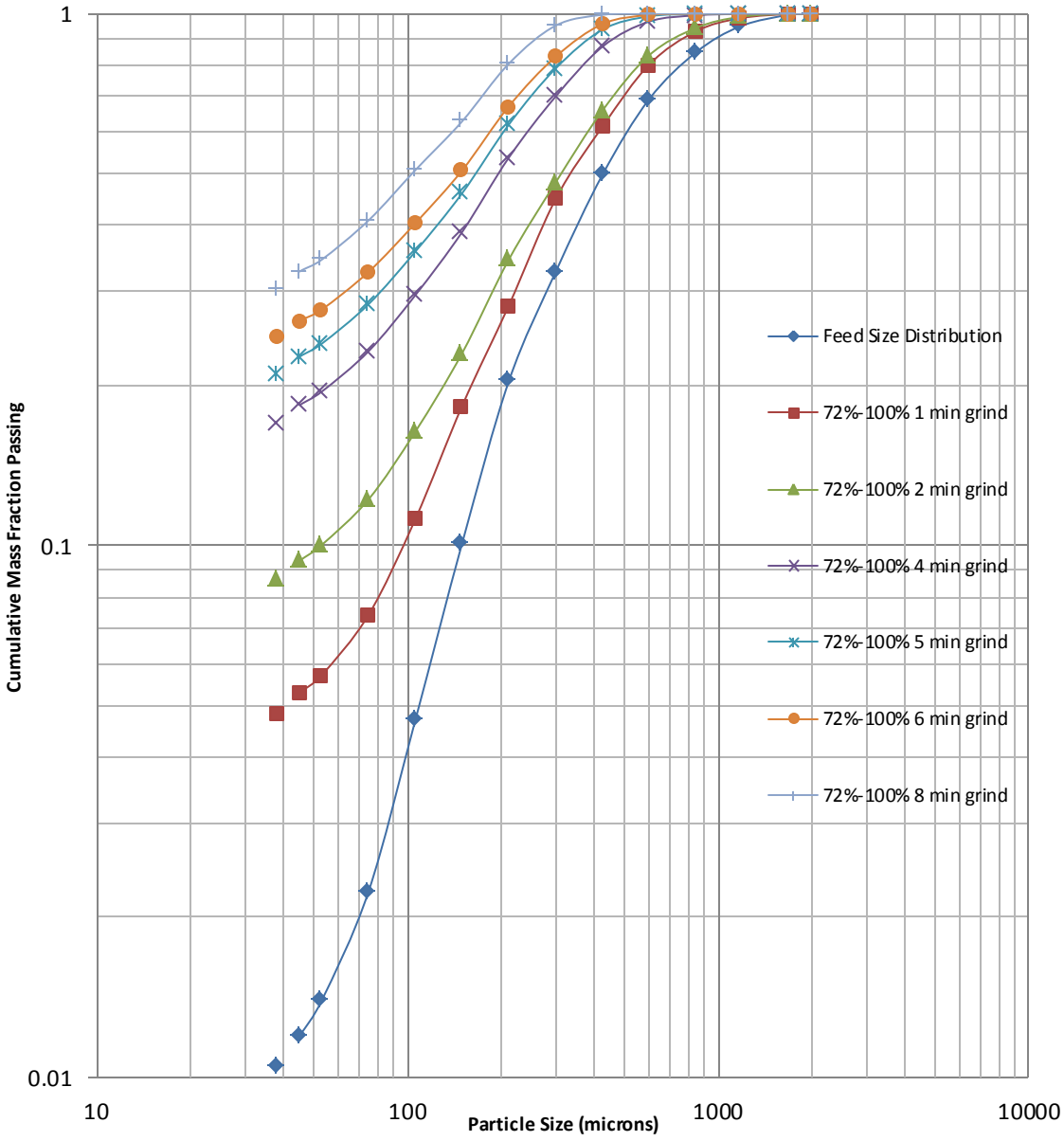

Figure A-2: Experimentally Derived Product Size Distribution (72% solids-100% slurry filling) for Limestone (-10 mesh natural size).

Table A-3 (Limestone)						
Mill Size: 10"		Medium: Wet		Feed Size: -10 mesh (Natural)		
M^*_B = 0.3	Average Power (kW) = 0.0584			Mass Holdup (tons) = 0.00501		
Percent Solids (%) = 65			Percent Slurry Filling (%) = 260			
Mill Speed (rpm) = 61.9	Grind Time (min)					
Size	1	2	4	5	6	8
	Energy (kWh/ton)					
(Mesh)	0.1975	0.3905	0.7783	0.9659	1.1594	1.5482
-9	1.0000	1.0000	1.0000	1.0000	1.0000	1.0000
-10	0.9958	0.9979	0.9995	0.9998	0.9999	1.0000
-14	0.9526	0.9702	0.9917	0.9955	0.9972	0.9993
-20	0.8481	0.8805	0.9524	0.9704	0.9803	0.9933
-28	0.6979	0.7369	0.8412	0.8840	0.9071	0.9552
-35	0.5124	0.5512	0.6593	0.7117	0.7387	0.8147
-48	0.3460	0.3813	0.4759	0.5251	0.5474	0.6198
-65	0.2290	0.2489	0.3371	0.3730	0.3969	0.4549
-100	0.1321	0.1445	0.2167	0.2453	0.2683	0.3168
-150	0.0790	0.0865	0.1450	0.1702	0.1923	0.2329
-200	0.0415	0.0550	0.1031	0.1242	0.1424	0.1759
-270	0.0241	0.0405	0.0822	0.1008	0.1170	0.1449
-400	0.0193	0.0335	0.0702	0.0869	0.1005	0.1256

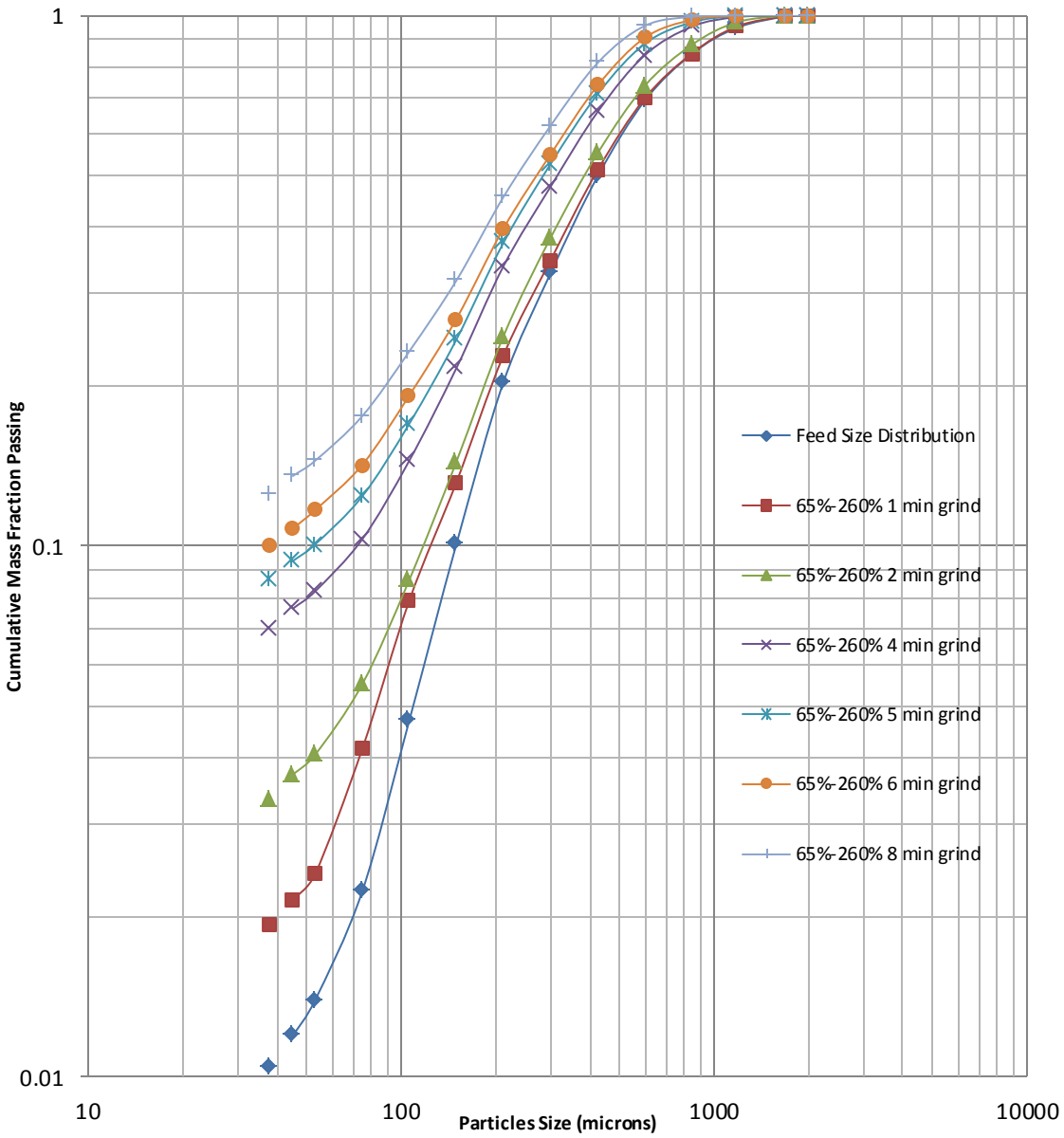

Figure A-3: Experimentally Derived Product Size Distribution (65% solids-260% slurry filling) for Limestone (-10 mesh natural size).

Table A-4 (Limestone)						
Mill Size: 10"		Medium: Wet		Feed Size: -10 mesh (Natural)		
M^*_B = 0.3	Average Power (kW) = 0.06107			Mass Holdup (tons) = 0.005852		
Percent Solids (%) = 72			Percent Slurry Filling (%) = 260			
Mill Speed (rpm) = 61.8	Grind Time (min)					
Size	1	2	4	5	6	8
	Energy (kWh/ton)					
(Mesh)	0.1743	0.3518	0.6951	0.8591	1.0405	1.3945
-9	1	1	1	1	1	1
-10	0.9953	0.9974	0.9985	0.9993	0.9997	0.9998
-14	0.9507	0.9633	0.9817	0.9891	0.9937	0.9960
-20	0.8482	0.8738	0.9210	0.9434	0.9630	0.9739
-28	0.7041	0.7331	0.7912	0.8313	0.8695	0.8864
-35	0.5273	0.5567	0.6101	0.6551	0.6972	0.7101
-48	0.3637	0.3913	0.4354	0.4802	0.5182	0.5280
-65	0.2336	0.2612	0.3000	0.3426	0.3754	0.3903
-100	0.1283	0.1531	0.1897	0.2254	0.2519	0.2708
-150	0.0698	0.0923	0.1262	0.1560	0.1767	0.1987
-200	0.0395	0.0584	0.0870	0.1113	0.1298	0.1504
-270	0.0281	0.0440	0.0687	0.0900	0.1056	0.1244
-400	0.0226	0.0362	0.0589	0.0779	0.0907	0.1078

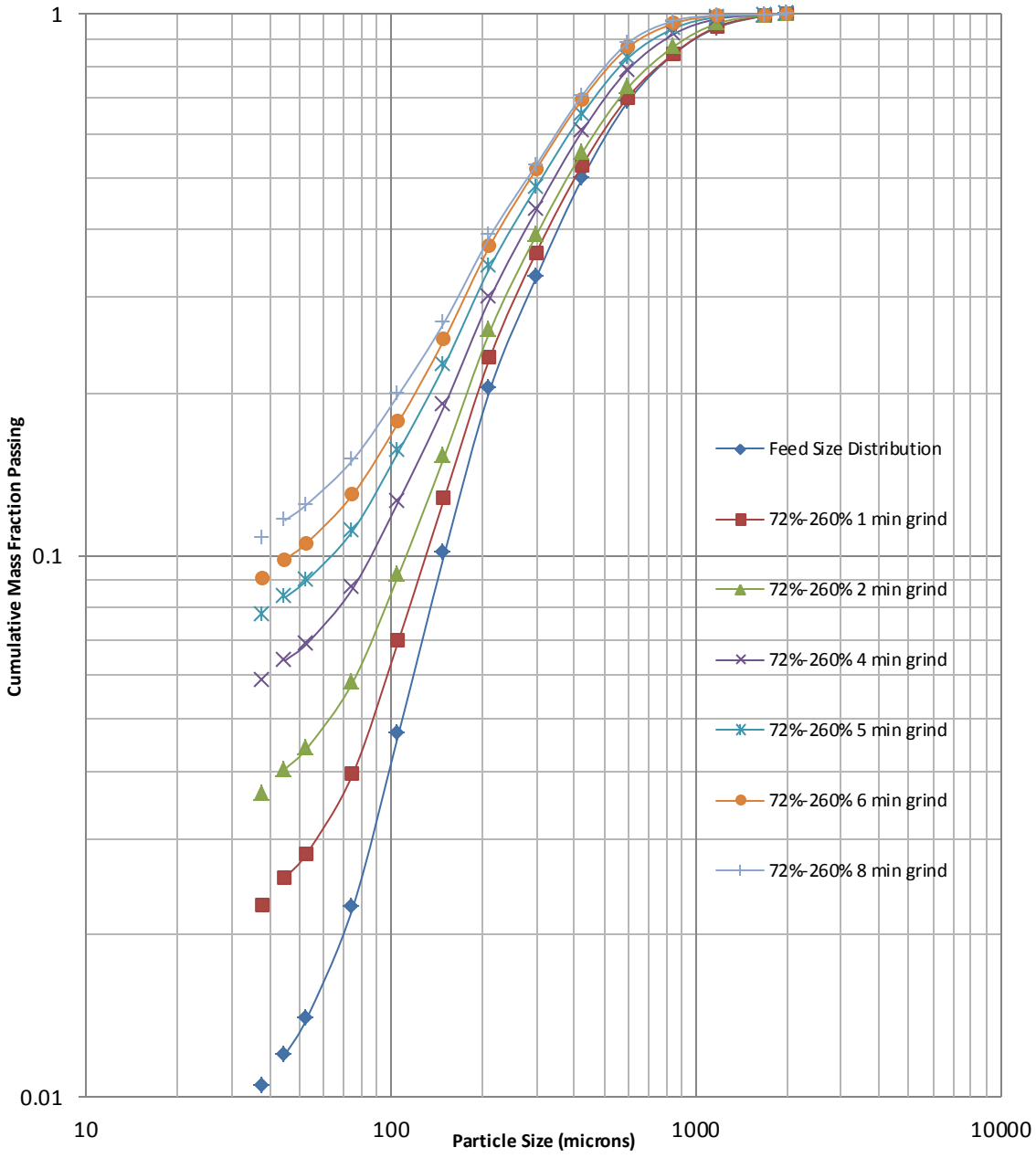

Figure A-4: Experimentally Derived Product Size Distribution (72% solids-260% slurry filling) for Limestone (-10 mesh natural size).

Table A-5 (Limestone)				
Mill Size: 10"	Medium: Wet	Feed Size: 10 x 14 (mono-size)		
M^*_B = 0.3	Average Power (kW) = 0.0644		Mass Holdup (tons) = 0.00225	
Percent Solids (%) = 72		Percent Slurry Filling (%) = 100		
Mill Speed (rpm) = 61.8	Grind Time (min)			
Size	1	2	4	6
	Energy (kWh/ton)			
(Mesh)	0.4631	0.9497	1.9198	2.9440
-9	1.0000	1.0000	1.0000	1.0000
-10	0.9786	0.9788	0.9956	0.9992
-14	0.3760	0.5745	0.8618	0.9692
-20	0.2045	0.3775	0.6844	0.9023
-28	0.1368	0.2640	0.5281	0.7757
-35	0.1010	0.1993	0.4069	0.6234
-48	0.0781	0.1556	0.3321	0.5162
-65	0.0625	0.1252	0.2700	0.4229
-100	0.0504	0.1014	0.2231	0.3481
-150	0.0427	0.0867	0.1915	0.3006
-200	0.0370	0.0744	0.1650	0.2589
-270	0.0327	0.0649	0.1455	0.2284
-400	0.0287	0.0567	0.1292	0.2048

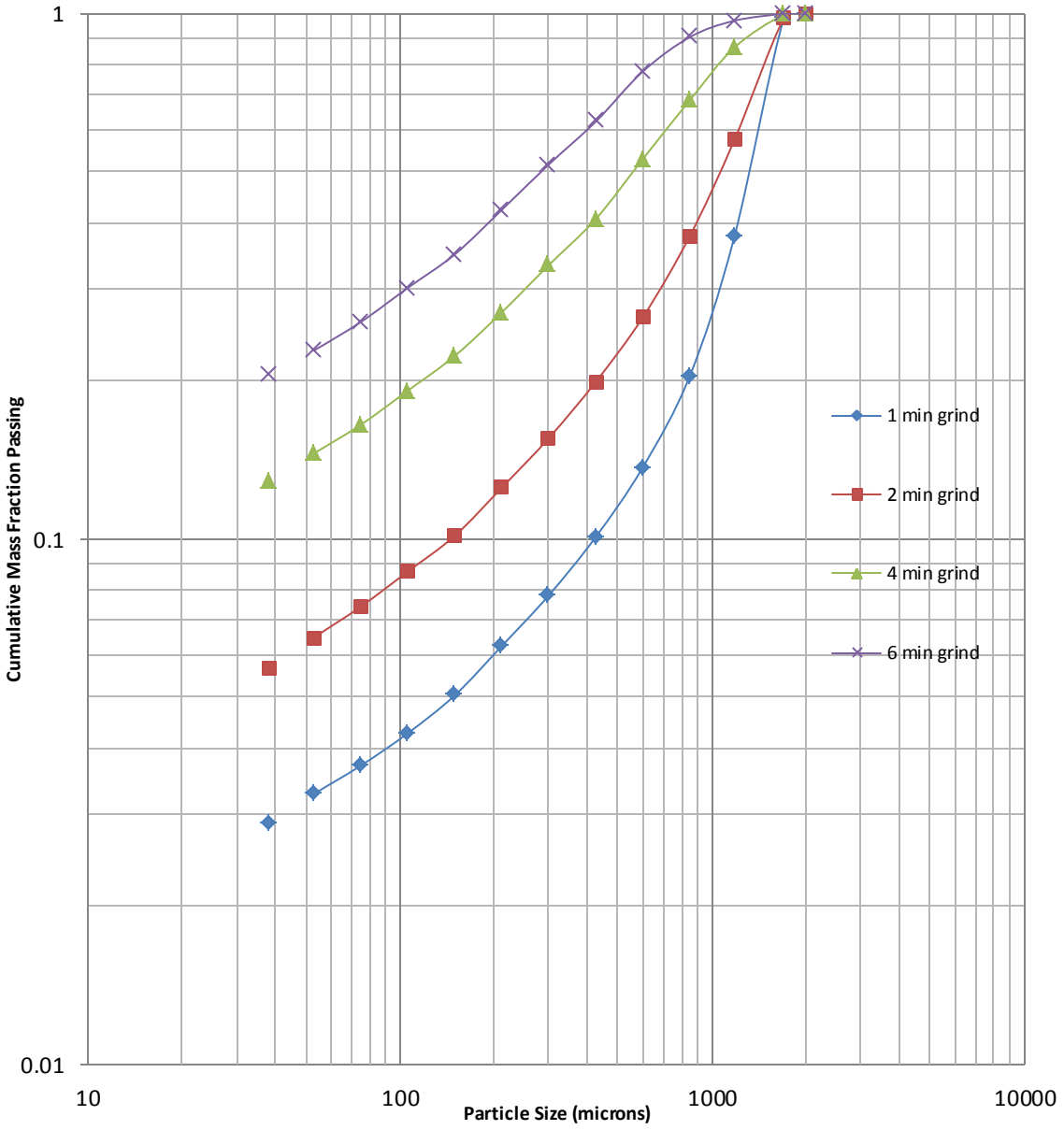

Figure A-5: Experimentally Derived Product Size Distribution (72% solids-100% slurry filling) for Limestone (10x14 mesh mono-size).

Table A-6 (Quartzite)						
Mill Size: 10"		Medium: Wet		Feed Size: -10 mesh (Natural)		
M^*_B = 0.3	Average Power (kW) = 0.0657			Mass Holdup (tons) = 0.00195		
Percent Solids (%) = 65			Percent Slurry Filling (%) = 100			
Mill Speed (rpm) = 61.8	Grind Time (min)					
Size	1	2	4	5	6	8
	Energy (kWh/ton)					
(Mesh)	0.5636	1.1213	2.2513	2.8054	3.3605	4.4885
-9	1.0000	1.0000	1.0000	1.0000	1.0000	1.0000
-10	0.9630	0.9889	0.9997	0.9997	1.0000	1.0000
-14	0.8974	0.9689	0.9986	0.9988	1.0000	1.0000
-20	0.8295	0.9407	0.9967	0.9982	0.9999	1.0000
-28	0.7579	0.8995	0.9919	0.9954	0.9993	0.9997
-35	0.6619	0.8236	0.9727	0.9859	0.9963	0.9992
-48	0.5431	0.6927	0.8911	0.9300	0.9670	0.9918
-65	0.4281	0.5544	0.7476	0.8023	0.8634	0.9379
-100	0.3463	0.4499	0.6165	0.6676	0.7328	0.8333
-150	0.2753	0.3531	0.4906	0.5408	0.5949	0.6992
-200	0.2044	0.2729	0.3783	0.4149	0.4638	0.5540
-270	0.1619	0.2114	0.2947	0.3249	0.3643	0.4405
-400	0.1255	0.1601	0.2358	0.2657	0.2934	0.3439

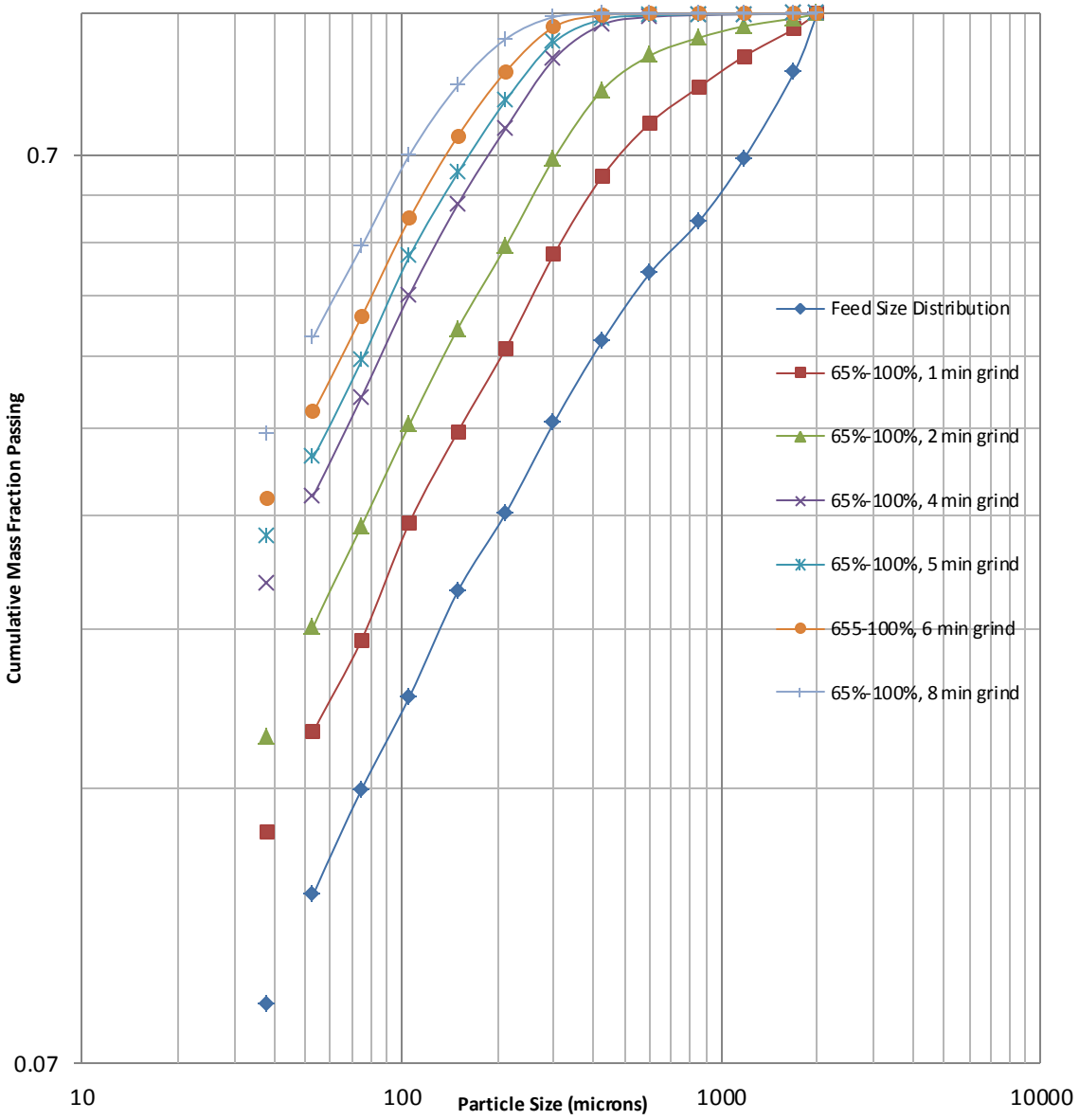

Figure A-6: Experimentally Derived Product Size Distribution (65% solids-100% slurry filling) for Quartzite (-10 mesh natural size).

Table A-7 (Quartzite)						
Mill Size: 10"		Medium: Wet		Feed Size: -10 mesh (Natural)		
M^*_B = 0.3	Average Power (kW) = 0.0667			Mass Holdup (tons) = 0.00234		
Percent Solids (%) = 72			Percent Slurry Filling (%) = 100			
Mill Speed (rpm) = 61.7	Grind Time (min)					
Size	1	2	4	5	6	8
	Energy (kWh/ton)					
(Mesh)	0.4746	0.9524	1.8937	2.3734	2.8551	3.7995
-9	1.0000	1.0000	1.0000	1.0000	1.0000	1.0000
-10	0.9628	0.9834	0.9993	0.9994	1.0000	1.0000
-14	0.8989	0.9575	0.9981	0.9988	0.9998	1.0000
-20	0.8223	0.9193	0.9958	0.9973	0.9993	0.9999
-28	0.7319	0.8571	0.9897	0.9925	0.9980	0.9995
-35	0.6315	0.7613	0.9629	0.9712	0.9913	0.9982
-48	0.5239	0.6368	0.8745	0.8960	0.9411	0.9851
-65	0.4197	0.5128	0.7360	0.7648	0.8116	0.9131
-100	0.3319	0.3999	0.5817	0.6234	0.6797	0.7642
-150	0.2565	0.3160	0.4652	0.5073	0.5548	0.6313
-200	0.1995	0.2472	0.3621	0.3998	0.4353	0.5023
-270	0.1539	0.1869	0.2802	0.3178	0.3464	0.4008
-400	0.1146	0.1267	0.2125	0.2386	0.2663	0.3092

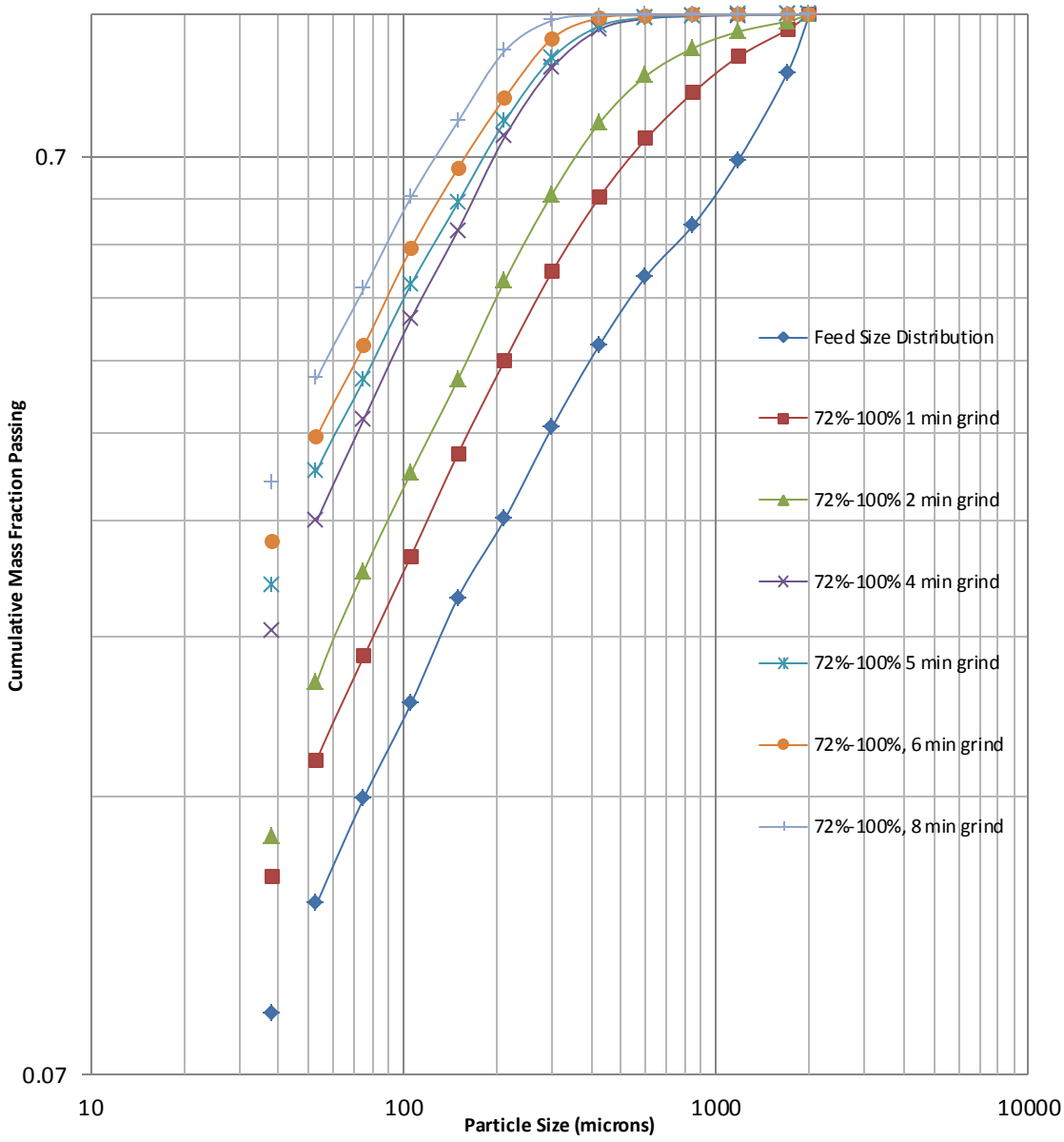

Figure A-7: Experimentally Derived Product Size Distribution (72% solids-100% slurry filling) for Quartzite (-10 mesh natural size).

Table A-8 (Quartzite)						
Mill Size: 10"		Medium: Wet		Feed Size: -10 mesh (Natural)		
M^*_B = 0.3	Average Power (kW) = 0.05746			Mass Holdup (tons) = 0.00508		
Percent Solids (%) = 65			Percent Slurry Filling (%) = 260			
Mill Speed (rpm) = 61.8	Grind Time (min)					
Size	1	2	4	5	6	8
	Energy (kwh/ton)					
(Mesh)	0.1943	0.3822	0.7525	0.9318	1.1189	1.4774
-9	1.0000	1.0000	1.0000	1.0000	1.0000	1.0000
-10	0.9415	0.9780	0.9960	0.9984	0.9990	0.9998
-14	0.8204	0.9126	0.9826	0.9933	0.9964	0.9994
-20	0.7168	0.8271	0.9503	0.9752	0.9873	0.9976
-28	0.6249	0.7283	0.8788	0.9300	0.9556	0.9872
-35	0.5302	0.6190	0.7732	0.8375	0.8736	0.9426
-48	0.4292	0.5052	0.6289	0.6879	0.7237	0.8265
-65	0.3381	0.3941	0.4906	0.5389	0.5680	0.6733
-100	0.2730	0.3179	0.3920	0.4326	0.4555	0.5255
-150	0.2122	0.2514	0.3054	0.3299	0.3519	0.4117
-200	0.1655	0.1902	0.2340	0.2558	0.2754	0.3159
-270	0.1272	0.1461	0.1786	0.1942	0.2109	0.2372
-400	0.1041	0.1067	0.1367	0.1520	0.1718	0.1764

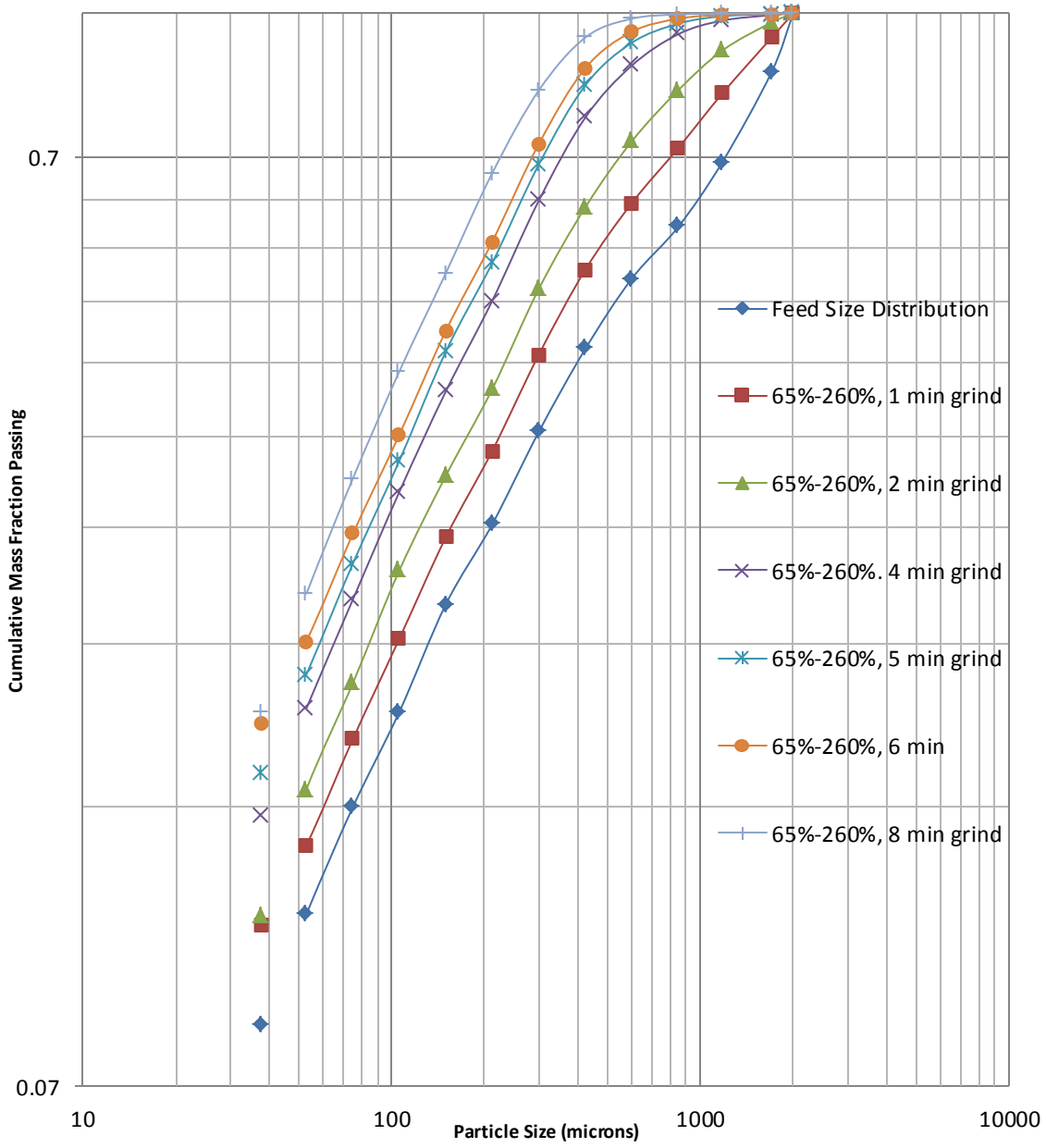

Figure A-8: Experimentally Derived Product Size Distribution (65% solids-260% slurry filling) for Quartzite (-10 mesh natural size).

Table A-9 (Quartzite)						
Mill Size: 10"		Medium: Wet		Feed Size: -10 mesh (Natural)		
M^*_B = 0.3	Average Power (kW) = 0.0590			Mass Holdup (tons) = 0.00608		
Percent Solids (%) = 72			Percent Slurry Filling (%) = 260			
Mill Speed (rpm) = 61.7	Grind Time (min)					
Size	1	2	4	5	6	8
	Energy (kWh/ton)					
(Mesh)	0.1664	0.3285	0.6462	0.8007	0.9617	1.2640
-9	1.0000	1.0000	1.0000	1.0000	1.0000	1.0000
-10	0.9216	0.9644	0.9911	0.9955	0.9977	0.9996
-14	0.7917	0.8807	0.9622	0.9822	0.9905	0.9982
-20	0.6801	0.7814	0.9047	0.9493	0.9701	0.9932
-28	0.5821	0.6859	0.8120	0.8828	0.9140	0.9707
-35	0.4937	0.5852	0.6952	0.7738	0.8053	0.8963
-48	0.4071	0.4749	0.5718	0.6300	0.6686	0.7659
-65	0.3261	0.3743	0.4524	0.4976	0.5352	0.6131
-100	0.2560	0.3030	0.3518	0.4003	0.4174	0.4767
-150	0.2047	0.2328	0.2727	0.3061	0.3276	0.3704
-200	0.1573	0.1832	0.2135	0.2397	0.2580	0.2945
-270	0.1220	0.1416	0.1633	0.1837	0.2013	0.2265
-400	0.0995	0.1048	0.1227	0.1383	0.1546	0.1687

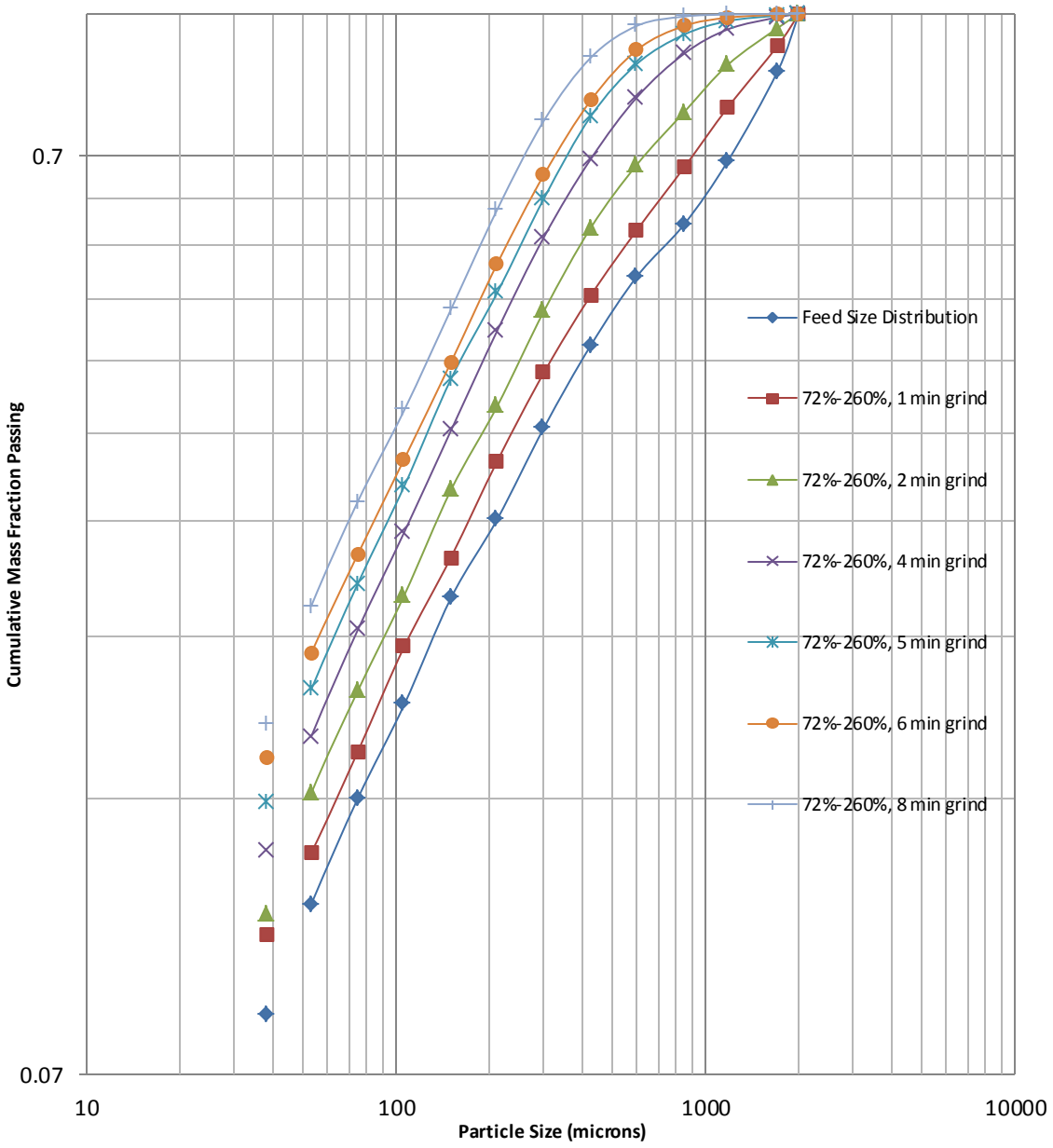

Figure A-9: Experimentally Derived Product Size Distribution (72% solids-260% slurry filling) for Quartzite (-10 mesh natural size).

Table A-10 (Quartzite)				
Mill Size: 10"	Medium: Wet	Feed Size: 10 x 14 (mono-size)		
$M^*_B = 0.3$	Average Power (kW) = 0.06338		Mass Holdup (tons) = 0.00234	
Percent Solids (%) = 72		Percent Slurry Filling (%) = 100		
Mill Speed (rpm) = 61.75	Grind Time (min)			
Size	1	2	4	6
	Energy (kWh/ton)			
(Mesh)	0.4323	0.8964	1.8429	2.7867
-9	1.0000	1.0000	1.0000	1.0000
-10	0.9411	0.9475	0.9896	0.9984
-14	0.5350	0.7854	0.9675	0.9955
-20	0.3720	0.6471	0.9313	0.9905
-28	0.2951	0.5439	0.8725	0.9786
-35	0.2343	0.4299	0.7644	0.9321
-48	0.1836	0.3557	0.6272	0.8148
-65	0.1407	0.2690	0.4895	0.6528
-100	0.1149	0.2196	0.3943	0.5331
-150	0.0890	0.1718	0.3033	0.4135
-200	0.0725	0.1322	0.2391	0.3310
-270	0.0585	0.1051	0.1909	0.2609
-400	0.0472	0.0793	0.1420	0.2023

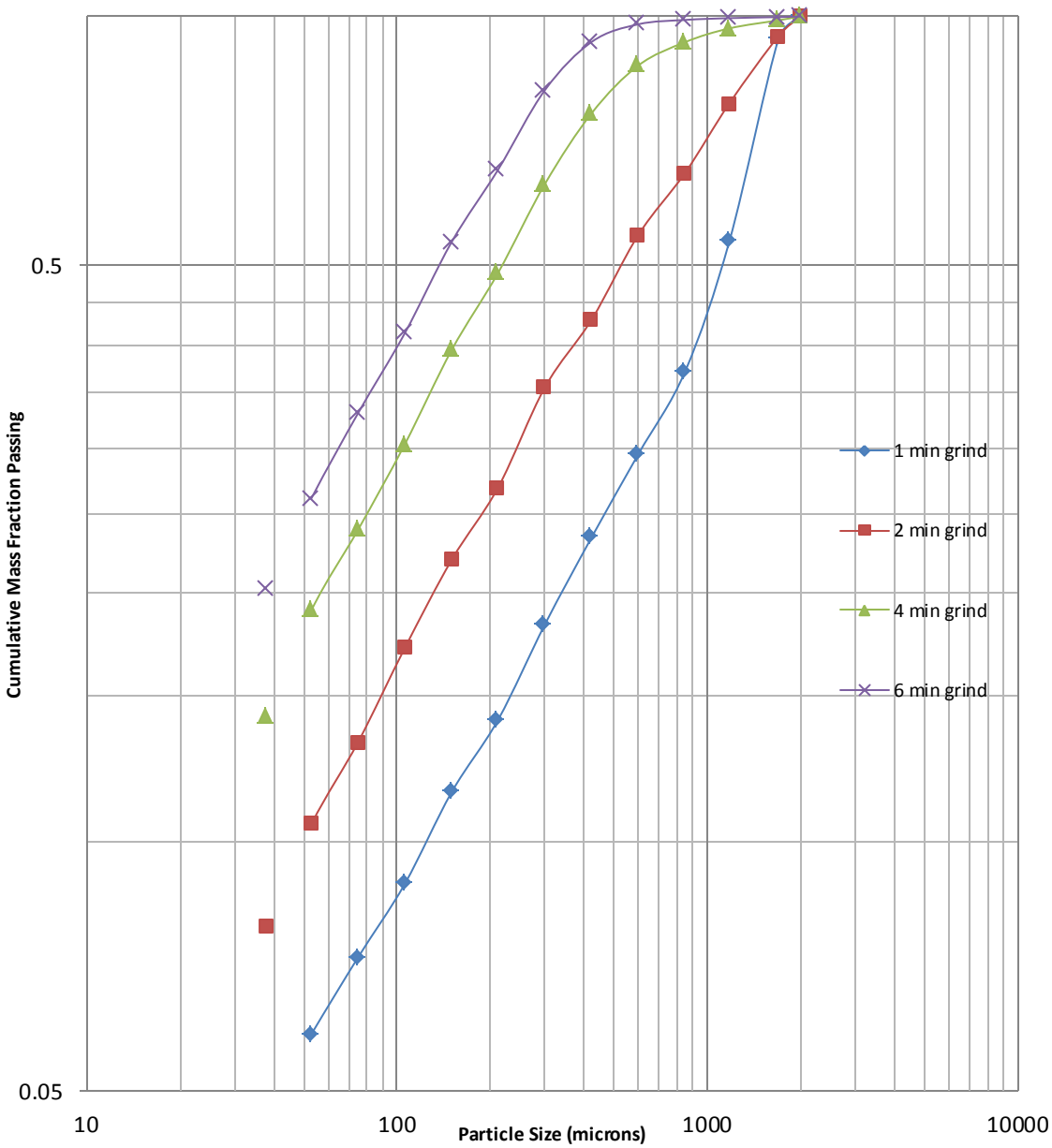

Figure A-10: Experimentally Derived Product Size Distribution (72% solids-100% slurry filling) for Quartzite (10x14 mesh mono-size).

Table A-11 (Gold Ore)						
Mill Size: 10"		Medium: Wet		Feed Size: -10 mesh (Natural)		
M^*_B = 0.3	Average Power (kW) = 0.06944			Mass Holdup (tons) = 0.0022034		
Percent Solids (%) = 65			Percent Slurry Filling (%) = 100			
Mill Speed (rpm) = 61.9	Grind Time (min)					
Size	1	2	4	5	6	8
	Energy (kWh/ton)					
(Mesh)	0.5289	1.0455	2.0819	2.6605	3.1780	4.1418
-9	1.0000	1.0000	1.0000	1.0000	1.0000	1.0000
-10	0.9986	0.9996	1.0000	1.0000	1.0000	1.0000
-14	0.9786	0.9914	0.9986	0.9995	0.9998	1.0000
-20	0.9202	0.9589	0.9893	0.9946	0.9973	0.9993
-28	0.8077	0.8815	0.9559	0.9733	0.9839	0.9942
-35	0.6448	0.7501	0.8784	0.9158	0.9419	0.9726
-48	0.4749	0.5925	0.7580	0.8146	0.8584	0.9181
-65	0.3344	0.4456	0.6192	0.6858	0.7414	0.8260
-100	0.2120	0.3107	0.4756	0.5439	0.6040	0.7029
-150	0.1355	0.2164	0.3581	0.4199	0.4764	0.5748
-200	0.0916	0.1557	0.2713	0.3235	0.3723	0.4606
-270	0.0679	0.1183	0.2105	0.2529	0.2932	0.3677
-400	0.0530	0.0927	0.1660	0.2001	0.2327	0.2940

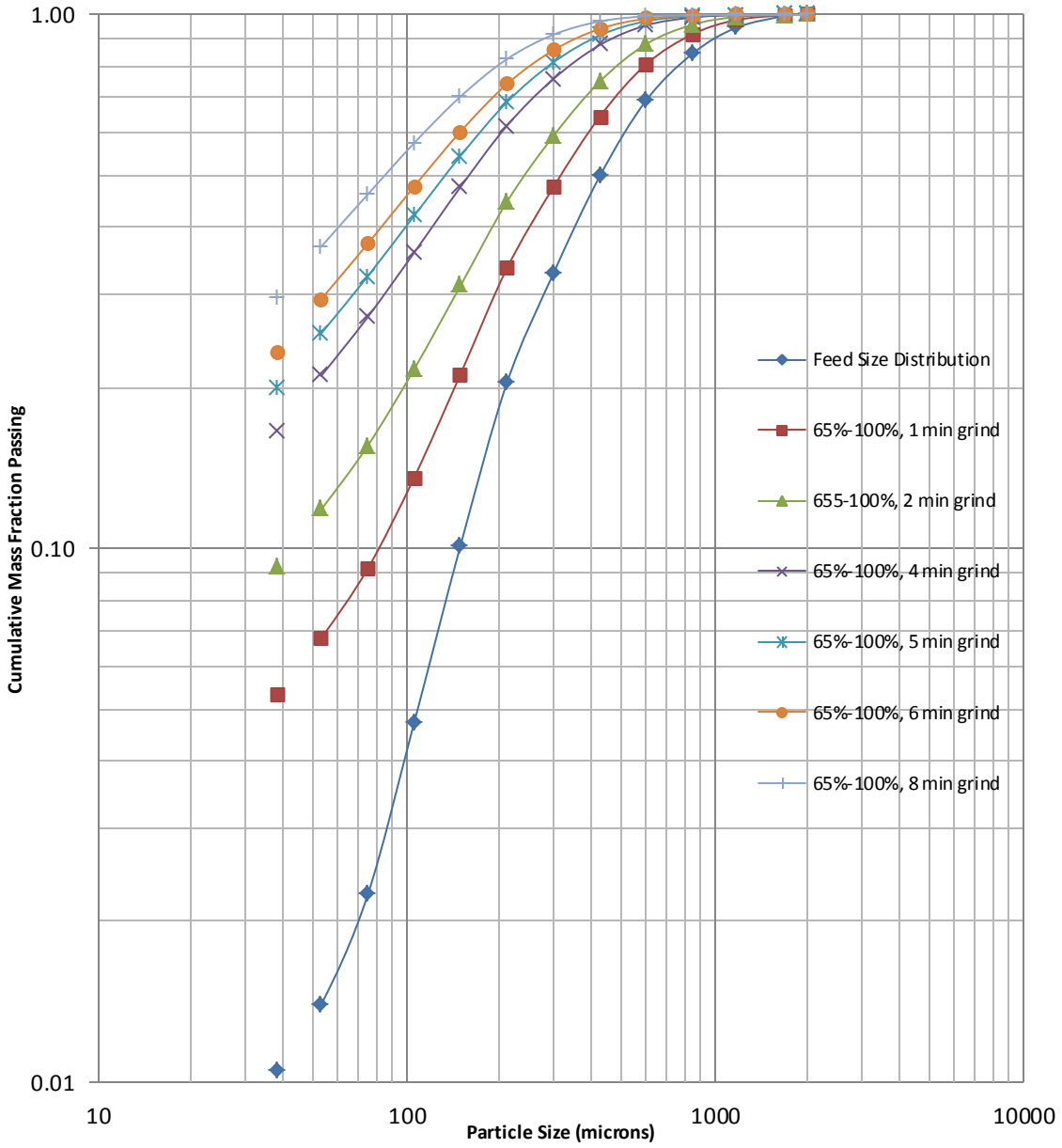

Figure A-11: Experimentally Derived Product Size Distribution (65% solids-100% slurry filling) for Gold Ore (-10 mesh natural size).

Table A-12 (Gold Ore)						
Mill Size: 10"		Medium: Wet		Feed Size: -10 mesh (Natural)		
M^*_B = 0.3	Average Power (kW) = 0.0667			Mass Holdup (tons) =0.002389		
Percent Solids (%) = 72			Percent Slurry Filling (%) = 100			
Mill Speed (rpm) = 61.7	Grind Time (min)					
Size	1	2	4	5	6	8
	Energy (kWh/ton)					
(Mesh)	0.4649	0.9329	1.8550	2.3249	2.7968	3.7219
-9	1.0000	1.0000	1.0000	1.0000	1.0000	1.0000
-10	0.9982	0.9993	0.9999	1.0000	1.0000	1.0000
-14	0.9740	0.9873	0.9970	0.9985	0.9993	0.9998
-20	0.9087	0.9460	0.9814	0.9891	0.9937	0.9979
-28	0.7886	0.8565	0.9348	0.9563	0.9708	0.9871
-35	0.6206	0.7143	0.8401	0.8811	0.9118	0.9518
-48	0.4502	0.5527	0.7071	0.7641	0.8105	0.8785
-65	0.3126	0.4082	0.5650	0.6283	0.6832	0.7710
-100	0.1936	0.2779	0.4240	0.4868	0.5434	0.6401
-150	0.1208	0.1897	0.3137	0.3694	0.4211	0.5135
-200	0.0801	0.1346	0.2351	0.2815	0.3254	0.4064
-270	0.0590	0.1017	0.1816	0.2191	0.2549	0.3224
-400	0.0459	0.0797	0.1431	0.1731	0.2020	0.2571

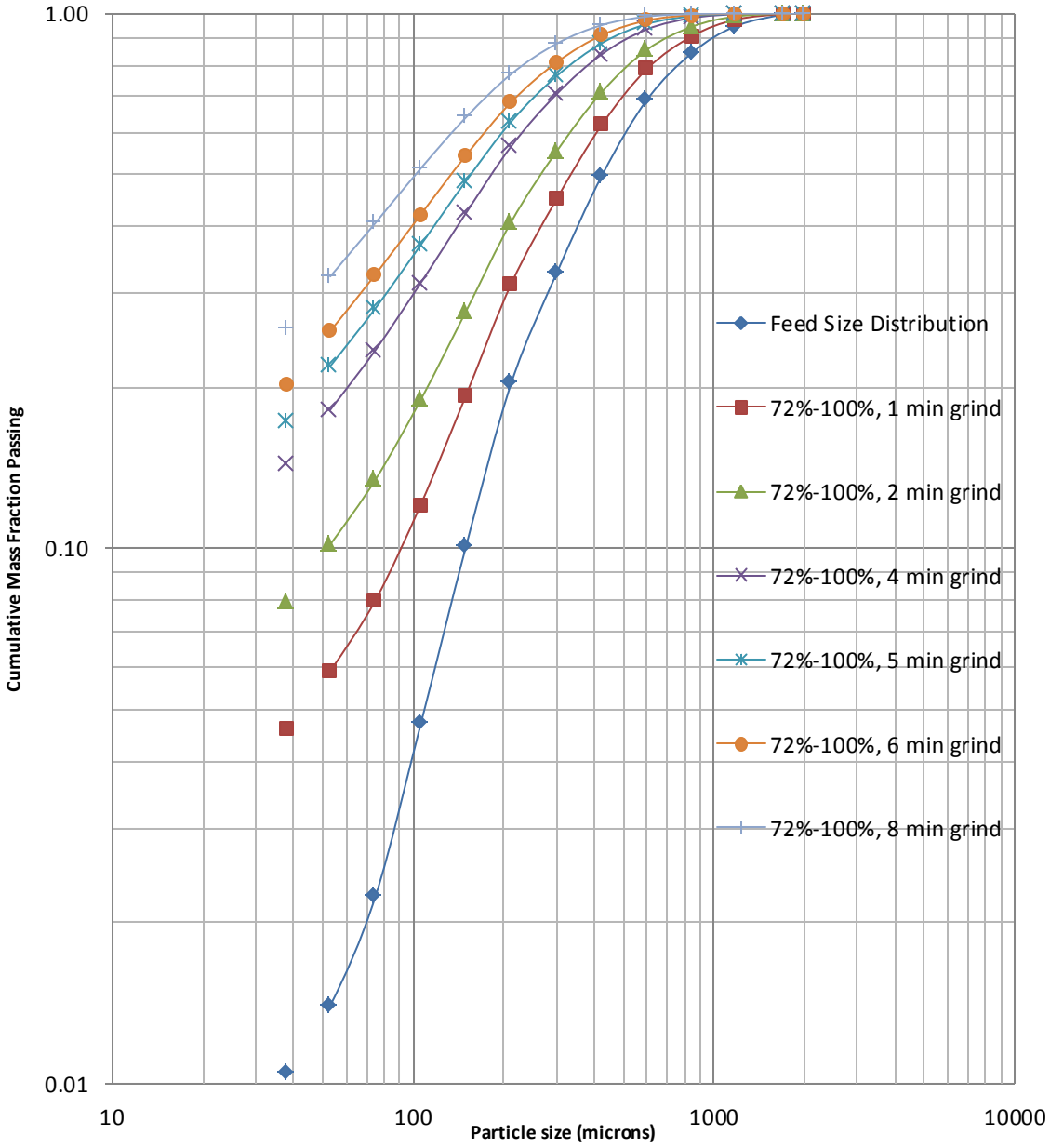

Figure A-12: Experimentally Derived Product Size Distribution (72% solids-100% slurry filling) for Gold Ore (-10 mesh natural size).

Table A-13 (Gold Ore)						
Mill Size: 10"		Medium: Wet		Feed Size: -10 mesh (Natural)		
M^*_B = 0.3	Average Power (kW) = 0.057456			Mass Holdup (tons) = 0.0057288		
Percent Solids (%) = 65			Percent Slurry Filling (%) = 260			
Mill Speed (rpm) = 61.8	Grind Time (min)					
Size	1	2	4	5	6	8
	Energy(kWh/ton)					
(Mesh)	0.1723	0.3389	0.6673	0.8263	0.9923	1.3101
-9	1	1	1	1	1	1
-10	0.9972	0.9982	0.9993	0.9995	0.9997	0.9999
-14	0.9619	0.9727	0.986	0.99	0.9929	0.9963
-20	0.8773	0.9021	0.9378	0.9504	0.9606	0.9751
-28	0.7348	0.7726	0.8332	0.8572	0.8779	0.9107
-35	0.5489	0.594	0.6714	0.7045	0.7344	0.7855
-48	0.3741	0.4179	0.4965	0.5317	0.5646	0.6236
-65	0.2433	0.2806	0.3495	0.3813	0.4116	0.4677
-100	0.1333	0.164	0.2217	0.2488	0.2748	0.324
-150	0.0722	0.0963	0.1419	0.1635	0.1844	0.2242
-200	0.0419	0.0607	0.0962	0.113	0.1294	0.1607
-270	0.0292	0.0439	0.0715	0.0847	0.0974	0.1219
-400	0.0225	0.0341	0.0559	0.0662	0.0763	0.0955

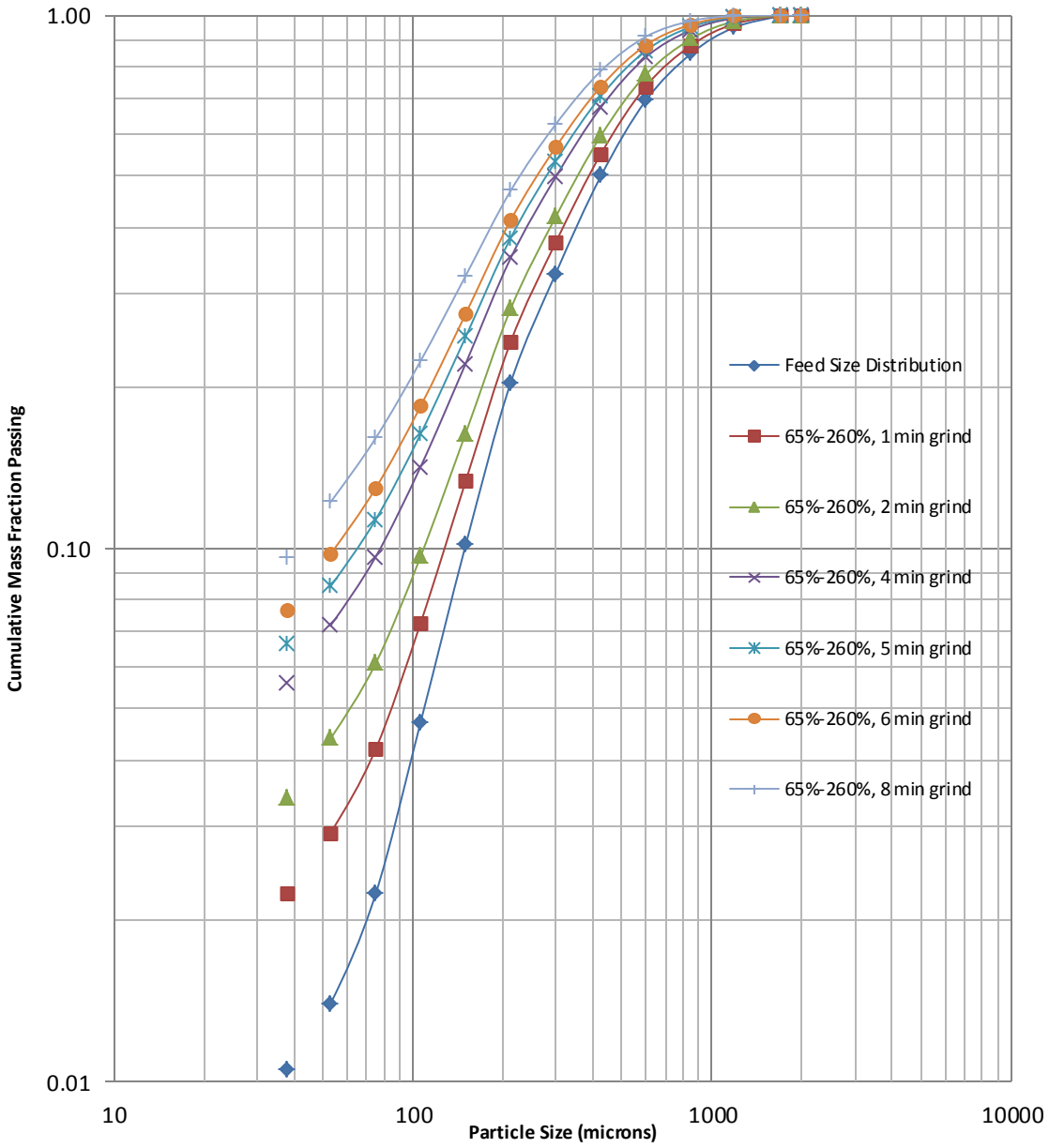

Figure A-13: Experimentally Derived Product Size Distribution (65% solids-260% slurry filling) for Gold Ore (-10 mesh natural size).

Table A-14 (Gold Ore)						
Mill Size: 10"		Medium: Wet		Feed Size: -10 mesh (Natural)		
M^*_B = 0.3	Average Power (kW) = 0.0590			Mass Holdup (tons) = 0.00621		
Percent Solids (%) = 72			Percent Slurry Filling (%) = 260			
Mill Speed (rpm) = 61.7	Grind Time (min)					
Size	1	2	4	5	6	8
	Energy (kWh/ton)					
(Mesh)	0.1629	0.3217	0.6327	0.7840	0.9416	1.2376
-9	1.0000	1.0000	1.0000	1.0000	1.0000	1.0000
-10	0.9966	0.9973	0.9984	0.9988	0.9990	0.9994
-14	0.9565	0.9644	0.9761	0.9804	0.9840	0.9893
-20	0.8669	0.8847	0.9135	0.9252	0.9353	0.9517
-28	0.7212	0.7487	0.7962	0.8166	0.8350	0.8666
-35	0.5351	0.5688	0.6296	0.6569	0.6822	0.7278
-48	0.3625	0.3962	0.4588	0.4878	0.5154	0.5666
-65	0.2344	0.2638	0.3197	0.3463	0.3719	0.4204
-100	0.1266	0.1515	0.1993	0.2224	0.2448	0.2880
-150	0.0672	0.0869	0.1253	0.1439	0.1621	0.1976
-200	0.0381	0.0535	0.0835	0.0982	0.1126	0.1407
-270	0.0262	0.0382	0.0616	0.0731	0.0844	0.1065
-400	0.0201	0.0295	0.0480	0.0570	0.0659	0.0834

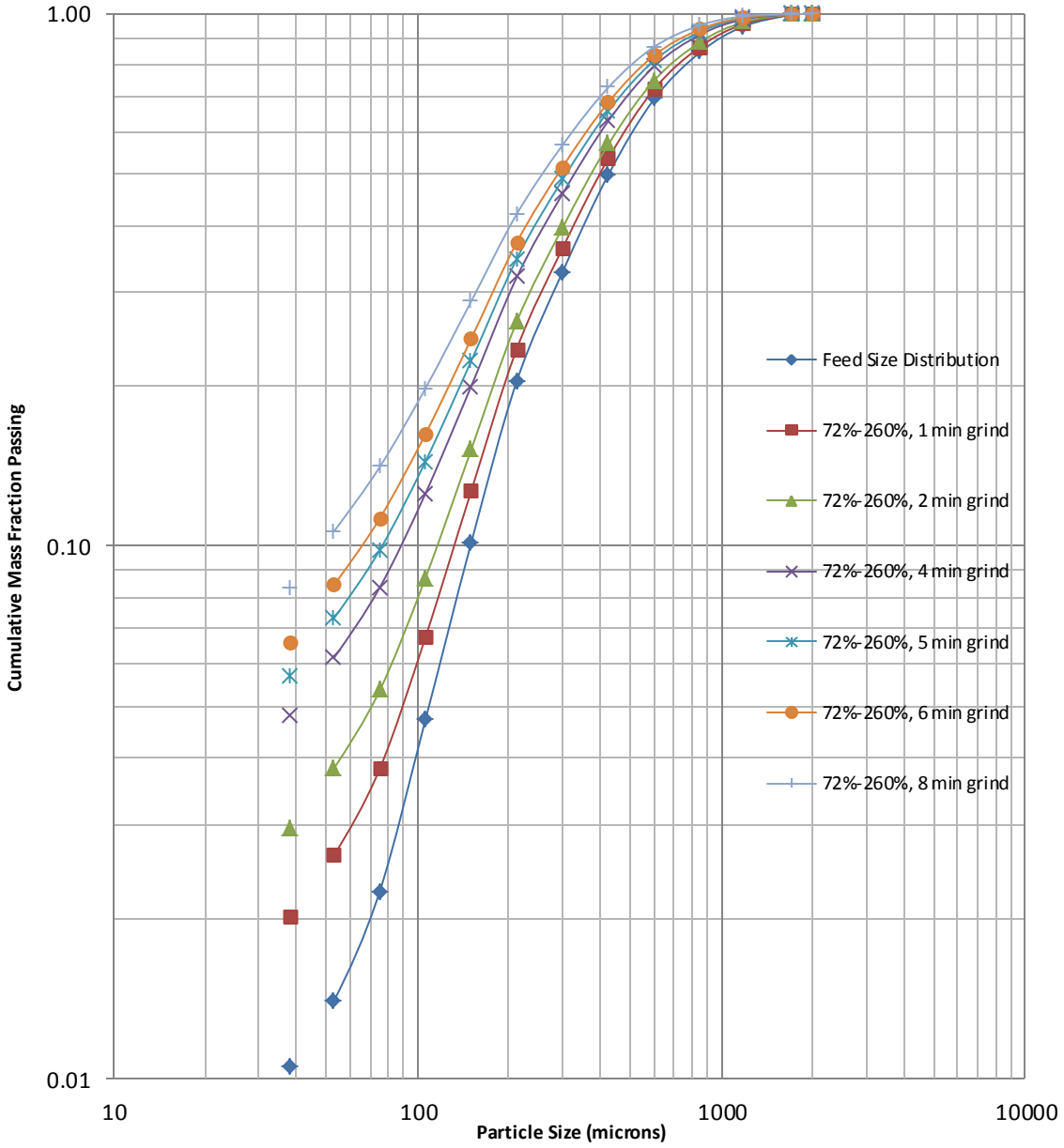

Figure A-14: Experimentally Derived Product Size Distribution (72% solids-260% slurry filling) for Gold Ore (-10 mesh natural size).

Table A-15 (Gold Ore)				
Mill Size: 10"	Medium: Wet	Feed Size: 10 x 14 (mono-size)		
M^*_B = 0.3	Average Power (kW) = 0.06112		Mass Holdup (tons) = 0.002389	
Percent Solids (%) = 72		Percent Slurry Filling (%) = 100		
Mill Speed (rpm) = 61.7	Grind Time (min)			
Size	1	2	4	6
	Energy (kwh/ton)			
(Mesh)	0.4046	0.8338	1.7413	2.6887
-9	1.0000	1.0000	1.0000	1.0000
-10	0.9445	0.9698	0.9909	0.9990
-14	0.4564	0.6252	0.8590	0.9658
-20	0.2289	0.3855	0.6685	0.8793
-28	0.1532	0.2700	0.5101	0.7540
-35	0.1133	0.2024	0.3939	0.6190
-48	0.0882	0.1545	0.3133	0.4978
-65	0.0719	0.1232	0.2550	0.4047
-100	0.0594	0.1052	0.2123	0.3494
-150	0.0507	0.0874	0.1826	0.2957
-200	0.0428	0.0758	0.1543	0.2555
-270	0.0353	0.0627	0.1288	0.2123
-400	0.0275	0.0502	0.1016	0.1764

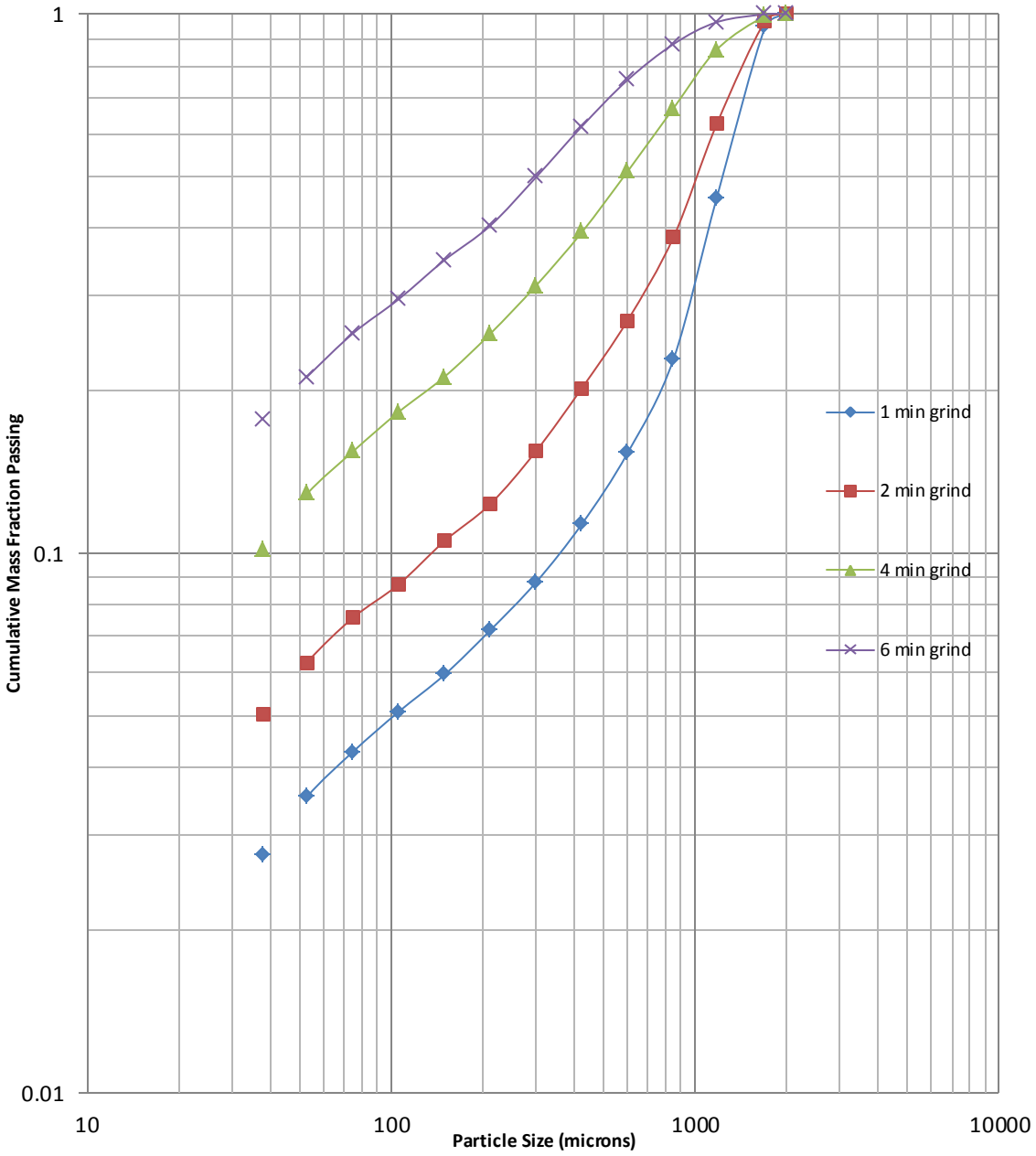

Figure A-15: Experimentally Derived Product Size Distribution (72% solids-100% slurry filling) for Gold Ore (10x14 mesh mono-size).

APPENDIX B

ILLUSTRATIVE COMPARISON OF PSD FROM METHOD I AND METHOD II

Table B-1: Illustration of Product Size Distribution Simulated from Method I for Quartzite (65% solids-100% slurry filling, -10 mesh natural size)

Method I- Cumulative Grind Times/Specific Energy						
	Cumulative Specific Energy					
(MESH)	0.56	1.12	2.25	2.81	3.36	4.49
	1 min	2 min	4 min	5 min	6 min	8 min
-9	1	1	1	1	1	1
-10	0.9677	0.9922	0.9996	0.9999	1	1
-14	0.9032	0.9704	0.9975	0.9993	0.9998	1
-20	0.8296	0.9329	0.991	0.9967	0.9988	0.9999
-28	0.7528	0.8791	0.9744	0.9884	0.9949	0.999
-35	0.6602	0.8011	0.9368	0.9647	0.9805	0.9942
-48	0.5565	0.6986	0.865	0.9094	0.9395	0.9734
-65	0.4529	0.5825	0.7566	0.8123	0.8551	0.914
-100	0.3681	0.4764	0.6336	0.6896	0.7359	0.8079
-150	0.2856	0.3731	0.5054	0.555	0.5977	0.6685
-200	0.2242	0.2927	0.3978	0.4381	0.4734	0.5335
-270	0.1724	0.2255	0.3075	0.3391	0.367	0.4149
-400	0.1316	0.1725	0.2359	0.2604	0.282	0.3193

Table B-2: Illustration of Product Size Distribution Simulated from Method II for Quartzite (65% solids-100% slurry filling, -10 mesh natural size)

Method II - Incremental Grind Times/Specific Energy						
kWh/ton	0-0.56, 1.12	0.56-1.12, 2.25	1.12-2.25,2.80	2.25-2.80, 3.36	2.25-2.80, 3.36	3.36-4.49
Microns	0-1 min, 2min	1-2 min, 4 min	2-4 min , 5 min	4-5 min, 6 min	5-6 min , 8 min	6-8 min
2000	1	1	1	1	1	1
1700	0.9611	0.9922	1	1	1	1
1180	0.899	0.9731	1	1	1	1
850	0.8338	0.9425	0.9993	0.9997	0.9998	1
600	0.7617	0.8961	0.9983	0.9981	0.9991	0.9999
425	0.6669	0.8197	0.975	0.9883	0.995	0.9993
300	0.5543	0.7046	0.8879	0.9332	0.9631	0.9903
212	0.4424	0.5717	0.7491	0.8104	0.8648	0.9377
150	0.3551	0.4615	0.6168	0.6785	0.7359	0.8347
106	0.2725	0.3653	0.4913	0.5454	0.6027	0.6983
75	0.2133	0.2741	0.3843	0.4237	0.4672	0.5539
53	0.1637	0.2155	0.2997	0.3308	0.3663	0.4362
38	0.1248	0.1667	0.2298	0.2639	0.2978	0.3492

REFERENCES

1. Herbst, J.A., Grandy, G.A., and Fuerstenau, D.W., "Population Balance Models for the Design of Continuous Grinding Mills," paper 19, X International Mineral Processing Congress, London, 1973.

2. Blasket, K.S., "Estimation of the Power Consumption in Grinding Mills," Mineral Processing and Extractive Metallurgy, London: IMM, pp. 631-49, 1970).

3. Rose, H.E. and Sullivan, R.M.E., "A Treatise on the Internal Mechanics of Ball, Tube and Rod Mills," 1958, Chemical Publishing C o., Inc ., 212 Fifth Avenue, New York.

4. Agar, G.E., and Brown, J.H., "Energy Requirements in Size Reduction," Can. Min. and Met. Bull., No. 622, February 1964.

5. Charles, R.J., "Energy-Size Reduction Relationships in Comminution," AIME Transactions, Vol. 208, 1957, pp. 80-88.

6. Schuhmann, R., "Energy Input and Size Distribution in Comminution," AIME Transactions, Vol. 217, 1960, pp. 22-25

7. Bond, F.C., "The Third Theory of Comminution," AIME Transactions, Vol.193, 1952, pp. 484-494.

8. Harris, C.C., "On the Role of Energy in Comminution: A Review of Physical and Mathematical Principles," Trans. I.M.M., Vol. 75, 1966, pp. C37-C56.

9. Harris, C.C., "On the Limit of Comminution," AIME Transactions, Vol.238, 1967, pp. 17-30.

10. Schonert, K., "Modellrechmungen fur Zerkleinerungsprozesse mit den Ergebnissen der Einzelkorn-Druckzerkleinerung," in Zerkleinern, 2nd European Symposium on Comminution, Amsterdam, 1966; Dechema-Monographien, Vol. 57, Part 1, 1967.

11. Herbst, J.A., and Fuerstenau, D.W., "The Zero Order Production of Fine Sizes in Comminution nd its Implications in Simulation," AIME Transactions, Vol. 241, 1968, pp. 538-549.

12. Herbst, J.A., "Batch Ball Mill Simulation: An Approach for Wet Systems," D. Eng. Dissertation, University of California, Berkeley, California, 1971.

13. Herbst, J.A. and Fuerstenau, D.W., "Mathematical Simulation of Dry Ball Milling Using Specific Power Information," Trans. AIME,Vol. 254, 1973, p. 343

14. Malghan, S.G., Fuerstenau, D.W., "The Scale-up of Ball Mills Using Population Balance Models and Specific Power Input," Symposium Zerkleinern, Dechma-Monographien, V o l. 79., Part I I, No. 1586, 1976, p. 613.

15. Malghan, S.G., "The Scale-up of Ball Mills Using Population Balance Models," D. Eng. Dissertation, University of California, Berkeley, California.

16. Kim, J.H., "A Normalized Model for Wet Batch Ball Milling," Ph.D. Dissertation, University of Utah, Salt Lake City, Utah, 1974.

17. Austin, L.G., Process Engineering of Size Reduction: Ball Milling, MME, 1984, 1-60 and 79- 117.

18. AMS Committee on Milling, Metals Handbook, 7, 56070.

19. Benjamin, J.S., Scientific American, l970.234, 40-48.

20. Mishra, B.K. and Rajamani, R.K., Comminution Theory and Particles, Editor S. Komar Kawatra, Soc. for Mining, Metall. and Exploration, Inc. Littleton CO., 1992, 427-440.

21. Gaudin, **A.** M., Principles of Mineral Dressing. Mcgraw-Hill, London, **1** 939, 92-140.

22. George Charles Lowrisen, Crushing and Grinding: The Size Reduction of Solid Materials, Butterworths, London, **1** 974, 225-254.

23. Takova, K., Developments in Mineral Processing, Mechanical Activation of Minerals, Volume 1 1, Elsevier, 1989, 70- 108.

24. Davice, R.M., McDennont and **C.** C. Koch. Metall. Trans., 19A, 1988, 2867.

25. Hashimoto, H. and Watanabe, R., Materials Science Forum, 88-90, 1992, 89-96.

26. Bond, F.C., "Crushing and Grinding Calculations, " Canadian Min. and Met. Bulletin, Vol. 47, 1954, p. 466.

27. Bond, F.C., "More Accurate Grinding Calculations, " Cement Lime and Gravel, 1963, p. 69.

28. Pryor, E.J., "Mineral Processing," 3rd Edition Elsevier Publishing Co. Ltd., Amsterdam-London-New York, 1965.

29. Reid, K.J., "A Solution to the Batch Grinding Equations," Chem. Eng. Sci. , Vol. 20, 1965, p. 953.

30. Austin, L.G., "Understanding Ball Mill Sizing, " Ind. Eng. Chem. Process Design and Development, Vol. 12, No. 2, 1973, p. 121.

31. Grandy, G.A. and Fuerstenau, D.W., "Simulation of Non-Linear Grinding Systems: Rod-Mill Grinding, " Trans. AIME, Vol. 247, 1970, p. 348.

32. Herbst, J.A. and Fuerstenau, D.W., 'The Zero Order Production of Fine Sizes in Comminution and its Implications in Simulation," Trans. AIME, Vol. 241, 1968, p. 538.

33. Austin, L.G. and Bhatia, V.K. "Experimental Methods for Grinding Studies in Laboratory Mills," Powder Technology, Vol. 5, 1971-72, p. 261.

34. Herbst, J. A. and Kim, J. H., "Nearly Equal Selection Functions in Linear Size - Discretized Grinding Models," Trans. IMM, Vol. 82, 1973, p. cl69.

35. Herbst, J.A., Grandy, G.A. and Mika, T.S., "On the Development and Use of Lumped Parameter Model for Continuous Open-and Closed- Circuit Grinding Systems," Trans._ IMM, Vol. 80, 1971, p. cl93.

36. Herbst, J.A., and Mika, T.S., "Linearization of Tumbling Mill Models Involving Nonlinear Breakage Phenomena," Eleventh International Symposium on Computer Applications in Mineral Industries, Tucson, Arizona, April 1973.

37. Tanaka, T., "Scale-up Formula For Grinding Equipment Using Selection Function, " Journal of Chemical Engineering of Japan, Vol. 5, No. 3, 1972.

38. Verma. R., and Rajamani, R.K., "Effect of Milling Environment on the Breakage Rates in Dry and Wet Grinding," In S.K.Kawatra (Ed), Comminution: Theory and Practice, pp. 261-271.

39. King, R.P., "Modeling and Simulation of Mineral Processing Systems", Butterworth Heinemann, 2001.

40. Siddique, M., "A Kinetic Approach to Ball Mill Scale-up for Dry and Wet Systems," MS Thesis, University of Utah, 1977.

41. Fuerstenau, D.W., Abouzeid, A.Z.M., Phatak, P.B., "Effect of Particulate Environment on the Kinetics and Energetics of Dry Ball Milling," Int. Journal of Min. Pro, Vol. 97, 2010, pp. 52-58.

42. Tangsathitkulchai, C. and Austin, L.G., "Rheology of Concentrated Slurries of Particles of Natural Size Distribution Produced by Grinding," Powder Technology, Vol. 56, 1989, pp. 293-299.